P-04-250

Oskarshamn site investigation

Fracture mineralogy and wall rock alteration

Results from drill core KSH01A+B

Henrik Drake
Department of Geology, Earth Science Centre
Göteborg University

Eva-Lena Tullborg
Terralogica AB, Gråbo

June 2004

Svensk Kärnbränslehantering AB
Swedish Nuclear Fuel
and Waste Management Co
Box 5864
SE-102 40 Stockholm Sweden
Tel 08-459 84 00
+46 8 459 84 00
Fax 08-661 57 19
+46 8 661 57 19

ISSN 1651-4416
SKB P-04-250

Oskarshamn site investigation

Fracture mineralogy and wall rock alteration

Results from drill core KSH01A+B

Henrik Drake
Department of Geology, Earth Science Centre
Göteborg University

Eva-Lena Tullborg
Terralogica AB, Gråbo

June 2004

Keywords: Fracture minerals, Simpevarp, Fracture mineralogy, Formation temperatures, Ductile/brittle deformation, Wall rock alteration, Oxidation-reduction, Subsidence-uplift, Metamorphic facies, Burial metamorphosis, Low-temperature minerals, Calcite, Stable isotopes.

Abstract

Fracture mineralogical studies have been carried out on the first deep core borehole on the Simpevarp peninsula (KSH01A+B) as part of SKB's site investigation programme. The Simpevarp area is situated in Precambrian crystalline rocks, at site consisting mainly of granitoids belonging to the Transscandinavian Igneous Belt (TIB).

40 samples have been collected from fractures, which include fillings of several generations. The samples have been analysed using mainly polarised light microscope and scanning electron microscope. For identification of fracture minerals, additional analyses have been made with stereomicroscope, X-ray diffraction and ICP-MS. Fracture calcites have been analysed for their stable isotope composition (C, O and Sr) and trace element contents. The aim of this study has been to: 1) provide fracture mineral identification, especially of clay minerals, to the macroscopic core mapping, 2) establish a sequence of fracture mineralisations that can add to the geological description and understanding of the site 3) give support to the selection of samples to be used for measurements of transport properties and 4) to give input to the palaeohydrogeological interpretations.

The fracture minerals identified are chlorite, calcite, epidote, quartz, low temperature K-feldspar (adularia), prehnite, laumontite, albite, fluorite, Ba-zeolite (harmotome), barite, pyrite, titanite, anatase/rutile, apatite, muscovite, hematite, apophyllite, REE-carbonate, amphibole, ilmenite and clay minerals, dominantly illite, mixed layer clays (illite-smectite), corrensite and to lesser degree smectite. Rarely, additional sulphides like chalcopyrite, galena and sphalerite have been found.

Several generations of mineralisations have been identified of which the first are quartz fillings, probably associated with post-magmatic circulation. Subsequent greenschist facies conditions (epidote, quartz, calcite, pyrite, muscovite and some albite and Fe-Mg chlorite with titanite) in combination with ductile deformation, resulted in the formation of epidote-mylonite. The epidote-mylonite seems to be associated with the oxidation and the formation of hematite, causing extensive red-staining of the wall-rock along the fractures. This relatively early formed mylonite has later been reactivated in association with brittle deformation conditions. The subsequent breccia sealing by prehnite-fluorite marks the ultimate ending point of the extensive red-staining of the wall-rock and also the change in conditions, from greenschist to prehnite-pumpellyite facies. Later fracture fillings consisting of calcite and Fe-Mg chlorite was followed by semi-ductile to brittle deformation, inducing dark-red coloured hematite-cataclasite formation together with adularia, Mg-chlorite and calcite. The latest hydrothermal mineralisation shows a decreasing formation temperature series as follows; Mg-chlorite, adularia, laumontite (Ca-zeolite), hematite, harmotome (Ba-zeolite), pyrite, Fe-chlorite (spherulitic), calcite + REE-carbonates and clay minerals. The appearance of zeolites infers formation conditions in the ranges of zeolite facies. These minerals might have been formed at one continuous event or at several different events with gradually lower temperatures. The outermost coatings along the hydraulically conductive fractures consist mainly of clay minerals of mixed layer clay type (corrensite = chlorite/smectite and illite/smectite) together with calcite and minor grains of pyrite. Low temperature calcites have been formed during various conditions and from both saline and fresh groundwaters. The stable isotope results from the fracture calcites support largely the above given sequence of events.

Sammanfattning

Sprickmineralogiska studier av det första djupa borrhålet på Simpevarpshalvön (KSH01A+B) har utförts inom ramen för SKB's platsundersökningar. Simpevarpsområdet är beläget i pre-kambrisk kristallin berggrundsterräng tillhörande det Transskandinaviska Magmatiska Bältet (TMB/TIB).

40 prover har insamlats från sprickor som innehåller sprickminerliseringar av flera generationer. Proverna har i huvudsak analyserats med polariserande mikroskop och svepelektron-mikroskop. Stereomikroskop, röntgendiffraktometri (XRD) och ICP-MS har använts för identifiering av sprickmineral och för kompletterande analyser. Stabila isotopförhållanden (C, O och Sr) och spårämnes-sammansättning har analyserats på kalciter bildade i sprickor. Syftet med studien är att: 1) komplettera den makroskopiska karteringen med bestämning av svår-identifierade faser t ex lermineraler, 2) ge bidrag till den geologiska beskrivningen och förståelsen av området genom att sammanställa en sekvens av sprickmineraliseringar, 3) ge en grund för valet av prover som skall användas vid analyser av transportegenskaper (Kd och diffusivitet) och 4) att ge information om palaeohydrogeologiska förhållanden.

De identifierade sprickmineralen är klorit, kalcit, epidot, kvarts, lågtemperatur-kalifältspat (adularia), prehnit, laumontit, albit, fluorit, Ba-zeolit (harmotom), baryt, pyrit, titanit, anatas/rutil, apatit, muskovit, hematit, apophyllit, REE-karbonat, amfibol, ilmenit and lermineral, främst illit, mixed layer clays (illit-smectit), corrensit och i mindre omfattning smectit. I ett par tillfällen har sulfider som kopparkis, blyglans och zinkblände noterats i sprickorna.

Flera generationer av mineraliseringar har identifierats. Den första av dessa generationer består av kvartsfyllningar, som antagligen kan kopplas samman med post-magmatisk cirkulation. Efterföljande grönskifferfacies-förhållanden (epidot, kvarts, kalcit, pyrit, muskovit och lite albite tillsammans med Fe-Mg klorit med titanit) i kombination med duktil deformation, resulterade i bildandet av epidot-mylonit. Epidot-myloniten ser ut att vara associerad med oxidering och hematit-bildning, vilken har givit upphov till omfattande rödfärgning av berget i nära anslutning till sprickorna. Denna relativt tidigt bildade mylonit har i ett senare skede blivit reaktiverad i samband med spröd deformation. Efterföljande breccia-läkning av prehnit och fluorit utgör slutskedet för den omfattande oxidationen av sidoberget, men markerar även övergången från grönskiffer till prehnit-pumpellyit-facies förhållanden. Senare sprickfyllnader av kalcit och Fe-Mg klorit följdes av semi-duktila till spröda förhållanden, vilket inducerade bildandet av en mörkt rödfärgad hematit-kataklasit, tillsammans med adularia, Mg-klorit och kalcit. Den senaste hydrotermala mineraliseringen visar på gradvis lägre bildningstemperatur som följer; Mg-klorit, adularia, laumontit (Ca-zeolit), hematit, harmotom (Ba-zeolit), pyrit, Fe-klorit (sfärulitisk), kalcit + REE-karbonat och lermineral. Uppträdandet av zeoliter visar på bildningsförhållanden liknande zeolit-facies. Mineralen i denna generation kan ha bildats vid ett och samma förlopp eller vid flera händelser med gradvis lägre temperaturförhållanden. De yttersta sprickmineralen i vattenförande sprickor består främst av lermineral av mixed-layer-clay typ (corrensit = klorit/smectit och illit/smectit) tillsammans med kalcit och mindre korn av pyrit. Lågtemperatur-kalcit har bildats under varierande förhållanden inkluderande både sött och salt grundvatten. Resultat från stabila isotop-analyser av kalciter stöder i stortbeskrivna sekvensen av händelser.

Contents

1 Introduction 7

2 Aim of the Study 9

3 Methods 11

4 Geological Setting 15
4.1 Rock Types 15
4.2 Subsidence and uplift of the present land surface 16

5 Geology of the drill-core 17
5.1 Fracture minerals identified 17
5.2 Results from XRD analyses 17

6 Facies and mineral characteristics 19
6.1 Greenschist facies 19
6.2 Zeolite facies/Prehnite-pumpellyite facies 19
6.3 Mineral characteristics 19

7 Fracture calcites 23

8 Generations 29
8.1 Generation 1 29
8.2 Generation 2 30
8.3 Generation 3 32
8.4 Generation 4 34
8.5 Generation 5 35
8.6 Generation 6 37
8.6.1 Generation 6-1: Calcite 37
8.6.2 Generation 6-2: Quartz, (albite) 38
8.6.3 Generation 6-3: Adularia, Mg-rich chlorite, Apatite, Laumontite etc 38
8.6.4 Generation 6-4: Adularia, Hematite, Harmotome, Pyrite, Fe-rich chlorite, Calcite, Fluorite 40
8.6.5 Generation 6-5: Calcite, Mixed layer clay, Pyrite, (REE-carbonate) 45
8.7 Götemar related fracture fillings 46
8.8 Detailed descriptions of the surface-samples 47
8.9 Wall rock alteration 48
8.10 Generation summary 50

9 Reducing/Oxidising conditions 53

10 Relation to different fracture orientations 55

11 Relation to geological events 57

12 Summary 61

13 Acknowledgement 63

14 References 65

Appendix 69

1 Introduction

The Swedish Nuclear Fuel and Waste Management Company (SKB) is currently doing a site investigation in the Simpevarp/Laxemar area in the Oskarshamns region. The site is situated in an area dominated by granitoids belonging to the Transscandinavian Igneous Belt (TIB). The first 1,000-meter deep drill-core (KSH01A+B) at the Simpevarp peninsula (Figure 1-1), has been sampled for detailed studies of fracture mineralogy and geochemistry. The mineral samples for the uppermost 100 m are taken from the adjacent KSH01B whiles the rest of the samples are from drillcore KSH01A. In this report, the general term KSH01 is used for all the samples.

40 samples, thin-sections and fracture surface samples, have been analysed using polarised light microscope and scanning electron microscope (SEM-EDS). Additional analyses for fracture mineral identification have been made using X-ray diffraction, ICP-MS and stereomicroscope. Calcite samples have been collected for d18O/d13C-, Sr-isotope-, and trace element analyses.

The work was carried out in accordance with activity plan SKB PS 400-03-045. In Table 1-1 controlling documents for performing this activity are listed. Both activity plan and method descriptions are SKB's internal controlling documents.

Figure 1-1. *Map showing the location of the KSH01 borehole on the Simpevarp peninsula.*

Table 1-1. Controlling documents for the performance of the activity.

Activity plan	Number	Version
Sprickmineralogiska undersökningar	AP PS 400-03-045	1.0
Method descriptions	**Number**	**Version**
Sprickmineralogy	SKB MD 144.000	1.0

2 Aim of the Study

The aim of the fracture mineral study is to 1) carry out fracture mineral identification e.g in support to the macroscopic core mapping 2) to find the relative sequence of fracture minerals which will also give support to the description of the geological evolution of the area, 3) give support to the selection of samples to be used for measurements of transport properties and 4) provide palaeohydrogeological information for the hydrogeochemical modelling

This study is partly done as master's thesis project at the Department of Geology, Earth Science Centre, Göteborg University.

3 Methods

Samples with fracture fillings suitable for microscopy were selected from the drill-core KSH01. Fractures that were assumed to have been filled with minerals of different generations were preferred. Approximately 40 samples were chosen from representative fractures at roughly every 50–100 m (see Table 3-1). The collecting of the samples was more based on the information that could be expected from each of the samples than to get a statistic overview from the whole drill-core. 30 thin-sections with a thickness of 30 µm each were then prepared and analysed with optical microscope and scanning electron microscope (SEM) equipped with an energy dispersive spectrometer (EDS). 5 samples from fracture surfaces were examined in detail with stereomicroscope and SEM. Additional fracture surfaces were only briefly examined with stereomicroscope. XRD identification of the fracture coatings were applied on a number of samples, included in which are the sections sampled for groundwater chemistry. Clay mineral compositions have been determined in the samples where possible. ICP-analyses have been used on some fracture coating samples and also on some separated minerals; e.g. for identification of a Barium-zeolite (harmotome) and also to trace the barium content in adularia and K-feldspar and biotite of the wall-rock

The thin-sections have been used to identify characteristic mineral parageneses from different fracture filling generations. The division into different generations has been based on textural and mineralogical observations. Textural observations include relative dating of fracture minerals in fractures of different age, cutting one another and low-temperature minerals penetrating and replacing earlier formed fillings in a pseudomorphic manner. Textural observations also include the suggestion of the rate (ductile/brittle) of the deformation inducing the fractures. Mineralogical observations include crystal morphology and chemical signatures. The comparison of chemical signatures, enabled by SEM-analysis in particular, makes the identification of different characteristic mineral compositions possible.

Indications of oxidising or reducing conditions have been recorded from the presence of hematite and pyrite, respectively. To further establish the dividing of the generations and the relation of the generations to different facies, well-founded facies and mineral characteristics from literature have been gathered in the “Facies and mineral characteristics” chapter.

Other observations that have been made are the characterisation of the wall-rock alteration. The result of the wall rock examination depends on the amount of wall rock present in the thin sections since these primarily were positioned in order to get as much information of the fracture minerals as possible. The task of analysing the fracture surfaces has been to identify the very latest fracture minerals in open fractures. Detailed studies of the fracture surfaces enable identification of the crystal morphology of the minerals. Relative age differences between the lately formed minerals can also be detected.

By comparing and combining the results from the thin-section analyses and the analyses of the fracture surfaces, a scheme of different fracture filling generations could be created. An attempt to relate the different generations to geological events has been made, resulting in suggestions of when the fracture fillings of the different generations could possibly have been formed.

Table 3-1. Table of all the samples in this study. (* = calcites only).

Depth	Thin Section	Surface Sample	XRD	ICP-MS*	Stable Isotopes*	$^{87}Sr/^{86}Sr$*
1.25–1.45					x	
3.7–3.87			x		x	
11.60–11.80	x					
20.77–21.01					x	
24.0–24.1	xx		x			
40.1–40.38					x	
44.65–44.74	x					
46.44–46.74						
67.8–67.9			x		x	
72.6–72.7					x	
81.35			x			
82.2			x			
94.8–94.9			x		x	
121.72–121.81	x					
130.83–131.19	x		x		xx	
159.2			xx		x	
178.25–178.34			x			
198.00–198.9	x			x	xxx	xx
208.60–208.64	x			x	x	x
211.74–211.77		x			x	
213.15–213.24	xx					
242.40–242.48		xx				
249.65			x	x	x	x
250.40–250.50			x		x	
255.78–255.93			x		x	
256.90–257.10	xx			x	x	x
259.4			x		xx	
267.97–268.02			x		xx	
275.70–275.75	x					
287.40–287.47	x				x	x
289.80–289.95	x	x	x		xx	x
290.9			x			
306.70–306.85			x		x	
325.93			x			
363.65–363.67	x			x	xxx	x
376.44–376.56	x					
401.05–401.23	x			x	x	x
409.85–410.00	x					
447.34			x			
514.46			x			
557.30–557.50					x	
558.60–558.65			x			
590.36–590.52			x		x	
596.00–596.10	x					
600.22–600.32	x				x	x
602.45–602.55	x					
603.18				x	x	x
610.60–610.70		x	x	x	x	x
626.00–626.05	x			x	xx	xx
793.70–793.80	x					
873.55–873.60	x				x	x
879.08–879.35	x					

The SEM-EDS analyses were carried out on an Oxford Instruments Link EDS mounted to a Zeiss DSM 940 SEM at the Earth Science Centre in Gothenburg. Polished thin-sections were coated with carbon and fracture surface samples were coated with gold for electron conductivity. The acceleration voltage were 25 kV, the working distance 24 mm (18 mm for fracture surface samples) and the specimen current was about 0.7nA. The instrument was calibrated at least once an hour using a cobalt standard linked to simple oxide and mineral standards to confirm that the drift was acceptable. ZAF calculations were maintained by an on-line LINK ISIS computer system. The quantitative microprobe analyses supply mineral compositions but Fe(II) and Fe(III) are not distinguished and the H_2O content is not calculated. Detection limits for major elements are higher than 0.1 oxide %, except for Na_2O with a detection limit of 0.3%.

For the XRD analyses the fracture material was scraped of the fracture walls. The amounts of the different samples were highly variable. The clay-rich samples were dispersed in distilled water, filtered and oriented according to /Drever, 1973/. In samples of small volumes the suspension was repeatedly put on glass and dried. Three measurements were carried out on each of the fine fraction samples for clay mineral identification; 1) dried samples 2) saturated with ethyleneglycol for two hours and finally 3) after heating to 400°C in two hours. Coarser material was wet sieved and dried. The > 35 μm fraction was ground by hand in an agate mortar. The sample powder was randomly orientated in the sample holder (or on the glass if very small sample volumes).

The radiation (CuK_α) in the diffractometer was generated at 40 kV and 40 mA, and the X-rays were focussed with a graphite monochromator. Scans were run from 2°–65° (2-theta) or from 2°–35° (samples with preferred crystal orientation) with step size 0.02° (2-theta) and counting time 1 s $step^{-1}$. The analyses were performed with a fixed 1° divergence and a 2 mm receiving slit. The XRD raw files were taken up in the Bruker/ Siemens DIFFRAC^{PLUS} software (version 2.2), and evaluated in the programme EVA. The minerals were identified by means of the PDF (1994) computer database.

ICP analyses were carried out on powdered material. 0.125 g of sample material was melted together with 0.375 g $LiBO_2$ and dissolved in HNO_3. The sample volumes were to small to do LOI (Loss on ignition measurements). The main element and some of the trace elements (Ba, Be, Co, Cr, Cu, Ni, Sc, Sr, V, Y, Zn and Zr) were analysed using ICP-AES according to the EPA-method descriptions 200.7. Additional trace elements including REE and U, Th were analysed by ICP-QMS according to EPA-method 200.8. The inhomogeneity of the samples makes the results more dependent on the actual sample than on the accuracy of the analyses.

The stable carbon and oxygen isotope analyses carried out on calcite samples were made accordingly: Samples, usally between 200 and 300 μg each, were roasted in vacuo for 30 minutes at 400°C to remove possible organic material and moisture. Thereafter, the samples were analysed using a VG Prism Series II mass spectrometer with a VG Isocarb preparation system on line. In the preparation system each sample was reacted with 100% phosphoric acid at 90°C for 10 minutes, whereupon the released CO2 gas was analysed in the mass spectrometer. All isotope results are reported as ð per mil relative to the Vienna Pee Dee Belemnite (VPDB) standard. The analysing system is calibrated to the PDB scale via NBS-19.

For the Sr isotope analyses about 30 to 40 mg of the carbonate samples were transferred to 2 ml centrifuge tubes, added 200 µl 0.2 M HCl, and shaken. The samples were let to react for 10 minutes while shaken in order to release the CO_2 gas. Then 20 µl 2 M HCl is added once or twice until most of the calcite has been decomposed. The samples were centrifuged for about 4 minutes and the liquids transferred to new clean centrifuge tubes

by use of a pipette. The centrifuge tubes are put on a hotplate and evaporated to dryness. To avoid disturbances in measuring the isotopic composition, strontium had to be separated from other elements present in the sample. After evaporation to dryness the samples were dissolved in 200 µl ultrapure 3M HNO_3, centrifuged and loaded onto ion-exchange columns packed with a Sr-Spec crown-ether resin from EIChrom, which retained Sr and allowed most other elements to pass. After rinsing out the remaining unwanted elements from the columns, strontium was collected with ultrapure water (Millipore). The collected Sr- fractions were then evaporated to dryness and loaded on pre-gassed Re filaments on a turret holding 12 samples and 1 NIST/NBS 987 Sr standard. The isotopic composition of Sr was determined by thermal ionization mass spectrometry (TIMS) on a Finnigan MAT 261 with a precision of about 20 ppm and a Sr blank of 50–100 pg. The $^{87}Sr/^{86}Sr$ ratio of the carbonate analysis are monitored by analysing one NIST/NBS SRM 987 Sr standard, for each turret of 12 samples, and the standard has a recommended $^{87}Sr/^{86}Sr$ value of 0.710248. The presented results are not corrected to the NBS 987 recommended value but given together with the specific measured NBS 987 value for the relevant turret.

The ICP-MS analyses on calcites leachates were carried out following the here given procedure: 12 mg calcite sample (weight registered ± 0.01 mg) was placed in a 50 ml tube, where 47 ml 5% HNO_3 was added containing 15 ppb of indium and rhenium respectively, to be used as internal standars. The sample was leached for 1 hour with stirring every 15 minutes. Thereafter, 20 ml of the solution was used for analyses carried out on a Hewlett-Packard ICP-MS, model HP 4500. Certified multielement standards from Merck (nr VI) and Agilent (nr 1) have been used.

To be able to relate the fractures in this study to different structures, information from the Borehole Imaging Processing System (BIPS) has been used. BIPS is a tool for visualization of the borehole walls. Information of the strike and dip of the fractures/structures can be estimated from the comparison of the drill-core samples to the BIPS-images of the borehole walls, using a specialized computer program.

4 Geological Setting

The bedrock in the Simpevarp area north of Oskarshamn is predominated by Småland granitoids belonging to the Transscandinavian Igneous Belt (TIB) /Gaál and Gorbatchev, 1987/ (Figure 3-1). This belt occupies an area between the older Svecofennian (c 1.9 Ga) crust in the east and the younger, westward younging, Gothian growth zones in the west /Larson and Berglund, 1992; Åhäll and Larsson, 2000/. The TIB granitoids were emplaced and extruded during several pulses of magmatism between 1.85 and 1.66 Ga with the younger of these rocks in the west /Larson and Berglund, 1992; Åhäll and Larsson, 2000/. The age of the volcanics related to the TIB granitoids, often called Småland porphyry, is c 1,800–1,835 Ma /Lindström et al. 1991, p. 37/. TIB is divided into three major magmatic events; TIB 1 (1.81–1.77 Ga), TIB 2 (1.72–1.69 Ga) and TIB 3 (1.69–1.66 Ga) /Larson and Berglund, 1992; Åhäll and Larsson, 2000/. The Småland granitoids in the Simpevarp area belong to TIB 1 rocks. Another magmatic episode in the region was the intrusion of the anorogenic granites, at e.g. Götemar /Kresten and Chyssler, 1976/. These coarse-grained granites were emplaced around 1.35–1.45 Ga /Åberg et al. 1984; Smellie and Stuckless, 1984; Åhäll, 2001/.

4.1 Rock Types

The dominating rocks in the area are TIB granitoids ranging in mineralogical compositions from true granites (some of the Ävrö granites) to granodioritic to dioritic composition (Quartz monzodiorite) /Kornfält and Wikman, 1988/. Other rocks in the area are fine-grained Småland granites, anorogenic granites (e.g. Götemar), metavolcanics, greenstones and dikes of pegmatites, aplites and dolerites /Kornfält and Wikman, 1987/.

The granitoids were probably formed by a continuous magma-mixing process as indicated by the presence of basic enclaves /Wikström, 1989/. All the rock units, except the anorogenic granites, show a general foliation in approximately ENE-WSW.

According to /Wahlgren et al. 2004/, the metavolcanic rock described above can not be classified as a volcanic rock since it does not show any characteristic volcanic texture. Therefore, the more neutral name fine-grained dioritoid is suggested for this rock, which probably is derived from the same magma as the earlier described granitoids

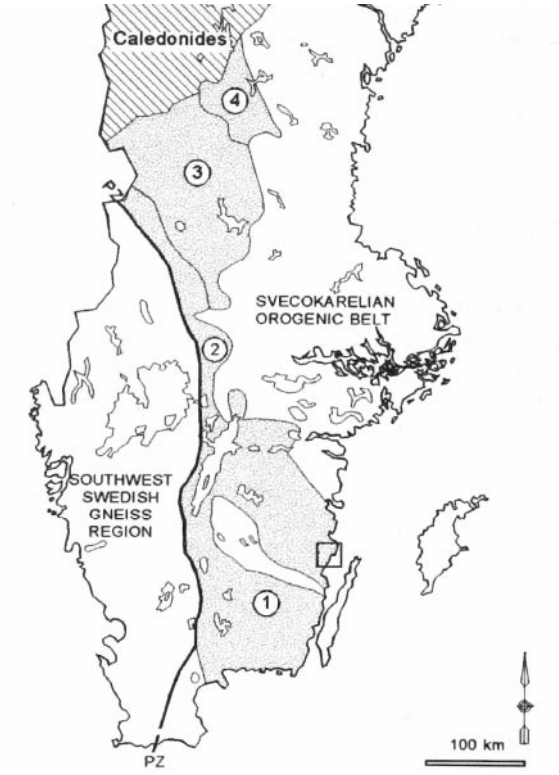

Figure 4-1. *Simplified map of the major Precambrian units in southern Sweden. "1–4" = Transscandinavian Igneous Belt. Square = Simpevarp area. From /Kornfält et al. 1997/.*

4.2 Subsidence and uplift of the present land surface

Datings of the the granitoids, produced c 1.8 Ga ages /Wikman and Kornfält, 1995; Wahlgren et al. 2004/. The combination of the zircon and the titanite ages indicate that the rocks have not been heated above 550–600°C since the crystallisation of the granitoids. Fission track analyses of apatite and titanite, together with other geochronological information reveal evidence for repeated uplift and subsidence of the present land surface /Tullborg et al. 1996/. Three major periods of subsidence related to sedimentation have been identified in the region. These periods are further discussed in the "Relating the generations to geological events" chapter since they are thought to have been important events for fracture inducing and subsequent fracture filling.

The present land surface corresponds closely to earlier denudation surfaces, which means that the erosion of the crystalline basement has been very slow /Lidmar-Bergström, 1991/. In places where the Sub-Cambrian peneplane is preserved, like in the Oskarshamn region, the sedimentary cover (produced in several events from Cambrian to Cretaceous) was not completely removed until the Tertiary /Lidmar-Bergström, 1991/. Changing hydrogeological conditions during the Late Tertiary and the Quaternary glacial and interglacial stages most likely caused dramatic changes in groundwater flow, which may be recognised in the fracture infilling /Stanfors et al. 1999/.

5 Geology of the drill-core

The KSH01 bore-hole was drilled in a rock-block bordered by major fracture zones/ lineaments. Rock types and fractures are shown in the WellCad plot in Appendix A8 /Ehrenborg and Stejskal, 2004/. Minor to moderate water-conducting fractures, are present in the bore-hole. These fracture zones appear at c 114–118, 155–160, 243–271, 286–291, 553–561, 585–590 m. The thin-section from 257 m is the only examined sample from a water-conducting fracture zone in this study. Practically all of the rock types described above (except for the Götemar Granite) is included in the KSH01 drill-core. The dominating rock types in the drill-core are: Quartz monzodiorite, equigranular to weakly porphyritic: c 0–205 m, 250–325 m, 340–350 m, 690–720 m, 730–765 m, 980–1,000 m) and "Fine-grained dioritoid" (c 205–250 m, 325–340 m, 350–630 m). The rock type of each of the examined samples in this study can be seen in the thin-section description and fracture surface-sample description in the Appendix A1 and A2 respectively. No dramatic dissimilarities have been noted between the fracture fillings in the different rock types.

5.1 Fracture minerals identified

Fracture minerals are determined macroscopically and mapped within the bore map system but many of the minerals are difficult to identify and small crystals are easily overlooked. Therefore fracture mineral analyses have been carried out for identification, mainly comprising:

- X-ray diffractometry; especially used for identification of clay minerals and gouge material composition (cf section 5.1).
- Identification of minerals carried on by transmissive light microscopy and SEM/EDS of fracture fillings (described in Chapter 6).

The most common fracture minerals at the site are chlorite and calcites which occur in several different varieties and are present in most of the open fractures. Other common minerals are epidote, prehnite, laumontite, quartz, adularia (low-temperature K-feldspar), fluorite, hematite and pyrite. A Ba-zeolite named harmotome have been identified in some fractures and apophyllite has been identified in a few diffractograms. Details about these minerals are given in Chapter 6.

Clay minerals identified are in addition to chlorite; corrensite (mixed layer chlorite/smectite or chlorite/vermiculite clay, the smectite or vermiculite layer are swelling), illite, mixed-layer illite/smectite (swelling) and a few notations of smectites.

5.2 Results from XRD analyses

Samples for XRD identification have mainly been taken from open and usually water conducting fractures with loose and clayish coatings, often of fault gouge type. All the fractures sampled belong to the uppermost 600 m of the borehole (KSH01A+B) as the deeper part has very low hydraulic conductivity and low frequency of originally open fractures. The fine fraction from each sample has been separated and oriented samples on glass were prepared for the clay mineral identification.

Most of the samples contain quartz, K-feldspar, and albite in addition to calcite, chlorite and clay minerals (Appendix A5). From earlier identifications of open fractures at Äspö (e.g. within the TRUE experiment sites) it is known that altered rock fragments dominate the gouge material /Andersson et al. 2002/. It is therefore probable that most of the quartz and feldspars together with the few observations of amphibole and biotite belong to these rock fragments even though contamination due to incorporation of material from the wall rock can not be ruled out. The total clay mineral contents in the open fractures is very difficult to determine in an appropriate way and the XRD analyses should not be regarded as necessarily representative for the entire filling but more of the specific sample. In fractures filled with fault gouge a reasonable estimate is, however, that the amount of clay mineral (chlorite not included) usually does not exceed 10–20 weight %. Thin coatings attached to the fracture wall can consist of 90–100% chlorite and clay minerals. The amounts are relatively small as these coatings are usually thin (< 100 μm) but their surface can be very large (cf SEM photo of mixed-layer clay coating Figure A-36, Appendix A2)

Minerals constituting less than 5–10% may not be detected in the diffractograms and e.g. hematite and pyrite, which have been detected in some of the XRD samples, are likely to be present in several of the others as well.

Smectite which is a significantly swelling clay mineral, has been identified in three of the samples (3.7 m, 24 m and 289.8 m)

6 Facies and mineral characteristics

This section presents some general characteristics (e.g. formation temperature, paragenesis, occurrence, alteration etc) of most of the minerals that have been identified in this study. Included is also a general introduction to the different temperature-pressure conditions (facies), which are thought to have been prevailing during different fracture filling events. All of the information listed below has been collected from mineralogical and petrological literature /Blatt and Tracy, 2000; Nesse, 2000; Deer et al. 1992 and references therein/. The purpose of this section is to provide additional information of the mineralogy and to give well-founded support to the dividing of the different fracture filling generations.

6.1 Greenschist facies

Rocks of the greenschist facies represent the beginning of regional metamorphism. Here, the rocks begin to show foliation as the effect of applied stress and deformation synchronous with mineral reactions. The rocks are also completely re-crystallised, in contrast to lower grade facies that commonly contain relict textures and mineralogy. Mineral assemblages include epidote-chlorite-actinolite, and calcite, muscovite etc. The lower limit of greenschist facies is placed at about 400°C.

6.2 Zeolite facies/Prehnite-pumpellyite facies

Zeolite facies metamorphism begins at burial depths of 1 to 5 km, depending on geothermal gradient and reactivity; these depths correspond with temperatures of 50° to 150°C. Transition to the prehnite-pumpellyite facies occurs at 3 to 13 km and at temperatures up to about 250°C. Incipient zeolite-facies metamorphism is indicated by the appearance of the calcium-aluminium zeolite laumontite and perhaps by albite or adularia. Relict grains, incomplete pseudomorphic replacements, and preserved igneous textures are typically present because very low grade reactions tend to approach equilibrium very slowly. Transition from the zeolite to prehnite-pumpellyite facies is marked by the elimination of laumontite in more aluminous compositions and the common occurrence of prehnite, pumpellyite, calcite, and quartz. Epidote with or without actinolite can appear. The upper temperature limit of prehnite-pumpellyite facies cannot be precisely set because it varies as a function of rock and mineral chemistry.

6.3 Mineral characteristics

Epidote: $Ca_2Al_2(Al,Fe^{3+})OOH[Si_2O_7][SiO_4]$

Epidote occurs in a wide range of metamorphic parageneses but is particularly characteristic in rocks of the greenschist and epidote-amphibolite facies. Iron-rich epidote occurs also in lower-grade rocks in association with chlorite. In greenschist-facies rocks, epidote is characteristically associated with chlorite, actinolite, albite, quartz and less commonly with mica, biotite and garnet. Epidote also occurs as a product of the hydorothermal alteration (saussuritization) of plagioclase, along joints and fissures and in amygdales and vugs. Epidote is relatively resistant to weathering environments.

Chlorite: $(Mg,Fe^{2+},Fe^{3+},Al)_{12}[(Si,Al)_8O_{20}](OH)_{16}$

The principal substitutions are of Mg, Fe^{2+}, Fe^{3+}, and Al in octahedral sites, and Si and Al in tetrahedral sites. Continuous solid solution extends from Mg-rich chlorite (clinochlore) to Fe-rich chlorite (chamosite).

Chlorite is a very common and often abundant mineral, particularly in low- to moderate-grade metamorphic rocks formed at temperatures up to about 400°C and pressures of a few kilo bars. Chlorite is a common constituent of igneous rocks in which it have usually been derived by the hydrothermal alteration of primary ferromagnesian minerals, such as biotite and hornblende. The composition of the chlorite is often related to that of the original igneous mineral. Partial and complete chloritization of biotite is particularly common in granites and in most cases the transformation is markedly pseudomorphic. Chlorite is a common constituent in rocks of the zeolite facies. In the lower part of the zeolite facies chlorite is associated with e.g. laumontite, stilbite and heulandite, and may contain appreciable amounts of Ca, K and Na due to the presence of interlayered di-octaedral clays, such as illite and smectite. In the upper part of the zeolite facies, chlorite occurs in assemblages with prehnite and pumpellyite. Chlorite-actinolite-epidote-albite assemblages are common in greenschists.

Prehnite: $Ca_2(Al,Fe^{3+})[AlSi_3O_{10}](OH)_2$

Most of the structure water in prehnite is lost only on heating to between 600 and 750°. The low-temperature alteration of prehnite may produce zeolites or chlorite. Prehnite is found in amygdules, veins, or other cavities in mafic to intermediate igneous rocks, often in association with zeolites and calcite. The most abundant occurrence is in low-grade regional metamorphic rocks derived from greywacke, basalt or other mafic to intermediate rocks. Associated minerals include pumpellyite, albite, epidote, chlorite and zeolites. The upper limit of prehnite stability occurs at about 400°C at 2–4 kbar.

Calcite: $CaCO_3$

Calcite is a common mineral of hydrothermal and secondary mineralization. Calcite frequently crystallizes in the later stages of hydrothermal deposition, occurring in veins and cavities. In amygdales it is often associated with quartz and zeolites. In many hydrothermal veins calcite is associated with fluorite, barite, dolomite, quartz or sulphides.

Hematite: Fe_2O_3

Hematite may be altered to iron hydroxide minerals. It is stable in the weathering environment and is commonly produced by weathering or hydrothermal alteration of iron-bearing minerals in almost all rock types. It is not common as a primary mineral. Associated minerals include magnetite, quartz, carbonates, and various Fe-silicates.

Muscovite (Sericite): $KAl_2(AlSi_3O_{10})(OH,F,Cl)_2$

Sericite is widespread in many igneous rocks, produced by the hydrothermal weathering of feldspars and other minerals. It may be converted to clay minerals by weathering.

Titanite: CaTiOSiO4

The usual alteration of titanite is an aggregate of titanium oxides, quartz and other minerals. Titanite may be produced by alteration of biotite or clinopyroxene.

Rutile/Anatase: TiO_2

Anatase is a low-temperature polymorph of rutile (TiO_2) and is found as a minor constituent of igneous and metamorphic rocks and in veins and druses in granite pegmatites. It also occurs as an alteration product of other Ti-bearing minerals such as titanite and ilmenite.

Albite: (Plagioclase) $NaAlSi_3O_8$

Plagioclase is commonly partly or completely altered to sericite, saussurite, calcite, clay or zeolites. Albite is often the common plagioclase in rocks subjected to relatively low-grade metamorphism. In felsic (granites, granodiorites etc) rocks the plagioclase often is albite or oligoclase. Albite and orthoclase-rich feldspar sub-grains can form from interaction of magmatic fluids at temperatures of < 450°C during cooling /Parsons, 1978/.

Pyrite: FeS_2

Pyrite is the most abundant of the sulphide minerals and occurs in large masses or veins of hydrothermal origin both as primary and secondary mineral.

Adularia: $KAlSi_3O_8$

Adularia is a low-temperature K-feldspar, defined based on its habitus and occurrence. In most cases adularia is crystallized at low temperatures (< roughly 450°C) in hydrothermal systems in veins or as a replacement after other minerals, or is produced during diagenesis of sediments. Studies made by /Hagen et al. 2001/ suggest authigenic adularia formation at temperatures as low as 100°C. The alteration products are sericite and clay. Paragenesis may include chlorite, quartz, albite, apatite and corrensite. The barium ion is present in small quantities in the great majority of feldspars. In adularia the barium content is noticeably high and may approach 1 per cent BaO.

Apophyllite: $(K,Na)Ca_4Si_8O_{20}F*8H_2O)$

Apophyllite is a hydrothermal sheet silicate with white to silvery surface often associated with hydrothermal minerals like prehnite.

Apatite: $Ca_5(PO_4)_3(OH,F,Cl)$

Apatite is a common accessory mineral in many types of rock. Apatite also occurs in hydrothermal veins and cavities and is found together with quartz, adularia, chlorite etc.

Zeolites:

Zeolites are chemically related to feldspars but have much more open structures and contain water molecules. In low-grade metamorphic rocks they occur as a result of hydrothermal activity and by burial metamorphism. Zeolite minerals may alter to clay or to other zeolite minerals.

Laumontite: $Ca_4[Al_8Si_{16}O_{48}] * 18H_2O$

Laumontite is a widespread zeolite that occurs in many environments, e.g. in vugs of plutonic rocks. Laumontite coexists with e.g. other zeolites, calcite, quartz, fluorite, plagioclase and chlorite.

Harmotome: $Ba_2(Na,Ca_{0.5})[Al_5Si_{11}O_{32}] * 12H_2O$

Harmotome occurs primarly as an amygdaloidal zeolite in metalliferous veins and vugs of plutonic (pegmatite and gabbro) and volcanic (basalt and andesite) rocks. Identified associations include e.g. other zeolites, prehnite, pyrite, quartz and calcite.

Clay minerals:

Illite: $(K, H_2O)Al_2[(Al,Si)Si_3O_{10}] (OH)_2$

Illite occur as micro – to cryptocrystalline, micaceous flakes

Smectite e.g. $(Mg_3(Si_4O_{10})(OH)_2xnH_2O)$,

Smectite can vary in composition and occurs as dominantly as Mg and Fe rich varities. Smectite is a swelling clay.

Mixed-Layer clays:

Mixed layer clay is usually applied on clays having alternating layers of e.g.illite and smectite. The ratio between the illite and smectite layers varies due to degree of recrystallisation; the larger the illite component the higher the formation temperature.

Mixed illite/smectite clay is swelling.

Corrensite: $((Mg,Fe)_9(Si,Al)_8O_{20}(OH)_{10}xH_2O)$

Corrensite is a chlorite-like mixed layer clay (swelling) with layers of chlorite and smecitite/vermiculite, usually with ratio of 1:1.

7 Fracture calcites

In order to sort out different generations and to provide palaeohydrogeological information 39 samples have been analysed for $\delta^{13}C$/ $\delta^{18}O$, of which 15 have been selected for $^{87}Sr/^{86}Sr$ and a smaller set (9 samples) analysed for chemical composition. Table A6 in appendix, shows all the calcites analysed for stable isotopes and trace element chemistry. The calcites represent both sealed and open fractures. In some open fractures it has been possible to sample calcites grown in open space showing euhedral crystal forms. Notations have been made of crystal morphology when possible since correspondence between calcite morphology (long and short C-axis) and groundwater salinity has been found in studies e.g. in Sellafield /Milodowski et al. 1998b/. The indication from the study is that fresh water carbonates usually show short C-axis (nailhead shaped crystals) whereas calcite precipitated from saline waters preferably show long C-axis (scaleohedral shapes). Equant crystals are common in transition zones of brackish water. Concerning the KSH01 samples (from depth between 129–361 m) all but one show equant to scalenohedral forms. This is in good agreement with the findings of saline water as high as 150 m depth /Laaksoharju et al. 2004/.

The $\delta^{13}C$/ $\delta^{18}O$ values for the KSH01 calcites are plotted together with previously analysed calcites from Äspö and Laxemar. (Figure 7-1). The KSH01 calcites show $\delta^{18}O$ values ranging from –6 to –22 o/oo and $\delta^{13}C$ values from –26 to –2 o/oo. The calcites showing the lowest δ18O values have the highest $\delta^{d\,13}C$, typical for hydrothermal calcites without signs of biogenic carbon. The calcites with higher $\delta^{18}O$ values (indicating possible precipitates from meteoric or brackish Baltic Sea water based on fractionation fratures by /O´Neil et al. 1969/ and ambient temperatures in the range of 7–15°C) also show larger spead in their $\delta^{13}C$ carbon isotope values supporting interaction with biogenic carbon. Extreme $\delta^{13}C$ values (as low as –84 o/oo) has been recorded in Äspö drillcores and indicate biogenic activity in the groundwater aquifers causing disequilibria in situ The lowest values in KSH01 (–20 to –26 o/oo) are indications of the same process. It should be noted that the fractionation between HCO_3^- and $CaCO_3$ is only a few per mille and the $\delta^{13}C$ value in the calcite reflects therefore largely the $\delta^{13}C$ value in the bicarbonate at the time of calcite formation.

Most of the calcites with euhdral crystals show $\delta^{18}O$ values between –6 and –10 o/oo, except for a group of three samples with scalenoedral shapes showing values around –12 to –13 o/oo. This population is earlier identified /Bath et al. 2000; Tullborg, 2004/ and are interpreated as “warm brine” precipitates.

The highest $\delta^{18}O$-values, close to zero, that have been found in the calcites from the Äspö drill cores interpreted as possible precipitates from marine waters of Ocean type, are not found in the analysed samples from the KSH01 drill core. This may be due to the relatively small set of samples analysed from the Simpevarp area.

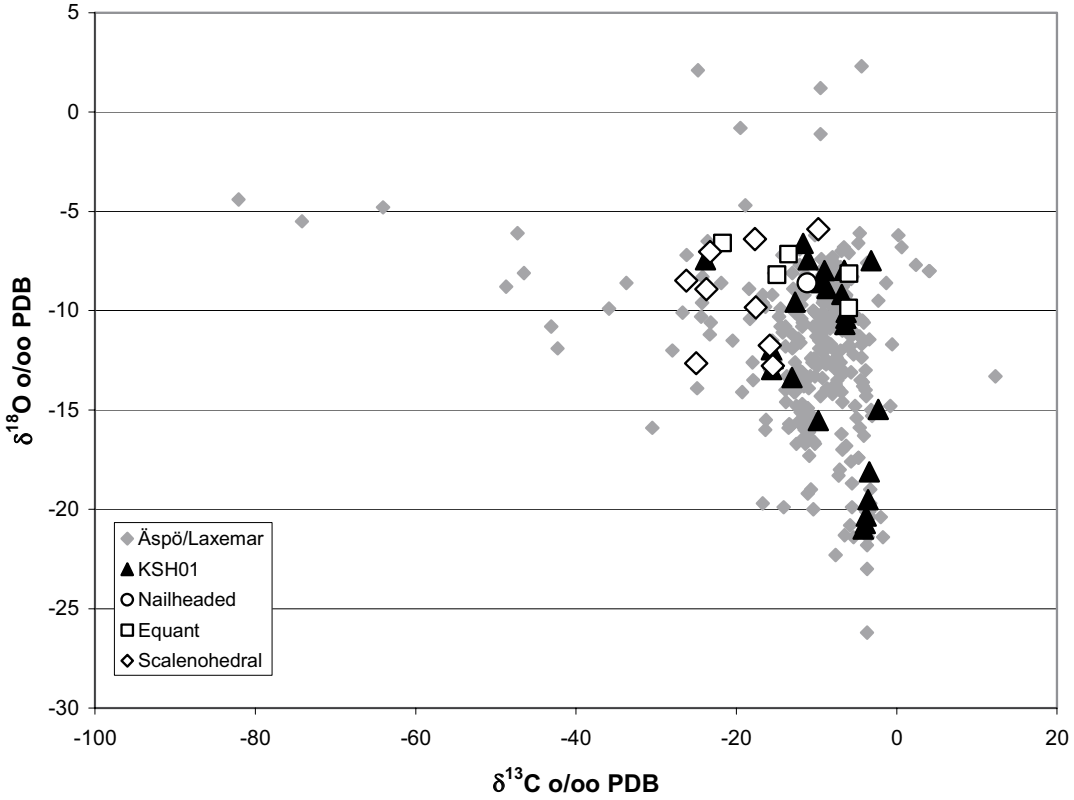

Figure 7-1. *$\delta^{13}C$/ $\delta^{18}O$ values for fracture calcites in KSH01A+B plotted together with earlier analysed samples from Äspö/Laxemar /Bath et al. 2000; Wallin and Peterman, 1999; Tullborg, 1997/. Note that crystal shapes have been distinguished when possible.*

Figures 7-2 and 7-3 show $\delta^{18}O$ and $\delta^{13}C$ plotted versus depth for KSH01A+B. These plots indicate that fractures in the upper 400 m have been more open to low temperature circulation (possible interaction with Meteoric/Baltic sea water) and that calcites with carbon of biogenic origin, are common down to 300 m. The distribution of the calcite isotope values versus depth are in agreement with the flow logging results, showing low hydraulic conductivity below 300 m and very tight rock in the lower 600 m of the borehole. The sections sampled for groundwater chemistry are 156–167 m, 245–261 m and 548–565 m corelegth (which is similar to vertical depth as the borehole is subvertical). The salinities of the present day groundwaters from these depth range from approximately 4,000 ppm to 8,000 ppm (increasing with depth) and the $\delta^{18}O$ values in the same waters are in the range of –12 to –14 o/oo.

The Sr isotope values in the fracture calcites range between 0.707551 and 0.715985 and when plotted versus $\delta^{18}O$ there is a positive correlation. The calcites showing the lowest Sr isotope and lowest $\delta^{18}O$ values are usually higher in Sr content and often precipitated with hydrothermal minerals. This is in accordance with earlier observations made by /Wallin and Peterman, 1999/ and can be explained by hydrothermal activity take place relatively early in the geological history of the bedrock. The calcites with Sr isotope values close to present groundwater (0.715 to 0.716) show $\delta^{18}O$ values around –6,4 and –8,5 o/oo i.e they are of possible recent origin, which in this case probably means Quaternary.

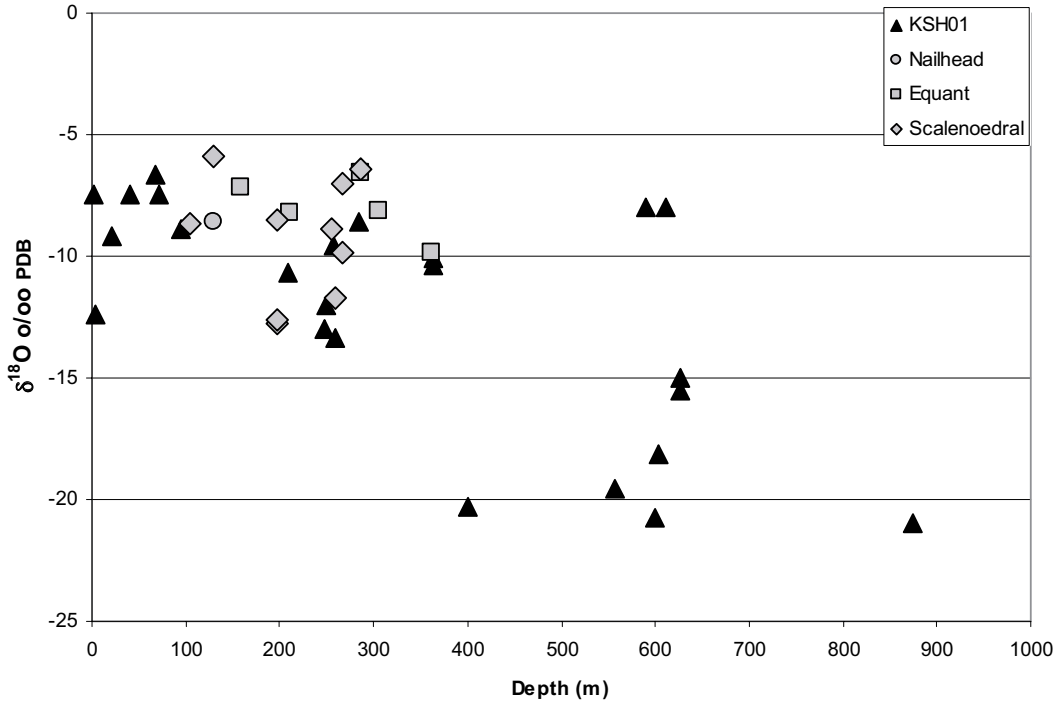

Figure 7-2. *$\delta^{18}O$ values for fracture calcites in KSH01 plotted versus depth. Crystal shapes distiunguised when possible.*

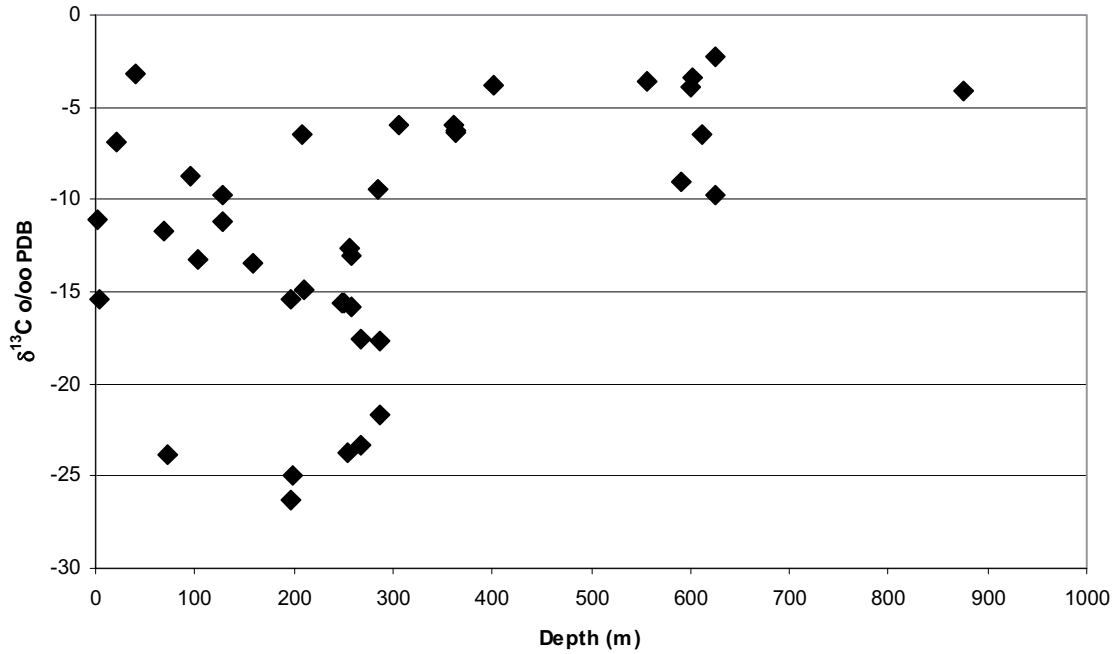

Figure 7-3. *$\delta^{13}C$ values for fracture calcites in KSH01versus depth.*

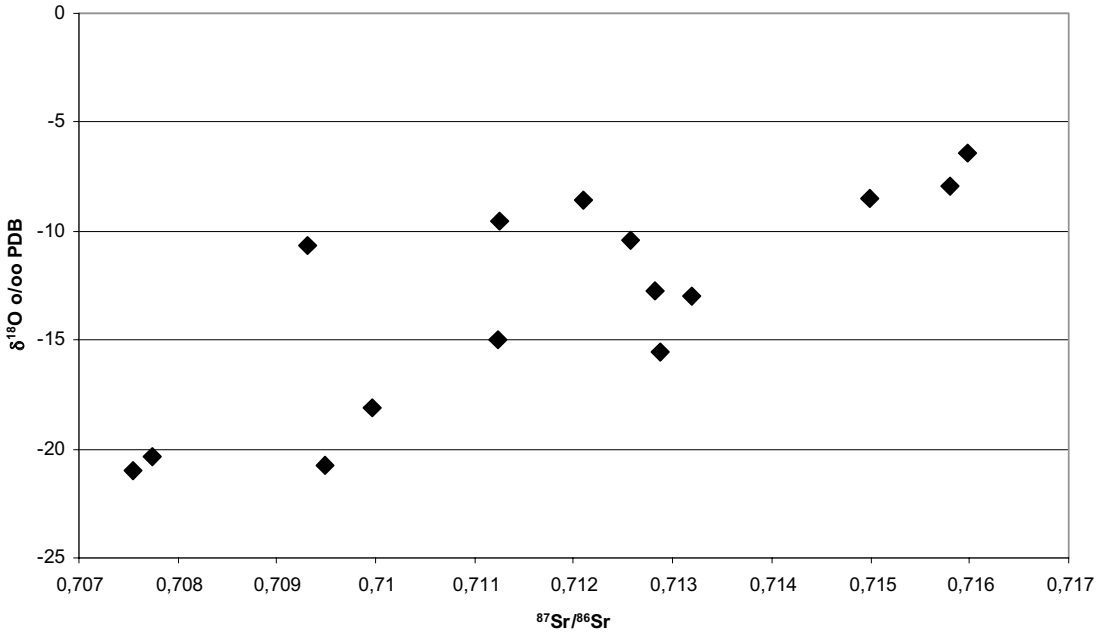

Figure 7-4. *Sr isotope ratio plotted versus $\delta^{18}O$ values for fracture calcites in KSH01.*

Trace element analyses are shown in Table A7. These analyses are made on leachates from calcite samples and it is obvious that some contaminant minerals have dissolved as well, or that ion exchanged elements are released from clayminerals included in the calcite samples. Sample 611 m show very high contant of Ba (4,852 ppm) which may be explained by dissolution of Ba-zeolite present in the sample.

Generally the trace elment contents of Sr, Mn and REE corresponds to earlier observations from Äspö/Laxemar /Bath et al.2000; Tullborg 2003/; Samples with hydrothermal calcites (low $\delta^{18}O$ and high $\delta^{13}C$) show generally Sr values higher than 100 ppm, low REE content and usually not fractionated REEs patterns, or like in the case of 401.25, enrichment of heavy REEs. Samples with highest La and Mn contents are found in the uppermost 400 m and are usually associated with calcites with lower d13C indicating reducing conditions due to microbial activity.

Small negative Ce anomalies are indicated in two samples 257.80 m and 208 m. The latter REE contents are so low that the significance can be questioned but in the 257 m sample it may indicate that groundwater have passed through a redox zone where Ce has been oxidised and immobilised and the resulting negative Ce-anomaly in the water can thereafter have been transposed to the fracture calcite. It can be noted that the Mn content in this sample is low.

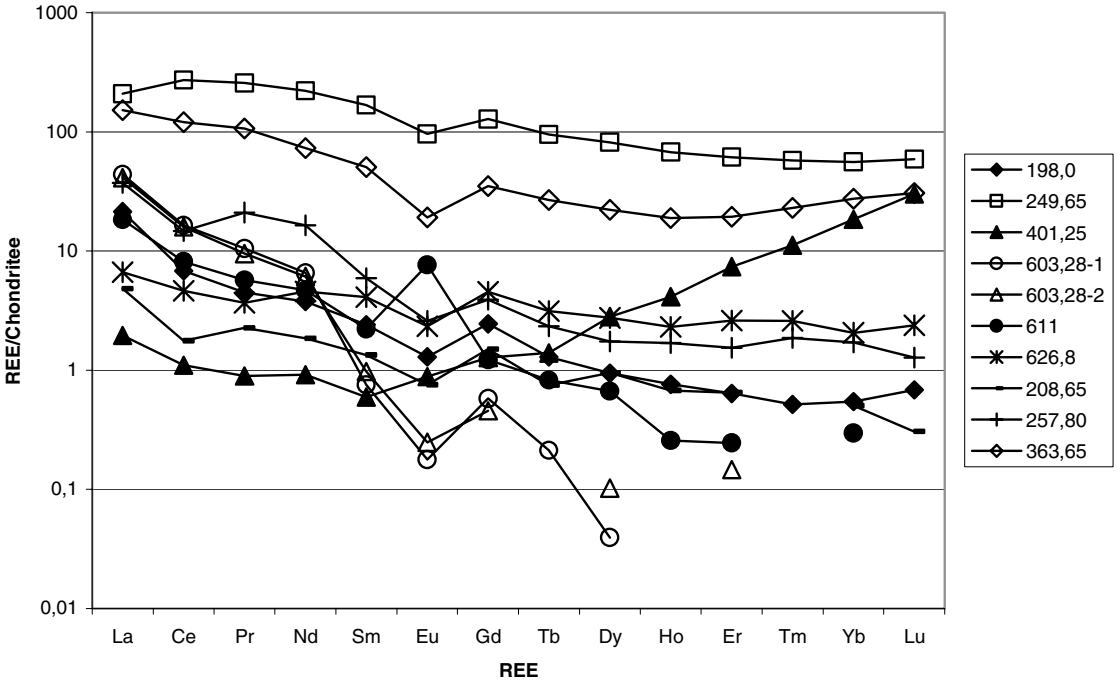

Figure 7-5. *Chondrite normalised REEs patterns for fracture calcites from KSH01. Note that these analyses are made on leacheates of calcite samples which contains small amounts of contaminant minerals.*

8 Generations

A sequence of different fracture mineralisations has been obtained by evaluation of textural and mineralogical observations. The procedure of dividing the different parageneses into generations is largely based on subjective conclusions. Most of the information has been gained from thin-section analysis, using transmissive light microscope and scanning electron microscope (SEM). Although the results from different thin-sections may vary, a pattern of different characteristic parageneses has been recognized. The generations listed below consist of mineral parageneses that are thought to be representative for the whole drill-core, based on the number of observations and the abundance of the different minerals in each sample. This means that several mineral observations have been left out of this scheme (see Appendix for a more detailed description of each sample). The observations from the thin-sections have also been correlated to the observations of the fracture surface-samples and to some extent to the data maintained from the X-ray diffraction (XRD) analyses. Analyses can be found in the appendix. All the analyses referred to in the text are SEM-EDS analyses, unless where indicated.

8.1 Generation 1

The earliest formed fracture filling identified in the KSH01 drill core consists of coarse-grained, idiomorphic, quartz crystals. These crystals had both the time and space to grow big. Crystals are still present, both as big idiomorphic crystals showing undulose extinction surrounded by re-crystallized quartz crystals and as remnants in later formed mylonites. This early fracture filling may be part of post-magmatic circulation after the formation of the Småland granitoids in the area. The quartz filling alone is not good pressure-temperature indicator and the lack of paragenetic minerals makes the relation to geological events difficult.

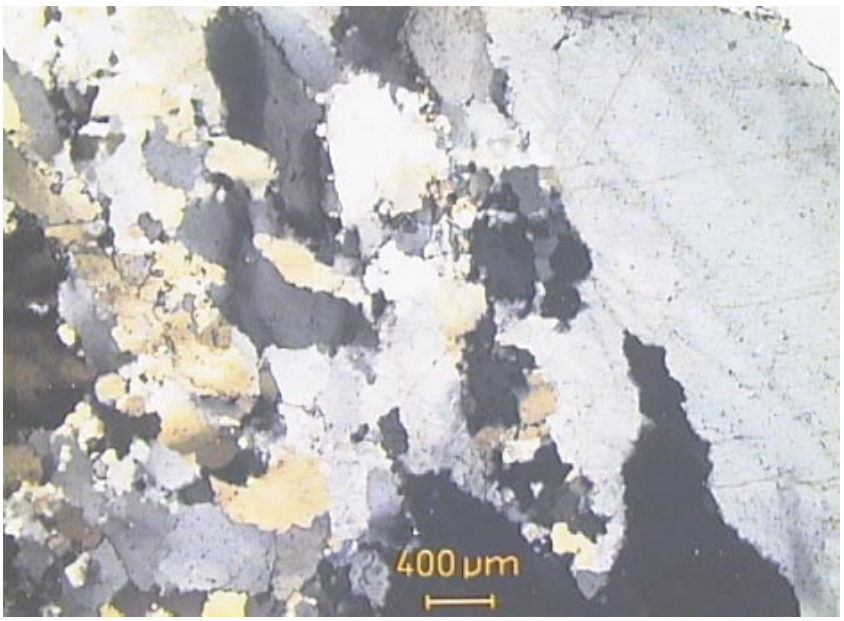

Figure 8-1. *Quartz crystals from the first fracture filling generation. The crystals are showing undulose extinction and sub-grain formation is present. Photomicrograph from thin-section KSH01: 130 m.*

8.2 Generation 2

At a following deformation stage the quartz crystals were deformed and partly re-crystallized, contemporary with the formation of idiomorphic pyrite (with small chalcopyrite crystals) and calcite crystals (KSH01: 24-2 m; KSH01: 873 m). These minerals typically form equigranular fillings with a thickness of about 5 mm, situated on the rim of the fractures. The deformation is indicated by quartz crystals showing undulose extinction and sub-grain formation and calcite crystals showing deformation-twin-lamellae. The calcite crystals have a detectable manganese content of in average 0.7–1.0% MnO_2. The stable isotope ratios give a hydrothermal signature and the sample (401 m) analysed for trace element composition indicate low REEs content showing an enrichment of HREE, and somewhat higher Sr value than the low temperature carbonates. Furthermore the Sr isotope ratios of calcites from this generation show the lowest values (around 0.707) indicating a formation early in the geological history of the area.

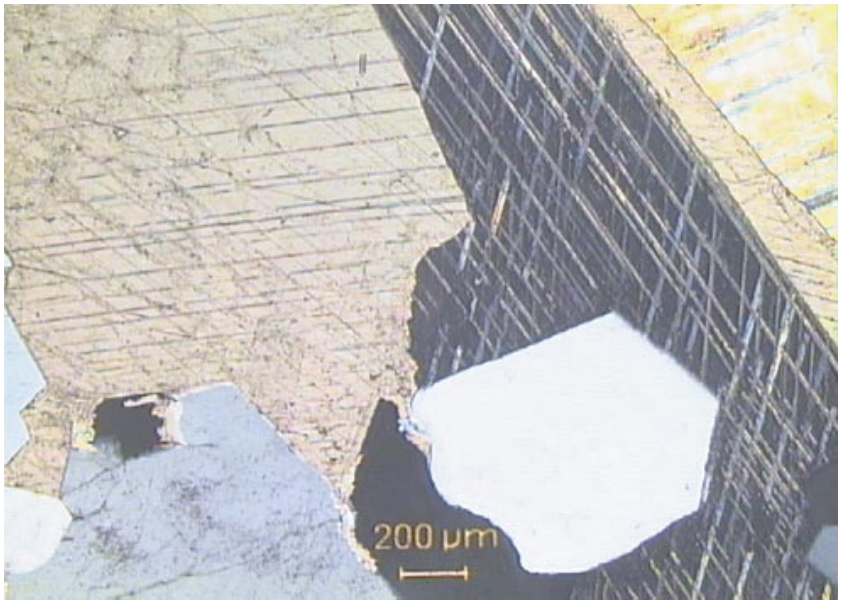

Figure 8-2. *Idiomorphic quartz crystals and calcite crystals. Photomicrograph from thin-section KSH01 873 m.*

Post-dating the quartz and pyrite formation but fairly contemporary, mylonites were formed in zones exposed to high deformation rates. The mylonites are here classified as two different mylonites, quartz mylonite and epidote mylonite, based on the mineral content. The time relation between these two can not be distinguished. However, indications of that the epidote mylonite is younger than the quartz mylonite and that they both are a bit younger than the re-crystallisation of quartz and the formation of idiomorphic calcite and pyrite, have been noted. The wall rock alteration adjacent to the fracture occupied by these three fillings respectively shows a slightly different appearance (see “Wall rock alteration”). Typical features of the wall rock alteration include the chloritization of biotite and the extensive red-staining of the wall rock adjacent to fractures, where micro-grains of hematite is found on mineral surfaces but also within their crystal structure, and within the plagioclase grains in particular. This alteration is caused by circulation of oxidising

fluids of hydrothermal origin. An interesting observation is that coarse-grained idiomorphic pyrite crystals (generation 2) only are identified in fractures coated by relatively fresh wall rock, in other words fractures that probably have not been exposed to oxidising fluids to a large extent. Further studies of these relations are however essential for the understanding of the current conditions. The lack of this early pyrite generation in fractures coated by a red-stained wall rock may infer that the pyrites, if once present, have been oxidised and completely altered.

The quartz mylonite typically consists of fine-grained quartz, muscovite and Fe/Mg-chlorite. The epidote mylonite consists of fine-grained epidote, quartz, Fe/Mg-chlorite, calcite and more coarse-grained epidote and quartz crystals. The fine-grained epidote often replace or partly replace larger crystals of quartz, calcite and titanite, which are found as remnants of older fracture fillings in the mylonite (KSH01: 11 m). The replacement is markedly pseudomorphic. Fe/Mg-chlorite also appears as big crystals unrelated to the epidote mylonite but related to fine-grained epidote. Titanite is probably not an earlier fracture filling but a part of the wall-rock, incorporated in the mylonite.

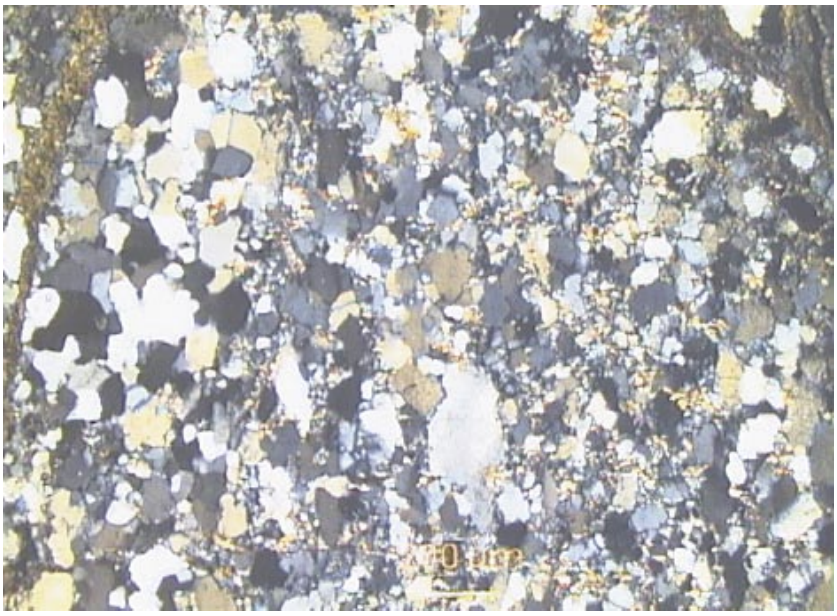

Figure 8-3. *Quartz mylonite from thin-section KSH01 24-1 m. Photomicrograph, width c 2.5 mm.*

The epidote mylonite is thought to be younger than the re-crystallization of quartz and the formation of calcite and pyrite. The formation of the mylonites indicates that some fracture zones have had ductile precursors. The ductile deformation and the mineral paragenesis, indicate a hydrothermal temperature-pressure interval in the ranges of epidote-amphibolite facies or greenschist facies, for the formation of the fracture minerals of this generation. The ductile event that is causing the mylonite formation might be related to a late phase of the regional deformation causing the E-W to ENE-WSW foliation in the granitoids. Field interpretations infer however that the mylonite formation postdates the development of the foliation /Munier, 1993/.

Figure 8-4. *Epidote mylonite (seen here as a more cataclastic variety), with complete pseudomorphic replacements of earlier quartz, calcite and some titanite. Photomicrograph from thin-section KSH01: 11 m.*

Chlorite and epidote have been derived by the hydrothermal alteration of primary ferromagnesian minerals, such as biotite, amphiboles and pyroxenes, demonstrated by the lack of biotite and amphiboles in the wall-rock of nearly all of the samples and the lack of pyroxenes in all of the samples, although pyroxenes are not a major constituent in felsic rocks. Epidote is formed from alteration of biotite and saussuritizion of plagioclase. Sericite, a kind of muscovite, is derived from hydrothermal alteration of the feldspars in the wall-rock.

Epidote, which is one of the major minerals of this generation, is particularly characteristic in rocks of the greenschist and epidote-amphibolite facies. In the greenschist facies it is characteristically associated with chlorite, actinolite, albite, quartz and calcite but also with some muscovite. These paragenetic minerals are more or less commonly associated in this fracture filling generation, which infers that the different pulses of this generation are formed during similar conditions. The formation temperatures of the minerals and the lack of minerals formed at lower temperatures suggest that the fillings in this, the second, generation were formed in the temperature-interval of roughly 400–550°C.

8.3 Generation 3

The third identified event in the KSH01 drill core is the appearance of pale green prehnite sealed fractures. This event is characterised by brittle deformation, breaking up earlier fracture fillings like the epidote- and quartz mylonites, but also creating new fractures, which may cut distinctly through earlier fracture fillings. These newly formed fractures and the space between the broken up mylonite fragments are filled with prehnite, leaving angular mylonite fragments in the prehnite (KSH01: 11 m; 600 m). Prehnite alone is a common fracture mineral in the area and is present in the majority of the samples in this

study. Macroscopically it can be distinguished from the darker and more distinctly green coloured epidote. The prehnite crystals range in size, from fine-grained to idiomorphic coarse-grained. The formation of prehnite is characteristically divided into several pulses where fillings of fine-grained crystals are followed by more coarse-grained, idiomorphic crystals. The

idiomorphic, bladed (almost fibrous), crystals are often growing perpendicular from the fracture rim, which is consisting of the host rock or of an earlier fracture filling, such as epidote mylonite, or of an earlier pulse of prehnite. In some fractures, single prehnite crystals are up to a couple of millimetres in size. The prehnite fillings are characteristically mono-mineralogical in opposite to the epidote mylonite. The only minerals identified to be related to this generation are fluorite and possibly some Fe/Mg-chlorite. Fluorite is only present, in small amount, in thin prehnite fillings. Although fluorite is found in small concentrations in relation with prehnite, several observations (KSH01; 24-1 m, 130 m, 793 m) of the coexistence of fluorite and prehnite, define them as to be of the same generation. The Fe/Mg-chlorite is more difficult to relate to any generation in particular. The wall rock next to the prehnite filled fractures is characteristically red-stained, in the same manner as the wall rock adjacent to epidote-mylonite filled fractures (see “Wall rock alteration”).

Figure 8-5. *Idiomorphic prehnite filling a fracture that is penetrating through earlier formed epidote mylonite (upper right). Microphotograph from thin-section KSH01: 11 m.*

Later dissolution of prehnite caused by circulating fluids appears more or less frequently throughout the drill core. The cavities left by the dissolution are filled by minerals of several subsequent generations, such as calcite, albite, Mg-rich chlorite, adularia and Fe-rich chlorite etc.

Prehnite is here thought to be formed within or just close to the borders of the prehnite-pumpellyite facies. This facies of low-grade regional metamorphism falls between the zeolite facies and the greenschist facies. The upper limit of prehnite stability occurs at about 400°C at 2–4 kbar /Blatt and Tracy, 2000 and references therein/. The transition from earlier ductile deformation to a more brittle deformation also indicates lower temperature-pressure conditions for the formation of the prehnite fillings. The fluorine in fluorite is probably derived from hydrothermal alteration of biotite and amphibole or by remobilisation of earlier formed fluorite.

8.4 Generation 4

White calcite fillings make up the next identified fracture filling generation. These fillings seal fractures which cut, both discordantly and concordantly, through the earlier fracture fillings. The fillings are often thin and appear to have crystallized rapidly. In some thin-sections, several pulses of thin fillings parallel to one another exist, which might infer that the fracture widened gradually, in close intervals (KSH01: 287 m; 600 m; 603 m; 626 m). The calcite crystals of this generation typically have a manganese content below the detection limit (SEM; < 0.2% MnO_2 supported by ICP-MS results as well, which show values between 80–215 ppm Mn for samples 208, 603 and 626 m), show deformation-twin-lamellae and have commonly been penetrated by later formed minerals, like adularia and Mg-rich chlorite. The stable isotope results indicate hydrothermal origin, showing high $\delta^{13}C$-values and $\delta^{18}O$-values ranging from –10.7 to –20.7‰ (Appendix A6). The Sr-values of the calcites are around 0.709 for this generation (Appendix A6). It is unclear whether the subsequent fracture filling minerals that are penetrating the calcite, like adularia, Mg-rich chlorite and hematite, are formed at more or less the same event as the calcite or clearly later. Fe/Mg-chlorite, with small individual crystals of titanite in the crystal structure, is present and the calcite and the chlorite are penetrating one another. This penetration is inconsequent between the different thin sections and infers that both chlorite and calcite are formed continuously over a long time span. The Fe/Mg-chlorite is present in generation 2-5. This fracture generation is distinguished by its distinct cutting of prehnite and that it is penetrated by later fracture filling generations.

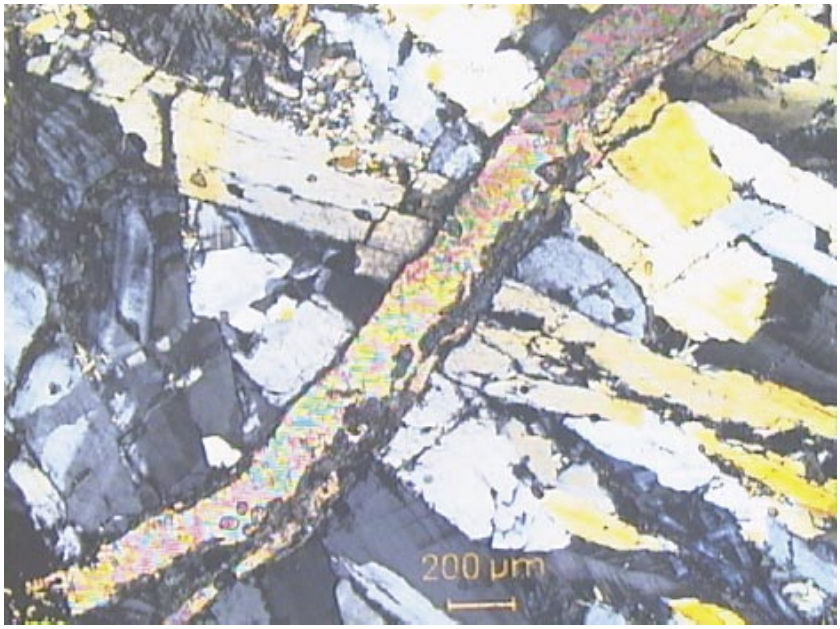

Figure 8-6. *Thin filling of calcite in a fracture cutting through an earlier filling of idiomorphic prehnite crystals. Microphotgraph from thin-section KSH01: 208 m.*

8.5 Generation 5

The calcites of the fourth generation are penetrated by a red and very fine-grained filling, consisting of adularia, Mg-rich chlorite, hematite and some Fe-rich chlorite (KSH01: 257 m; 275 m; 363 m; 626 m etc). This red, hematite-stained, filling is formed in an event marked by semi-ductile deformation, giving the filling a "mylonitic" appearance, but should however by classified as a cataclasite. Hematite is present as individual grains but also as thin layers on the other silicates, making them almost impossible to identify. See analysis of Fe-enriched chlorite in the appendix (257-Hematite-Chlorite(1-2)).

A later pulse of the same minerals is however penetrating the cataclasite in a more brittle manner, leaving the earlier fracture filling as angular fragments in the later filling (KSH01: 257 m). This later filling differs from the red stained cataclasite in that it is more coarse-grained, and it consists of less Fe-rich chlorite and of much less hematite. The lack of hematite makes this filling less red coloured. Although they differ in appearance they seem to be closely related in time. This means that, while deformation prevailed, semi-ductile conditions were successively replaced by brittle conditions.

Another fracture filling that is penetrating the calcite of the fourth generation is the spherulitic Fe/Mg-chlorite (KSH01: 130 m; 289 m; 873 m). This chlorite differs from the earlier formed Fe/Mg-chlorite both in texture and Fe/Mg-ratio (see analysis 130-Fe/Mg-chlorite(sph)). Both of the Fe/Mg-chlorites are related to titanite, although the relation seems to be more apparent in the earlier generations. No relation has been found between the spherulitic Fe/Mg-chlorite and the fine-grained fillings. All of the fracture fillings in this generation are however penetrated by fracture fillings of later generations.

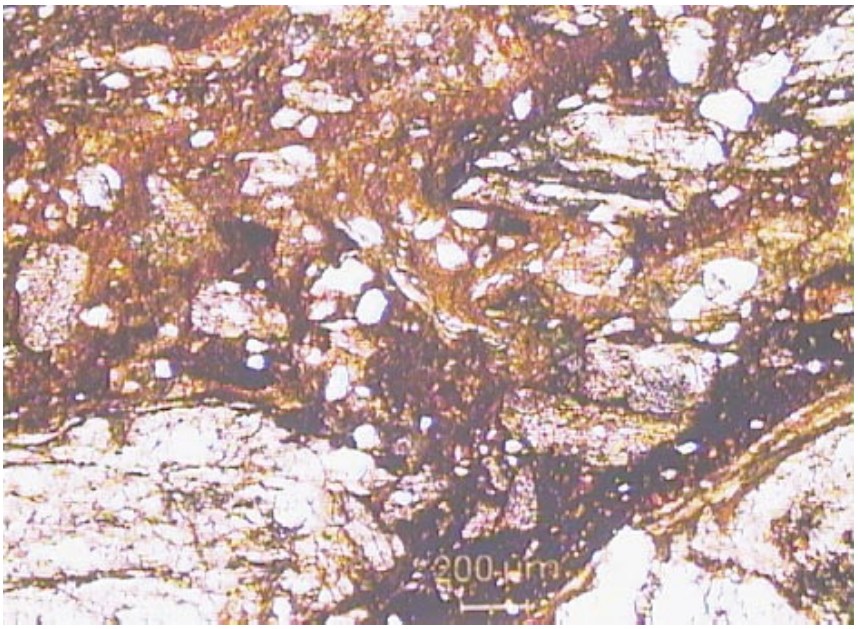

Figure 8-7. *Red coloured cataclasite penetrating earlier formed fillings in thin-section KSH01 363 m. Microphotograph in plane polarized light.*

The appearance of adularia and Mg-rich chlorite along with Fe-rich chlorite marks this event as an event with even lower formation temperatures than the earlier fillings. The lack of prehnite and zeolites place this event somewhere between the prehnite-pumpellyite facies and the zeolite facies. The adularia has probably been derived from hydrothermal alteration of K-feldspar, biotite and sericite in the host rock. The Mg-rich chlorite and the Fe-rich chlorite comes from alteration of earlier formed chlorite and other Fe/Mg-bearing minerals such as biotite and amphiboles but also from the alteration and dissolution of prehnite and maybe also from epidote. Hematite is formed from the oxidation of Fe(II) present in the chlorite, biotite and magnetite in the host rock. The presence of hematite marks this event as an event where oxidising fluids have been circulating in fracture zones and in individual fractures. This red-staining event differs from the earlier wall-rock red staining in that this red-staining is concentrated to the fracture fillings and is not common in the wall rock. These two red-staining events also differ in colour. The red-staining of this event gives the filling a dark red to brown appearance, caused by individual hematite grains in paragenesis with a dark Mg-rich chlorite, whereas the early red-staining event, which is fairly contemporary with generation 2 or generation 3, is characterised by a brighter red colour (see "Wall rock alteration"). These two events of oxidising conditions are separated by at least calcite of generation 4.

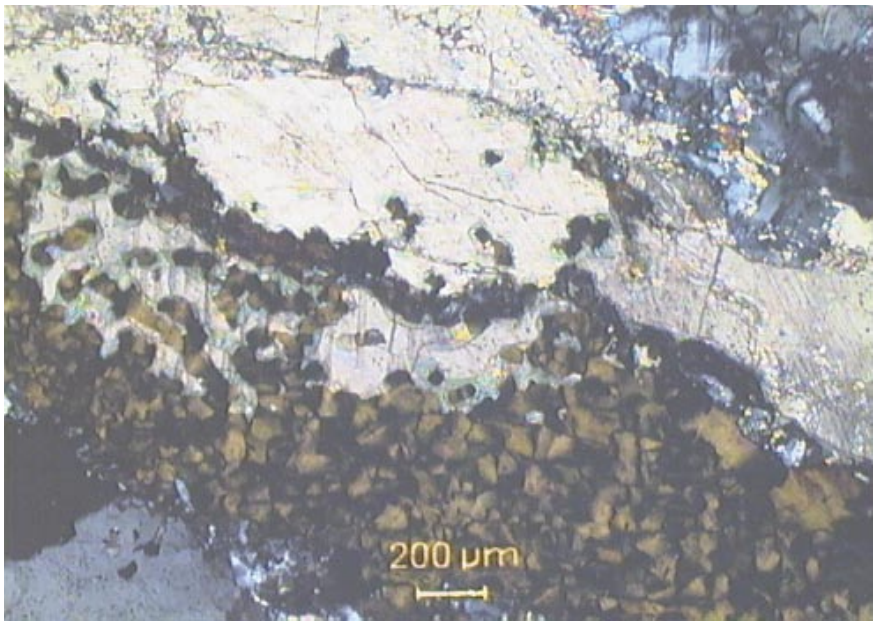

Figure 8-8. *Brown coloured, spherulitic, Fe/Mg-chlorite growing into calcite of the fourth generation. Microphotograph from thin-section KSH01: 873 m.*

8.6 Generation 6

The following fracture filling generations, here described as one generation divided into several sub-generations, are obviously of low temperature origin. The minerals formed here are penetrating old fracture fillings, leaving relict textures. The only fracture filling in generation 6 that is clearly macroscopically identifiable is calcite. These calcite fillings are often thin like in generation 4, although the crystals of this generations show less deformation-twin-lamellae and the manganese content can rise up to 2% MnO_2 (SEM) in lately formed fillings. ICP-MS analyses of samples 363 m and 257 m show values of 1.2% MnO_2 and 0.03% MnO_2, respectively (Appendix A7). These calcite fillings cut distinctly through the earlier fine-grained hematite-cataclasite, although they do not seem to be formed very distant in time. Some microscopically visible fractures cut through the earlier formed fracture fillings and the host rock. These fractures are of a late phase and are filled with harmotome (Ba-zeolite), spherulitic Fe-rich chlorite and less commonly pyrite. The lack of numerous discordantly cutting fractures, incomplete re-crystallization and remaining relict structures marks the formation conditions as low-temperature and make the separation of different fracture filling generations difficult. The fact that fracture minerals are penetrating one another inconsequent in different thin-section infers that they are fairly contemporary and thus considered to be of the same generation. Subdivisions of the generation can be made by dividing the minerals in to groups of characteristically identified parageneses, e.g. adularia is frequently related to Mg-rich chlorite and occasionally with apatite (KSH01: 198 m; 208 m). A sequence of hydrothermal mineral growths representing decreasing formation temperature can be constructed. This series might be the result of a continuous event of gradually lower temperatures. It might as well be the result of several different fracture filling events with big time gaps in between.

8.6.1 Generation 6-1: Calcite

As mentioned above, the calcite fillings are major constitutes of this facture filling generation. The fractures filled with calcite cut through the earlier red cataclasite fillings of the fifth generation (KSH01: 363 m). The calcite crystals are very thin. Commonly the fractures filled with calcite are occupied by only 2–3 calcite crystals, filling the whole fracture section that is present in the thin-section. Calcites are formed at several different stages of the sixth generation, but this early calcite (6-1) is characteristically penetrated by one or more of the later formed fracture fillings, often adularia and Mg-rich chlorite, followed by Fe-rich chlorite etc. Hematite stains originating from the red cataclasite are later occupying parts of the calcite fillings, showing that the hematitization is ongoing later than generation five. The calcite fillings are penetrated by later formed minerals, leaving the texture of the relict calcite filling intact. A low temperature Ti-oxide is present in relation to calcite in the thin section from 363 m. It is thought to be the low temperature polymorph of rutile, namely anatase, which has been formed from the alteration of titanite and ilmenite in the host rock and in the fracture fillings. From stable isotope analyses and microscopy it is evident that calcite have been precipiatetd during several events included in generation 6; $\delta^{18}O$ values ranging from –8 to –15‰ and $\delta^{13}C$ values ranging from –6.42 to –12‰ (the latter indicating some biogenic influence). Sr isotope values range from 0.711258 to 0.712686. The Sr contents in the two samples analysed (257 and 363 m) are low (45–55 ppm), which is typical for low temperature carbonates.

8.6.2 Generation 6-2: Quartz, (albite)

Fine-grained and occasionally idiomorphic quartz crystals are present in some thin-sections. They are characteristically growing from the rim of calcite filled fractures, penetrating the calcite fillings and leaving the relict texture of the calcite filling intact. The quartz fillings are evidently formed later than the calcite filling of the fourth generation and the red cataclasite of the fifth generation (KSH01: 600 m, 626 m). Since calcite is formed at several different events, there are calcites of the sixth generation that are both older and younger than the quartz fillings. Some relations between quartz and adularia (6-3) have been noted but adularia seems to be a little bit younger than quartz (KSH01: 600 m, 603 m). Fine-grained albite crystals appear to be of the same sub-generation (6-2) as quartz but the albite crystals are far less abundant than quartz.

8.6.3 Generation 6-3: Adularia, Mg-rich chlorite, Apatite, Laumontite etc

The fracture filling paragenesis, consisting of mainly adularia and Mg-rich chlorite, is one of the most abundant throughout the whole study. Although hardly macroscopically visible, this filling is present in almost every thin-section, characteristically penetrating calcite of earlier generations (and 6-1), leaving relict structures, which infer low temperature formation. The minerals of this generation are also frequently observed in dissolved cavities in prehnite and albite. The paragenesis of adularia and Mg-rich chlorite is the most reliable in the whole study. These two minerals almost always appear together. Notable is that the Mg-chlorite is typically growing into the adularia crystals. Included in this paragenesis are evidently apatite (KSH01: 198 m, 208 m) and laumontite (KSH01: 208 m, 213-1 m, 213-2 m), although these minerals are only identified in a narrow depth span although indications from other studies indicate that laumontite is present at a more wide depth span, e.g. down to 920 m in drillcore KOV01, Oskarshamn. Apatite forms fine-grained, idiomorphic, crystals, although not as needle shaped as its common habit. Textural relationships reveal that the apatite postdates adularia and is younger than Mg-rich chlorite, even though they are closely related in time. Laumontite forms relatively big crystals compared to adularia and apatite etc, but is difficult to relate to other minerals

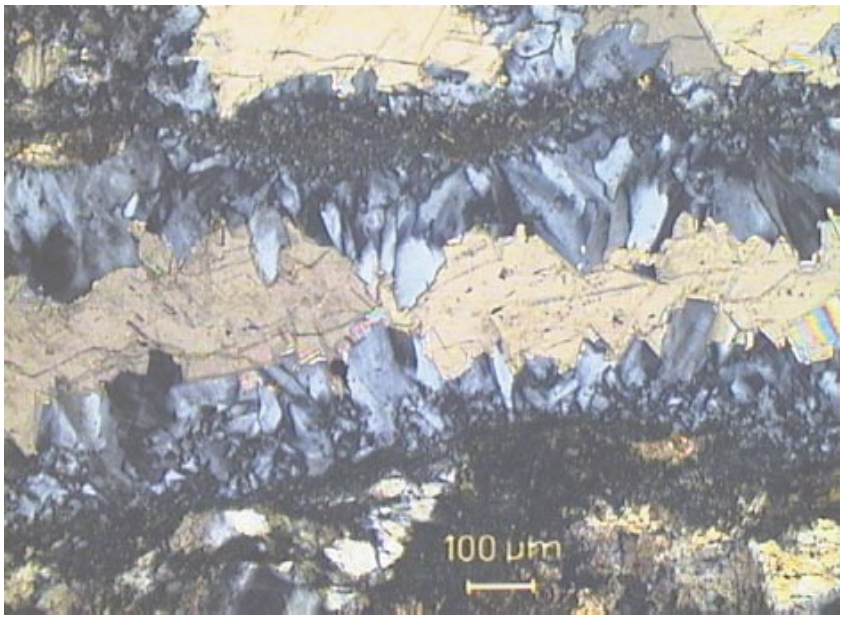

Figure 8-9. *Fracture coated by adularia is later sealed by calcite. Photomicrograph from thin-section KSH01: 287 m.*

in detail. In the thin-sections from 208 m, hematite and harmotome appear to be related to adularia and Mg-rich chlorite. The hematite often appears as stains on the surface of adularia and Mg-rich chlorite and can thus be classified as younger but in some cases hematite form crystals that seem to be contemporary with adularia and Mg-rich chlorite. Harmotome is described below as a mineral that is formed later and during lower temperature conditions than adularia and laumontite, but observations of harmotome in paragenesis with the other minerals in generation 6-3 has been noted (KSH01: 208 m), suggesting a not too distant relation between 6-3 and 6-4.

As mentioned earlier, chlorite is formed in a wide pressure-temperature interval. The Mg-rich chlorite is replacing the Fe/Mg-chlorite with decreasing temperature. The Mg-rich chlorite is richer in MgO and has a reduced amount of FeO, compared to the Fe/Mg-chlorite (see analyses of all the chlorite varieties in appendix). The later formed Fe-rich chlorite is replacing the Mg-rich chlorite. The higher amount of FeO might be derived from the present hematitization, were hematite is formed from oxidation of magnetite in the host rock and from alteration of Fe/Mg-minerals.

Adularia is a low-temperature K-feldspar, formed at temperature < 450°C /Nesse, 2000 and references therein/. Studies of /Hagen et al. 2001/ imply that adularia may be formed at temperatures as low as 100°C related to shallow burial by sedimentation. Adularia is formed from the hydrothermal alteration of K-feldspars and possibly also biotite and sericite in the host rock. The adularia in this generation is probably also derived from the breakdown of adularia of the fourth generation. The barium content in adularia is changing with time of formation. ICP-MS analyses show slightly different BaO contents for the K-feldspars in the host rock and the adularia in the fractures. The BaO content in the adularia seem to be higher than in the K-feldspars in the host rock. SEM-EDS analyses, which are less precise than the ICP-MS do however show quite the opposite (see analyses). The paragenesis of adularia, chlorite, quartz and apatite has been previously observed /Deer et al. 1992 and references therein/.

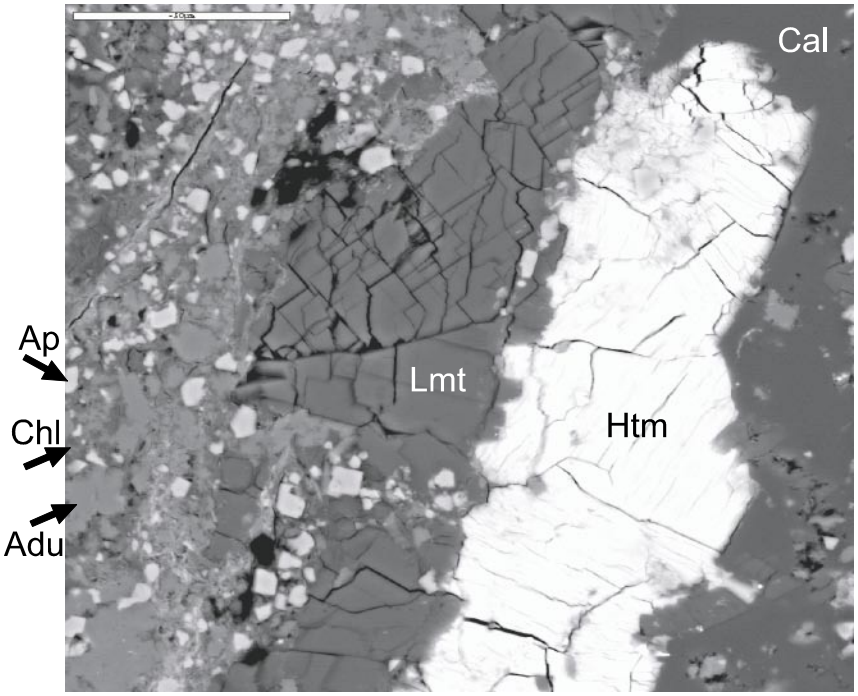

Figure 8-10. *Laumontite (Lmt) and Harmotome (Htm) looks to be fairly contemporary with a thin filling of calcite (Cal) and the fine-grained matrix consisting of Mg-rich chlorite (Chl), adularia (Adu) and apatite (Ap). All are from generation 6. Backscattered electron image from thin section KSH01: 208 m. Scale bar is 50 µm.*

8.6.4 Generation 6-4: Adularia, Hematite, Harmotome, Pyrite, Fe-rich chlorite, Calcite, Fluorite

The latest crystallization of adularia in this study is the idiomorphic crystals found in thin, partially open, fractures cutting through more fine-grained adularia and Mg-rich chlorite fillings formed in earlier generations. These adularia crystals are probably formed by re-crystallization of the earlier formed adularia, caused by hydrothermal alteration.

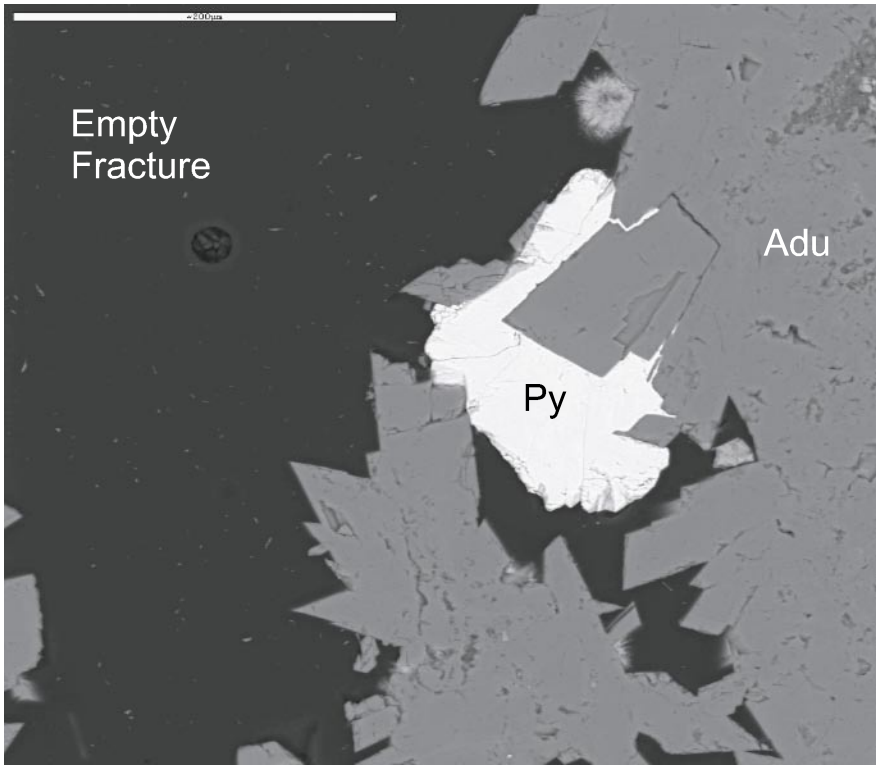

Figure 8-11. *Idiomorphic adularia (Adu – generation 6-4) with later pyrite (Py – generation 6-4) and Fe-rich chlorite (spherulitic crystal above pyrite – generation 6-4). Backscattered electron image KSH01: 257 m. Scale bar is 200 µm.*

The most abundant fracture mineral in this generation is however by far the Fe-rich chlorite (see analysis). This chlorite is often spherulitic and very fine-grained. It often fills very thin and winding fractures cutting through earlier formed fracture fillings, often consisting of adularia and Mg-rich chlorite. This chlorite is also abundant in cavities in prehnite and albite, caused by dissolution and can also be found as a characteristic spherulitic variety in late, partially and completely, open fractures, growing from the rim of the fracture. The paragenesis includes hematite and later harmotome and pyrite, but chlorite may also be included in a fine-grained, porous filling, together with adularia, apatite and sometimes also albite, present in open fracture (KSH01: 198 m).

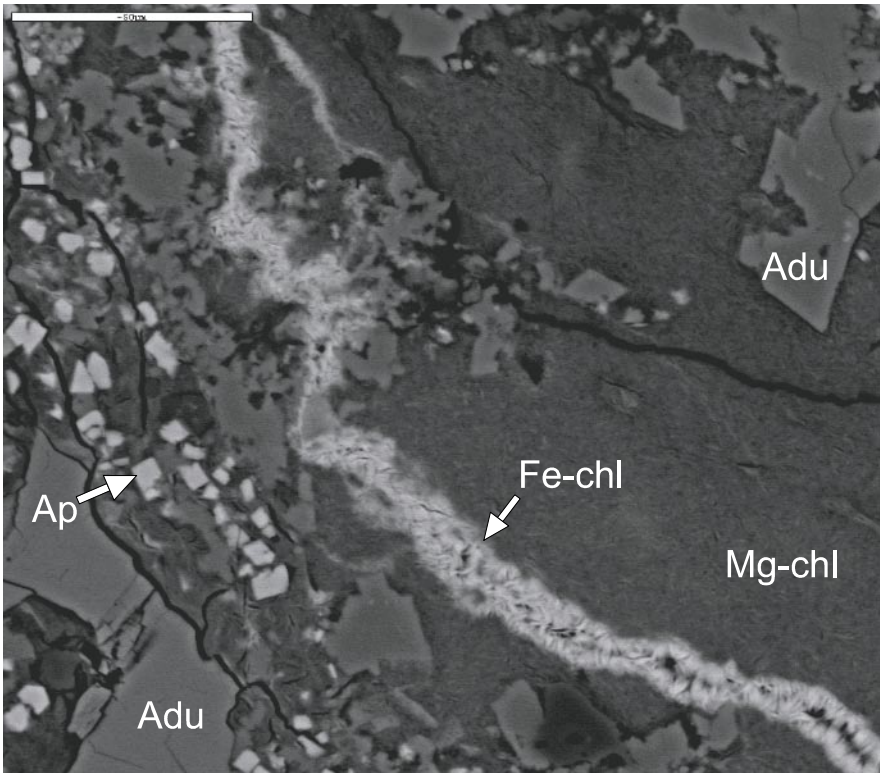

Figure 8-12. *Fine-grained matrix consisting of Mg-rich chlorite (Mg-chl), adularia (Adu) and apatite (Ap), of generation 6-3, is cut by a thin filling of Fe-rich chlorite (Fe-chl – generation 6-4). Backscattered electron image from thin-section KSH01: 208 m. Scale bar is 50 µm.*

Hematite is present, both in the form of small stains on the crystal surfaces and in the crystal structure of other minerals, sometimes forming circular dots of pure hematite and sometimes appearing merely as thin layers. Hematite also exist as fracture fillings in very thin fractures, often in relation with Fe-rich chlorite and sometimes with pyrite, but pyrite seams to be younger. Hematite can also, like Fe-rich chlorite, occupy cavities in earlier dissolved mineral phases. The hematite crystals in this generation are typically neither as fine-grained nor as abundant as the crystals in the fifth generation. The red hematite-stained fillings of the fifth generation are also more macroscopically evident.

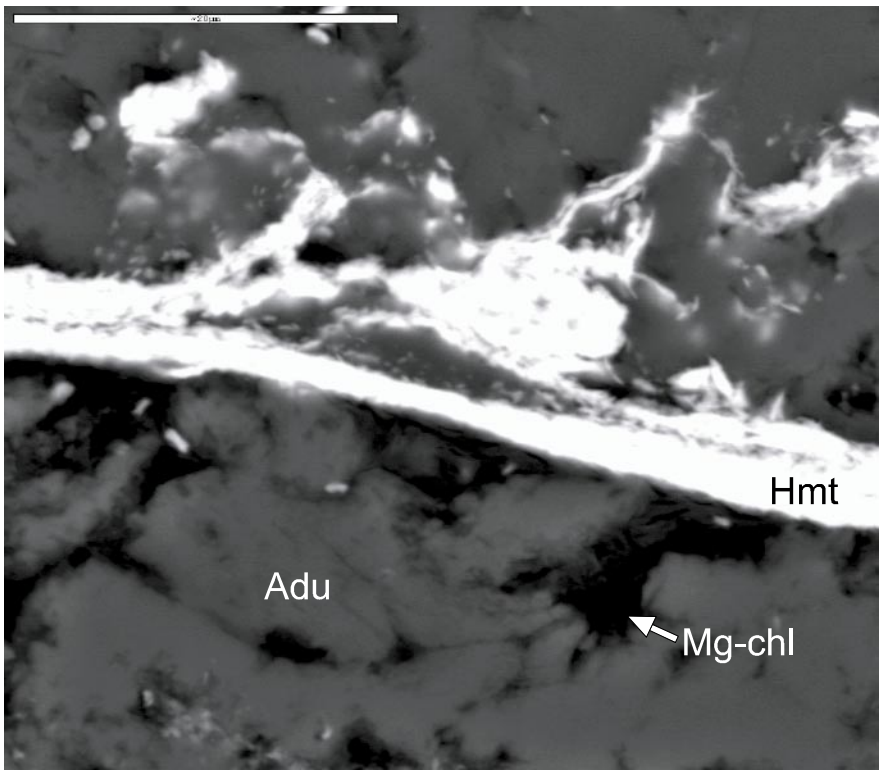

Figure 8-13. *Adularia (Adu – generation 6-3) and Mg-rich chlorite (Mg-chl generation 6-3) are cut by hematite (Hmt – generation 6-4). Backscattered electron image from thin-section KSH01: 287 m. Scale bar is 20 µm.*

Pyrite has been identified as a fracture filling mineral in relation to Fe-rich chlorite, but also as an unaccompanied fracture filling, present both in thin-sections and in fracture surface-samples. The pyrite crystals of this generation are neither as numerous nor as coarse-grained as the early formed pyrites (generation 2). The pyrite crystals are fine-grained and ranging from idiomorphic cubic crystals to xenomorphic crystals in thin fillings. The thin fillings consisting of a few xenomorphic pyrite crystals have been shaped in accordance to the structure of the fracture. The idiomorphic crystals have been observed in cavities in earlier formed Mg-rich chlorite filled fractures (KSH01: 24-2 m), together with fluorite. Other idiomorphic pyrite crystals have been identified in paragenesis with Fe-rich chlorite and a single sphalerite crystal (KSH01: 257 m). Xenomorphic pyrite crystals are characteristically found in paragenesis with Fe-rich chlorite but they also seem to appear in some sort of relation to the hematite, which is formed earlier in generation 6-4 (KSH01: 213 m; 257 m).

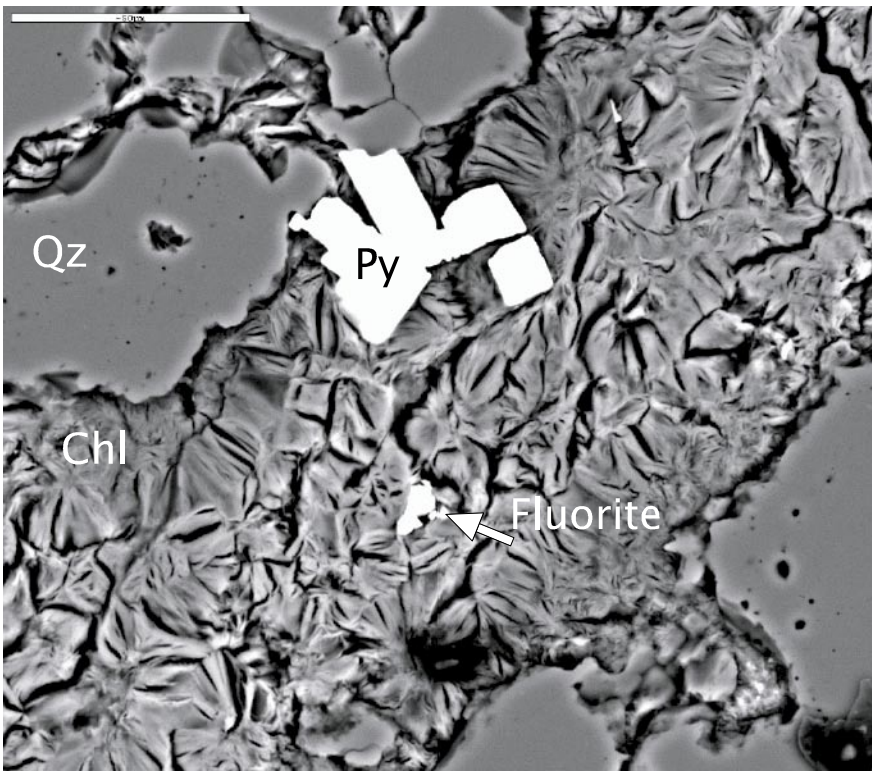

Figure 8-14. *Quartz (Qz – generation 1) is penetrated by Mg-rich chlorite (Chl – generation 6-4). Pyrite (Py) and fluorite, both of generation 6-4, have grown in cavities present in the Mg-chlorite filling. Backscattered electron image from thin-section KSH01: 24 m. Scale bar is 50 µm.*

The quite uncommon barium-zeolite, harmotome, also identified by Milodowski in the drill-core KLX01 from Laxemar (oral communications), is found in a fairly narrow span of the drill core. It has been identified in samples ranging form 130 m to 242 m, both in thin-sections and on fracture surface-samples. This narrow depth span is corresponding to that of Milodowski, who have observed harmotome in several samples from depths above 300 m in the drill-core KLX01 from Laxemar (oral communications). Small crystals, too small to get a decent analysis, consisting of a barium content up to 8% BaO, have however been observed in the thin-section from 11 m, suggesting that barium-rich solutions has been present in a wider span. The presence of idiomorphic crystals of barite on the fracture surface-sample from 242 m further indicates the presence of barium rich fluids. The harmotome present in thin-sections occupy very thin fractures, cutting through fillings as lately formed as the adularia and Mg-chlorite from generation 6-3. These fractures are often coated by Fe-rich chlorite, which is present wherever harmotome is identified. The harmotome seems to be an easily dissolved fracture filling since approximately 90% of the fractures occupied with harmotome are empty. In the thin-section from 208 m the harmotome seems to be related to minerals of generation 6-3. Generally, the harmotome has evidently been formed subsequent to the formation of laumontite. This further indicates that a series of gradually lower temperature conditions have been present since harmotome is known to be formed at lower temperatures than laumontite, specified by higher H_2O-content in the harmotome formula.

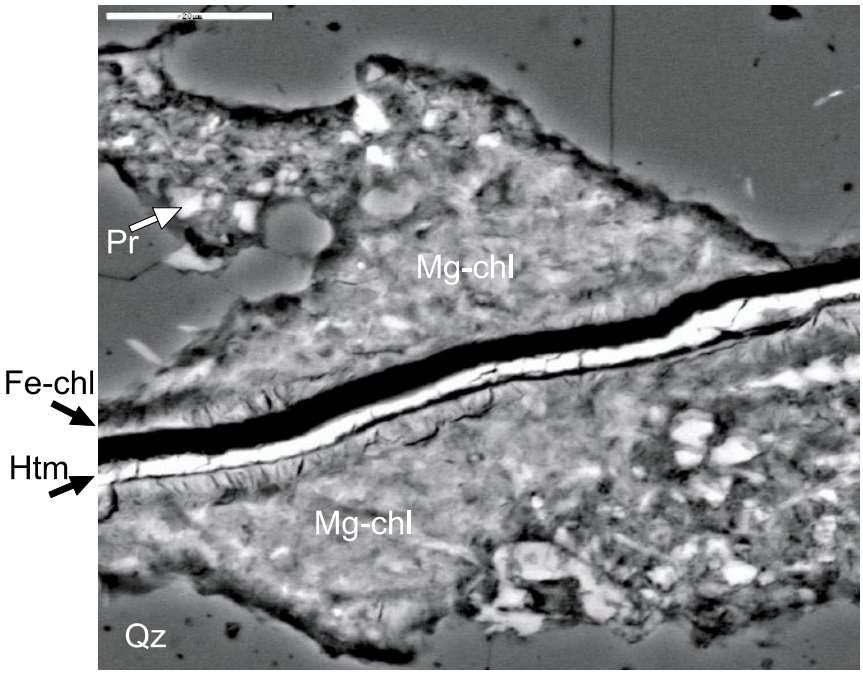

Figure 8-15. *Early quartz crystals (Qz – generation 1) are penetrated by prehnite crystals (Pr – generation 3) located in a fine-grained matrix. Mg-rich chlorite (Mg-chl – generation 6-3) is formed later than prehnite and is cut by a vein of Fe-rich chlorite (Fe-chl) and harmotome (Htm), both of generation 6-4. Backscattered electron image from thin-section KSH01: 130 m. Scale bar is 20 µm.*

Fluorite is classified as being a part of this sub-generation since it is observed in paragenesis with pyrite in cavities in earlier Mg-rich chlorite (generation 6-3, KSH01: 24-2 m) and since it is found in fractures both cutting through Mg-rich chlorite (generation 6-3), calcite (generation 6-1) and the red cataclasite of the fifth generation (KSH01: 363 m). The crystals found in cavities in other minerals are typically very small and rounded, while the crystals forming individual fillings in thin, distinct cutting, fractures are xenomorphic and formed by fluids flowing through the fracture. The fluorites in this kind of fractures are always partly dissolved (KSH01: 208 m, 363 m). Fluorite is observed to be an easily dissolved and commonly re-crystallized mineral. It is originally derived from hydrothermal alteration of the fluorine bearing mineral biotite. This late generation of fluorite probably consists of partly re-crystallized fluorite.

The easily dissolved Ba-zeolite harmotome is a mineral formed at low temperature conditions. The zeolites are mainly formed from the break down of feldspars in the host rock and in the fractures. Zeolites are also formed by the alteration of prehnite. The barium is possibly derived from the hydrothermal alteration of K-feldspar and biotite, which both are known to be barium bearing minerals. Other sources for the high Ba content might as well be some kind of sediments, covering the bedrock and burying the crust into burial metamorphosis regimes.

The presence of hematite reveals extensive oxidation conditions in this late crystallization phase. The formation of pyrite postdating the hematite indicates however that the oxidation phase was followed by reducing conditions. The Fe-rich chlorite appears to be related to both the hematite and the pyrite but the pyrite and chlorite have evidently often been formed later than hematite. All of these minerals have been derived from low-temperature hydrothermal alteration of earlier formed Fe/Mg-bearing fracture minerals and from minerals present in the wall rock. Pyrite has been formed from alteration of Fe-bearing minerals.

8.6.5 Generation 6-5: Calcite, Mixed layer clay, Pyrite, (REE-carbonate)

The outermost layers of the open fractures usually consist of clay minerals, calcite and pyrite. This is also the case for the fracture surface samples included in this study where also REE-carbonate was identified on one fracture surface. The relations between the analyses of the thin-sections and the surface-samples can be coordinated to a certain extent and show that the fracture fillings existing on the surface-samples are often formed at a very late stage. As mentioned earlier, calcites have been formed throughout the whole scheme of formation and are also present as at least two phases in generation 6-5. Some of these calcites are in paragenesis with harmotome and barite. These calcites have been formed earlier than REE-carbonate and a late phase of Fe-rich chlorite and pyrite. Small crystals of Fe-rich chlorites and pyrite are found on the crystal surfaces of harmotome, barite and calcite (KSH01: 242-2 m, 289 m), while the REE-carbonate forms a porous cover upon the calcite crystals (KSH01: 289 m). The late formation of pyrite, infers that reducing conditions have been present at this stage.

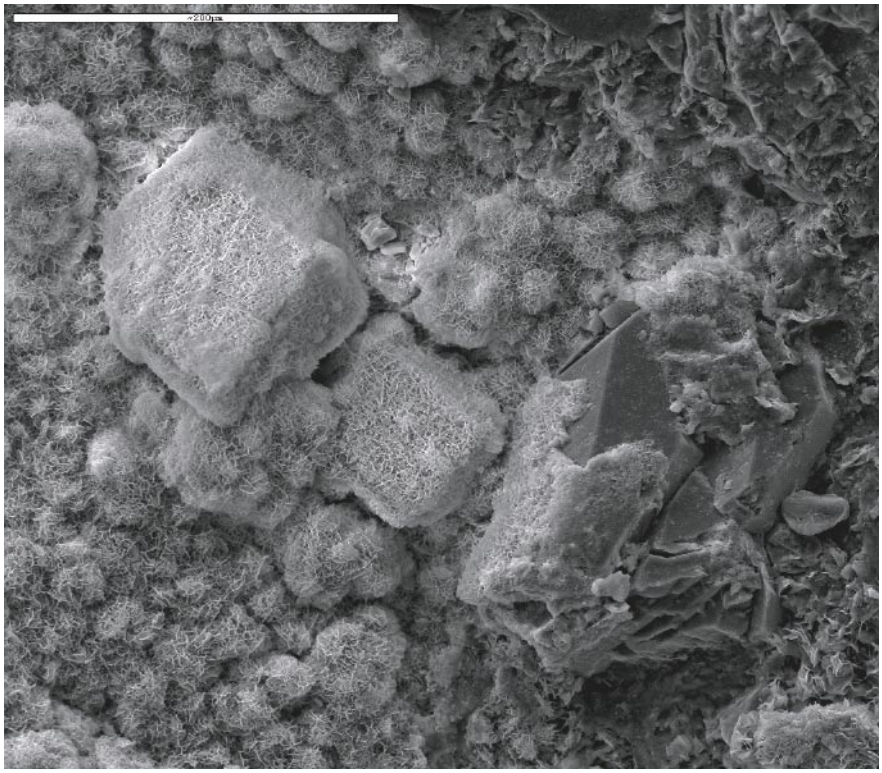

Figure 8-16. *Electron image of the fracture surface from 289 m, showing scalenoedral calcite crystals covered with a thin layer of REE-carbonate. Scale bar is 200µm.*

Although their presence can be assumed macroscopically, clay minerals have been difficult to identify using SEM. Identifications of clay minerals have only been confirmed using X-ray diffraction. Clay minerals and mixed-layer clay in particular are identified in all XRD analyses and the dominating minerals are chlorite, and mixed layer clays of chlorite/ smectite and illite/smectite types. The mixed layer clays are thought to be one of the latest formed mineral phases in this study, supported by studies made of /Maddock et al. 1993/. The results of the XRD analyses are further discussed in the “X-ray diffraction results” chapter.

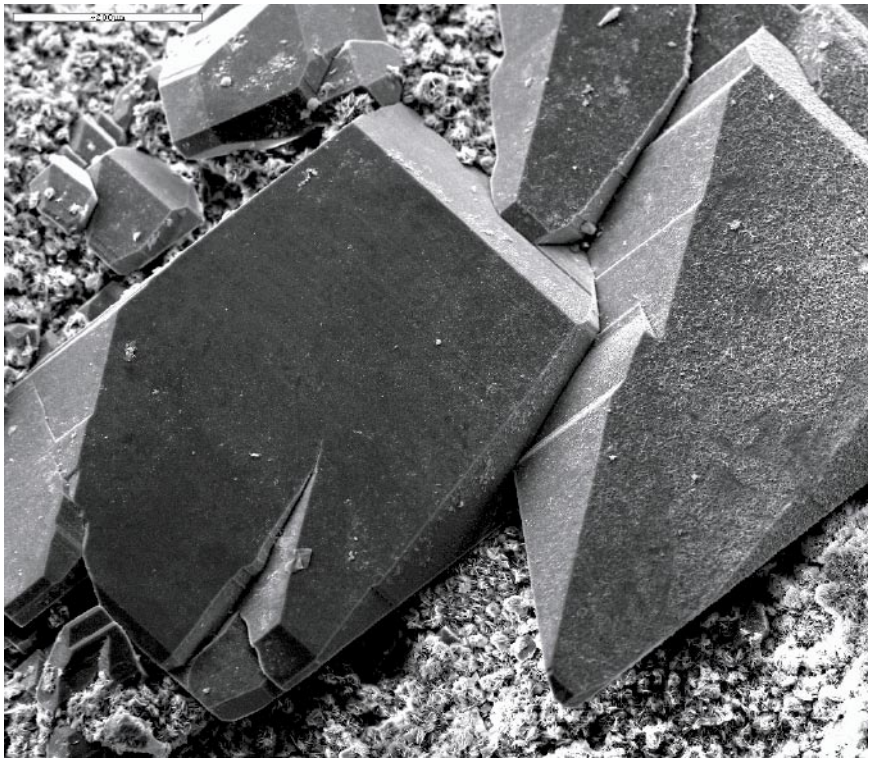

Figure 8-17. *Electron image of the fracture surface from 289 m, showing scalenoedral calcite crystals. Scale bar is 200µm.*

The sixth generation of fracture minerals have been formed at low-temperature conditions. The presence of the zeolites harmotome and laumontite, and the lack of prehnite indicate that the minerals in this generation have been formed within the zeolite facies and not in the prehnite-pumpellyite facies. Adularia and albite are also minerals known to be formed at low-temperature conditions. Generally the sub-divisions of the sixth generation form a low-temperature formation series, with decreasing formation temperatures. Characteristically, relict grains, incomplete pseudomorphic replacements, and preserved textures are present.

8.7 Götemar related fracture fillings

Some of the idiomorphic quartz fillings in the KSH01 drill-core may postdate the cataclasites, although the relations are indistinguishable. These quartz fillings are related to idiomorphic epidote and Fe/Mg-chlorite. A quartz-epidote-muscovite-fluorite fracture filling generation has been identified in other studies /Tullborg, 1988/ to be related to post-magmatic circulation of the Götemar granite. Since no relation between fluorite-muscovite-epidote has been identified in this study of the KSH01 drill-core, the Götemar-related fracture fillings can not be included in this study. In fact, no fluorite in this study has been identified as being older than generation 3 and no muscovite in this study has been identified as being younger than generation 2. Studies made by /Tullborg, 1988/ infer that the formation of the Götemar induced fracture filling took place subsequent to the formation of the epidote-mylonite (generation 2 in this study) but prior to the formation of prehnite (generation 3 in this study).

8.8 Detailed descriptions of the surface-samples

A small amount of surface-samples have been analysed (6 in total, 5 using SEM). The most abundant fracture minerals in these samples are harmotome (KSH01: 211 m, 242 m) and calcite (KSH01: 242 m, 289 m, 611 m) but the harmotome are not as abundant as calcite throughout the whole drill core. The harmotome crystals form a complete cover of idiomorphic crystals on the fracture surface (KSH01: 211 m). The crystals are well preserved, although they are evidently fragile and easily dissolved. The monoclinic harmotome have been identified in paragenesis with idiomorphic, unaltered calcite crystals of scalenoedral crystal structure. This infers that no major deformation has occurred in these fractures after the formation of these mineral phases. Later fluids have however been present in these open fractures and pyrite, Fe-rich chlorite and REE-carbonate have all been identified as later formed mineral phases on the surfaces of the harmotome and calcite crystals. Idiomorphic calcite crystals of different shapes have been identified on fracture surfaces and the stable istotope results from these indicate different origin concerning water types and chemistry, (cf Figure 7-1). Sr isotopes results show that some of these crystals have values in correspondence with present groundwaters (0.715 to 0, 716; Appendix A6). It is thus realistic to assume that calcite has precipitated in the open fractures during several periods and groundwater regimes up to recent time. Equant crystals of calcite have been observed at 611 m depth. Also present are barite crystals in paragenesis with calcite and harmotome (KSH01: 242-2 m) and laumontite in paragenesis with calcite (KSH01: 242-1 m). The presence of barite further infers the occurrence of barium-rich fluids in this late stage of formation. The presence of undeformed and unaltered laumontite, which is identified in the thin-sections as a fairly early formed mineral in the sixth generation, infers that no major deformation events have occurred since the formation of laumontite.

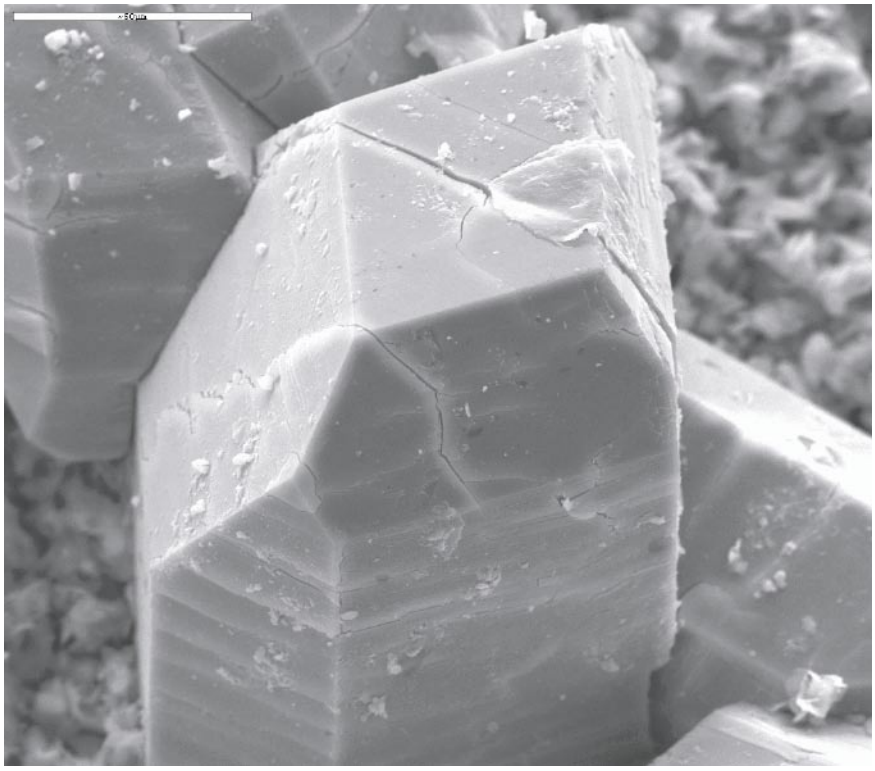

Figure 8-18. *Electron image of the fracture surface from 211 m, showing harmotome crystals. Scale bar is 50µm.*

8.9 Wall rock alteration

The alteration of the wall rock shows a similar pattern throughout the drill core. The most apparent alteration is the extensive red-staining of the host rock adjacent to a majority of the fractures. Other widespread alterations are the chloritization of biotite and saussuritization/ sericitization of feldspars. These alterations are evidently earlier than the formation of calcite of generation 4 and are thus considered to be a part of the earliest events in the geological record of the area.

All in all the wall rock shows an increasing alteration closer to the fractures. Amphibole and biotite crystals are replaced by idiomorphic chlorite crystals. This partial and complete chloritization of biotite in particular, has been confirmed in the wall rock in every thin-section. In most cases the transformation is markedly pseudomorphic. The biotite in the wall-rock is rich in TiO_2 (see analyses in appendix). When the biotite was transformed into chlorite the titanium formed small individual crystals of titanite, present within the chlorite crystals. The alteration of biotite into chlorite also leaves some exsolved K^+. This potassium has been participating in the formation of K-feldspar and sericite. Fluorine released from the biotite is incorporated in fluorite in the altered rock and the fracture coatings The number of idiomorphic epidote crystals is also rapidly increasing in the wall rock close to the fractures. The epidote and the chlorite (Fe/Mg) appear to be rather contemporary.

The alteration of the plagioclase crystals in the wall rock is, as usual in granites, marked by widespread saussuritisation. Sericitisation of K-feldspar has also been observed but this alteration has not been as extensive as the alteration of plagioclase. The degree of alteration is increasing closer to the fractures. The increased saussuritisation have been followed by an increased number of micropores within the altered grains, caused by the removal of the major part of the anorthite component of the plagioclase, related to albitisation of the crystals /Eliasson, 1993/. This albitisation of plagioclase would have given a volume reduction of plagioclase and also some exsolved Ca^{2+}, from which calcite may have been formed /Eliasson, 1993/.

Even more macroscopically noticeable is however the extensive red-staining of the feldspars and of the plagioclase crystals in particular, next to a great number of fractures in the drill core. Observations from the drill core show that the red-staining generally extends some centimetres but occasionally some decimetres in to the wall rock. Observations from outcrops show however that the red-staining can be present in big portions of the wall rock, sometimes reaching far from the fracture from which the oxidising fluids originates. The red colour comes from micro crystals of hematite, or Fe-oxyhydroxides that is present as thin layers in the crystal structure and on the surface of the plagioclase crystals in particular /Eliasson, 1993 and this study/. The red-staining of the granite coincides with hydrothermal metamorphic alteration assemblages, which occur along the fractures. This infers that the red-staining have been related to hydrothermal alteration. Studies made by /Landström et al. 2001/ show that there is not necessarily a corrpondence between how far from the fracture edge the alteration of biotite, plagioclase and the red staining reach, although it can be concluded that hydrothermal alteration is essential for the development of the red-staining. The red colouration has been concentrated to saussuritised plagioclase crystals, giving them a cloudy appearance. /Eliasson, 1993/, who concludes that the red-staining mainly have been caused by very fine-grained Fe-oxyhydroxides/hydroxides in saussuritic and clouded plagioclase, along grain boundaries and to some extent along microfractures within individual grains. More recent studies made by /Didriksen and Stipp (in manuscript)/ do however infer that the

majority of the red-staining is caused by hematite and not Fe-oxyhydroxide/hydroxide. The dominance of hematite in the red-coloured wall-rock and fracture fillings are also supported by the observations made in this study. /Eliasson, 1993/ further classify this red-staining event as being part of the final low-temperature stage of water-rock interactions with formation temperatures of 150–250°C. This would infer that the red-staining of the wall-rock have been formed at prehnite-pumpellyite facies or lower. Such precise indications have not been confirmed in this study. The hematite has been hydrothermaly derived from the oxidation of Fe(II) minerals, mainly magnetite and biotite in the host rock. This widespread hematite crystallisation marks the presence of oxidising, Fe(III)-rich, solutions throughout a large number of fractures and fracture zones.

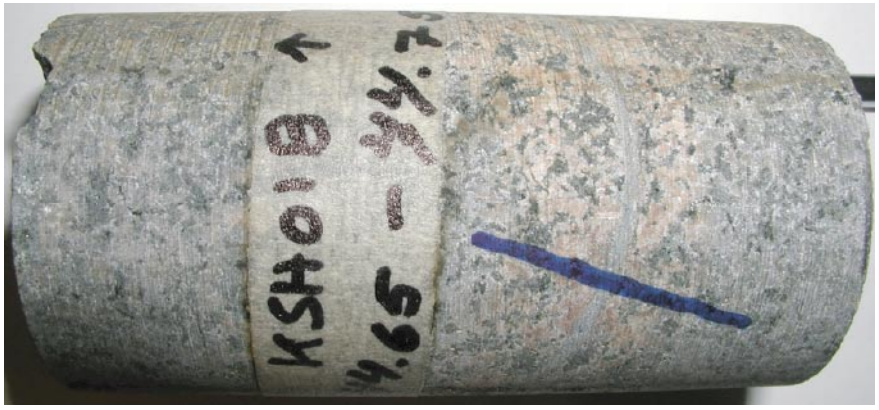

Figure 8-19. *Photograph of the drill-core sample from 44.65–44.75 m, showing red-staining of the wall-rock adjacent to a prehnite filled fracture. Drill-core is 5 cm in diameter.*

Both oxidised and un-oxidised wall rock occur also surrounding the old hydrothermal fractures and it is observed that fractures carrying early formed pyrite (generation 2; coarse-grained and idiomorphic) may have more fresh biotite and hornblende in the wall rock Another difference is that the red-staining evidently is more common in the wall rock next to fractures filled with epidote mylonite and prehnite than it is next to fractures occupied by idiomorphic quartz or quartz mylonite. This infers that the oxidising fluids are related to the epidote mylonite and that the oxidising may have continued throughout the formation of the prehnite filled fractures of generation 3. This further infers that some time difference has been present between the formations of the three different fillings in generation 2 and that the time difference between the epidote mylonite and the prehnite is not that big. The red-staining may however be related to the prehnite alone since the epidote-mylonite have only been observed in large quantities in fractures that have been re-activated and sealed by prehnite.

The quartz crystals in the wall rock are partially altered and are showing undulose extinction and in rare cases even sub-grain formation.

8.10 Generation summary

Generally, the whole scheme of thse different fracture filling generations resemble a series of gradually lower forming temperatures. The rock unit included in the drill core has visibly been exposed to deformation and a gradual filling of newly formed or re-activated fractures at several different events. Each of the events causing the fractures are characterised by the different pressure-temperature conditions, prevailing at the time. After the crystallisation of the magma and the formation of the early quartz filled fractures of generation 1, the rock unit has evidently been exposed to ductile deformation at pressure-temperature conditions in accordance to the greenschist facies, with temperatures in the range of 400–550°C. Further on, the rock has been exposed to prehnite-pumpellyite facies with temperatures < 400°C. The prehnite generation marks the definite end of the extensive wall rock alteration, including chloritization of biotite and widespread oxidation causing red-staining of the wall rock. In a period subsequent to the greenschist-facies ductile deformation conditions and the brittle deformation responsible for the prehnite filled fractures, semi-ductile to brittle deformation induced the fractures filled with the hematite-cataclasite of generation 5. The mineral-paragenesis of the hematite-cataclasite is of characteristic low-temperature origin but the lack of prehnite and zeolites makes a more precise classification of the temperature-pressure conditions difficult to establish. At one or several events postdating the hematite-cataclasite, minerals of gradually lower formation temperatures began to occupy the fractures. The appearance of different zeolites confirms that the fillings have been formed at zeolite facies pressure-temperature conditions. Furthermore, the conditions shifted from oxidising to reducing, demonstrated by the growth of pyrite. A summary of the mineral parageneses is listed below in Table 8-1.

Table 8-1.

1	Quartz, coarse-grained ***(Post-magmatic circulation)***
2	I) Re-crystallised quartz – idiomorhic pyrite, calcite
	II) Quartz-mylonite, muscovite, chlorite
	III) Epidote-mylonite, (Fe/Mg-chlorite), (calcite) ***(Greenschist-facies)***
3	Prehnite (fluorite) (Fe/Mg-chlorite) ***(Prehnite-pumpellyite facies)***
4	Calcite (Fe/Mg-chlorite)
5	Hematite-cataclasite: adularia, Mg-chlorite, hematite, (spherulitic Fe/Mg-chlorite) ***(Prehnite-pumpellyite/zeolite facies ?)***
6-1	Calcite
6-2	Quartz (albite)
6-3	Fine grained adularia, Mg-chlorite, apatite, laumontite, (hematite) (calcite)
6-4	Hematite, Fe-chlorite, harmotome, pyrite, (adularia) (calcite) (fluorite)
6-5	Calcite, Mixed-layer clay (chlorite, illite, smectite), (REE-carbonate) ***(Zeolite-facies to Surface Conditions ?)***

As shown in Table 8-2, one of the same fracture mineral was formed at different events. The results in the table further visualise the suggestion of gradually lower forming temperatures for the different fracture filling generations.

Table 8-2. Note that the hematite in generation 2 is only present in the wall rock.

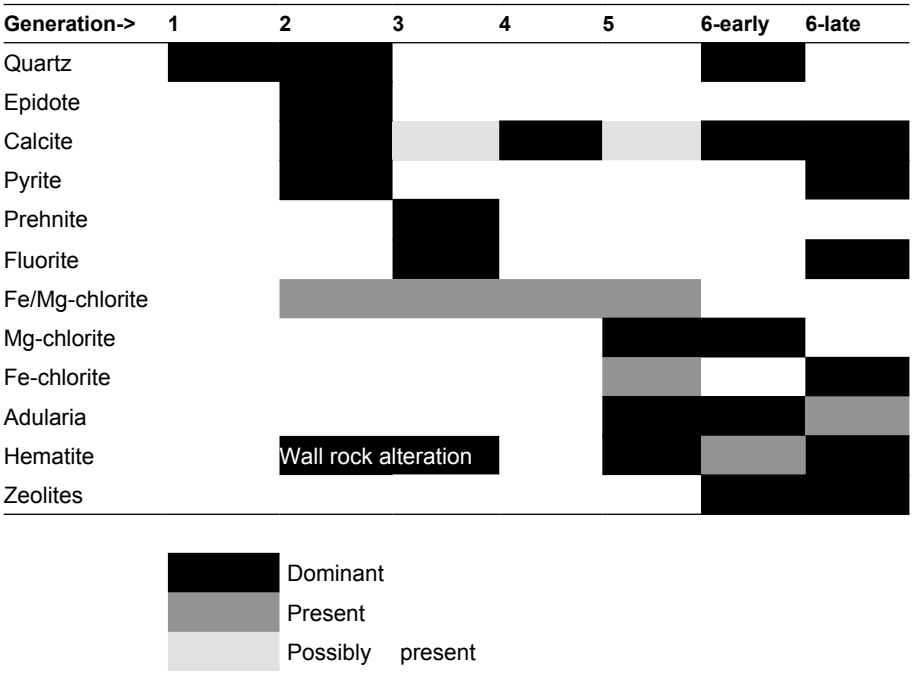

Most significant in this table is the existence of chlorite and calcite in roughly every generation. The crystals of different generations can be distinguished by chemical signatures and a change in crystal textures but also by different parageneses. The different chlorite generations can be recognized through the change in the Mg/Fe ratio and the different colours and textures of each different phase. As mentioned earlier the chlorite changes from Fe/Mg-chlorite (analyses: Fe/Mg-Chlorite) to a more spherulitic Fe/Mg-variety (analysis: Fe/Mg-Chlorite(sph)) in generation 5. Further on, the chlorite changes from Fe/Mg-chlorite to an Mg-rich chlorite (analyses: Mg-Chlorite) and eventually it changes to the Fe-rich variety (analyses: Fe-Chlorite) present from generation 6-4. The different calcite generations can be distinguished by the change in MnO_2, Sr isotope-ratio and O-and C -isotopes values The MnO_2-content in the calcites examined by SEM/EDS are usually below the detection limit for the SEM (< 0.1 wt %), but exceptions have been found in generation 2 (MnO_2 = 0.7–1.0%) and late in generation 6 (MnO_2 0.7–2.0%). The Sr isotope values show a general increace from the oldest to the youngest generation which indirectly confirms the geological interpretation and also points to a significant difference in age between e.g. generation 2 and 6. Furthermore, the extention in time possibly from Mid Proterozoic to present is indicated by the large span in Sr-isotope values within the calcites of generation 6 to recent. The $\delta^{18}O/\delta^{13}C$ values broadly confirm the sequence of events, and also underline that low temperature water have made significant contributions relatively early in the history (generation 4).

9 Reducing/Oxidising conditions

Indications of reducing and oxidising conditions are in this study partly demonstrated by the presence of pyrite (reducing conditions) and hematite (oxidising conditions). Both minerals can be formed at hydrothermal and low temperature conditions. Further indications on whether the conditions have been reducing or oxidising is gained from the analyses of the manganese content in calcites. Calcites formed in reduced conditions frequently contain detectable amounts of manganese (> 0.2 wt % MnO_2) often up to 1–2%, where Mn^{2+} substitute for Ca^{2+}. It can e.g. not be concluded that low Mn content necessarily is due to oxidising conditions, whereas high Mn content is a more reliable indicator of reducing environment. Figure 9-1 shows the abundance of pyrite and hematite in the different generations. Also included in the figure is the manganese-content in the calcites of the different generations.

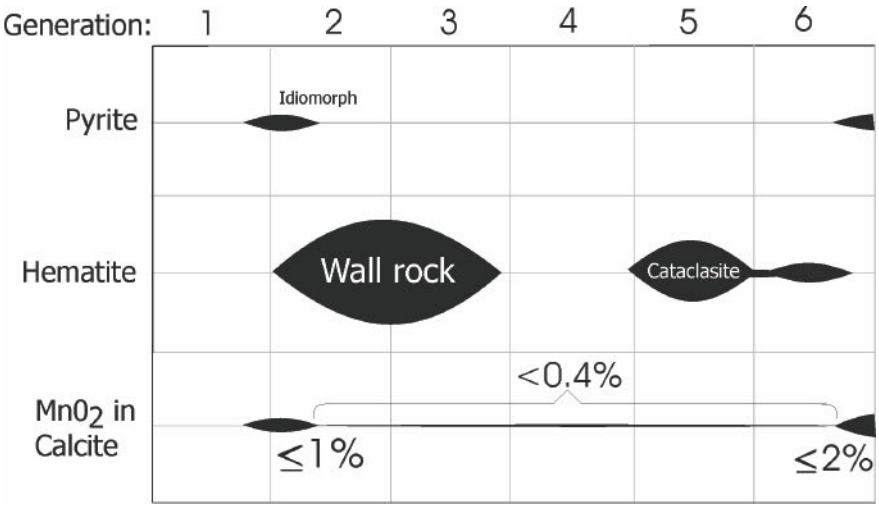

Figure 9-1. *Scheme showing the abundance of pyrite and hematite in the different generations. The abundance of each mineral is proportional to the vertical extension of the marker. The scheme also displays the different manganese contents throughout the different calcite generations, where the vertical extension of the marker indicates the average manganese content in each generation and not the abundance of calcite.*

The figure displays that reducing conditions, indicated by the existence of pyrite and possibly also by the existence of Mn-rich-calcite, have been prevailing in a phase earlier than the extensive oxidation of the wall rock. This red-staining of the wall rock is the earliest indication of oxidising conditions and is thought to have been contemporary with generation 2 and/or generation 3. This is thought to have been the most extensive oxidising conditions throughout the history of the rock unit although it has only been confirmed in the wall rock adjacent to fractures. Generation 4 lacks both pyrite and hematite but the low manganese content in the calcites might mark this event as an event where oxidising conditions still prevailed. Oxidising conditions have further been confirmed in generation 5, displayed by the dark red coloured hematite-cataclasite, which is concentrated in fractures and fracture zones. This hematite-cataclasite has clearly been formed later than the red-staining event in generation 2/generation 3. Indications of oxidising conditions have however been observed early in generation 6,

clearly later than the hematite-cataclasite, confirmed by the presence of micro-grains of hematite and also by low contents of manganese in calcite. Sometime during the late stages of generation 6 the conditions changed from oxidising to reducing. This change in conditions is demonstrated by the lack of hematite and the presence of pyrite and also by high manganese contents in calcite. The manganese content can rise up to 2% MnO_2 but MnO_2-contents of 0.7–1.0% are more common. Since the calcites have been formed more or less continuously throughout generation 6 the correlation of the calcites with different manganese-contents to the hematite and pyrite observations is somewhat imprecise. The reducing conditions are thought to represent the current conditions in the rock unit. This is in agreement with the results from U-series analyses from the Äspö area presented in /Tullborg et al. 2004/, where oxidising conditions were only detected in the uppermost 15–20 m of the bed rock

10 Relation to different fracture orientations

A minor part of the study was the task of relating different fracture filling generations to different fracture orientations. The relatively small amount of fractures studied in this work, makes a more statistically precise model practically unachievable. Some trends can be distinguished but a more widespread study is essential for a decent analysis. Table 10-1 shows the orientation of the fractures occupied with the most common minerals in this study. The amount of fractures with a specific orientation is indicated by a number. More detailed values for the strike/dip of each of the fractures can be found in the appendix (thin-section and fracture surface-sample description).

The information from the table shows that prehnite and epidote often occupy fractures with similar orientation. The prehnite is often filling fractures formed from re- activated of epidote-mylonite but single fractures of prehnite are also present. The calcites of the different generations and quartz of generation 2 are filling fractures of similar orientations. The calcites of generation 2 are characteristically related to quartz crystals. The calcites may have been formed from reactivation of fractures that have been filled with earlier formed calcite. The earlier formed calcite in the fracture may have been dissolved and new calcites have been formed from precipitation of the Ca^{2+}-rich solutions still present in the fracture.

Table 10-1. Orientation fractures occupied with some of the most common fracture minerals.

Mineral(s):	Several observations	Few observations
Prehnite	NNW-NNE to SSE-SSW (7)	ENE-WSW (1)
Epidote	NNW-NNE to SSE-SSW (4)	ENE-WSW (1)
Calcite – generation2	N-S to NE-SW (7)	E-W (1), NW-SE (1)
Calcite – generation4	N-S to NE-SW (2)	
Calcite – generation6	N-S to NE-SW (2)	
Quartz	N-S to NE-SW (2)	
Hematite-cataclasite		N-S, NW-SE, NE-SW, E-W
Harmotome		NW-SE (1)

11 Relation to geological events

To be able to relate the different generations to certain geological events, a model showing the subsidence and uplift of the region is a crucial tool. The model (Figure 11-1) used in this study was maintained by /Tullborg et al. 1996/ and gives an indication of the pressure-temperature conditions prevailing throughout the history of the region. The present land surface has been subjected to repeated subsidence and uplift, caused by several events of e.g. burial through sediment covering and subsequent erosion.

The model provides information of at least four events related to subsidence of the region ("A–B", E, G, H). The first event ("A–B"), marked by ductile deformation, responsible for the E-W foliation/lineation and the formation of the mylonites in generation 2, is positioned in a period of 1.8–1.4 Ga /Larson et al. 1990; Munier 1993; Wikman and Kornfält 1995/. K-Ar datings of biotite indicate that the E-W ductile deformation is older than 1.5 Ga /Åberg, 1978; 1988/. The 1.4 Ga anorogenic Götemar granite (C), is considered to have been intruding at relatively shallow depths, which infers that the present rock surface of the region was situated at depths of about 2 km at the time /Kresten and Chyssler 1976; cf Åberg et al. 1984; Smellie and Stuckless 1985; Åberg 1988/. Subsequent to both the Sveconorwegian and Caledonain orogens, thick layers of sediments is beleaved to have covered the surface of the region, subsiding the present rock surface to depths of approximately 8 km (E) and 4 km (G), respectively /Tullborg et al. 1996/. The depths are estimated from fission-track studies in the Oskarshamn region, showing 250 ± 50°C at 820 ± 88 Ma (E) and 130 ± 20°C at 375 ± 20 Ma (G) /Tullborg et al. 1996/.

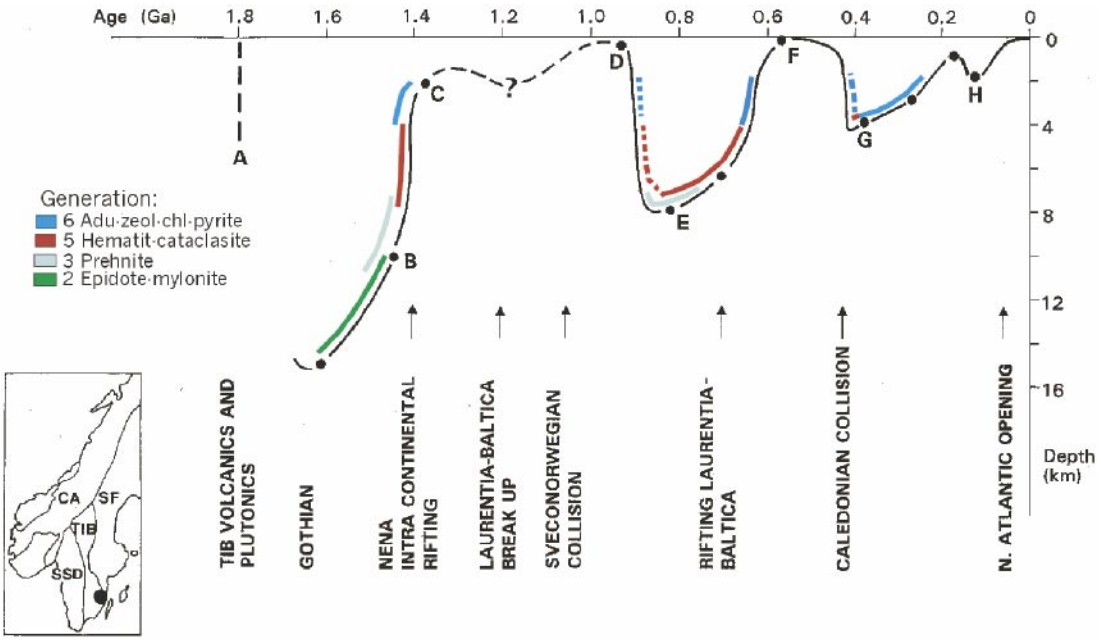

Figure 11-1. *Reworked figure of subsidence and uplift of the present land surface in the Oskarshamn-Västervik area from /Tullborg et al. 1996/. Inserted are possible fracture-filling-events for the different generations. A. Intrusion of the TIB granitoids (the Gothian event). B. K-Ar ages of biotite in TIB granitoids. C. Intrusion of the Götemar Granite. D. Intrusions of dolerite into unconsolidated Almesåkra conglomerate. E. Titanite fission-track ages. F. Sub-Cambrian peneplain. G. Apatite fission-track ages. H. Cretaceous marine sedimentation.*

These events were both followed by intense erosion followed by uplift of the bedrock, shown by gradually lower fission-track temperatures /Tullborg et al. 1996/. At lower Cambrian (F), in-between the two orogens, the rock surface, referred to as the Sub-Cambrian peneplane, coincided with the present rock surface /Lidmar-Bergström, 1991/. Furthermore, the transgression in Cretaceous time (H), is thought to have been adding sediments that buried the present rock surface to depths of maximum 2 km /Tullborg et al. 1996/.

If the formation temperatures of the minerals in the different generations are correlated to the model provided by /Tullborg et al. 1996/, a new model can be constructed (inserted coloured lines in Figure 11-1.). This new model provides crucial information concerning the possible events where the minerals of the different generations could have been formed. Eventually these correlations give useful suggestions to the geological history of the region. The formation temperature interval of the different generations has been roughly estimated from information provided by /Blatt and Tracy, 2000, Figure 11-2/ and mineralogical data from /Nesse, 2000/ and /Deer et al. 1992/ and references therein.

These intervals have been related to the formation temperatures of the different minerals and are only to be seen as hypothetical. The correlation between depth and temperature is one of the major dilemmas since the value of the geothermal gradient at the different events is unknown. This uncertainty is one of the reasons why the interval of the different generations in the model are somewhat overlapping.

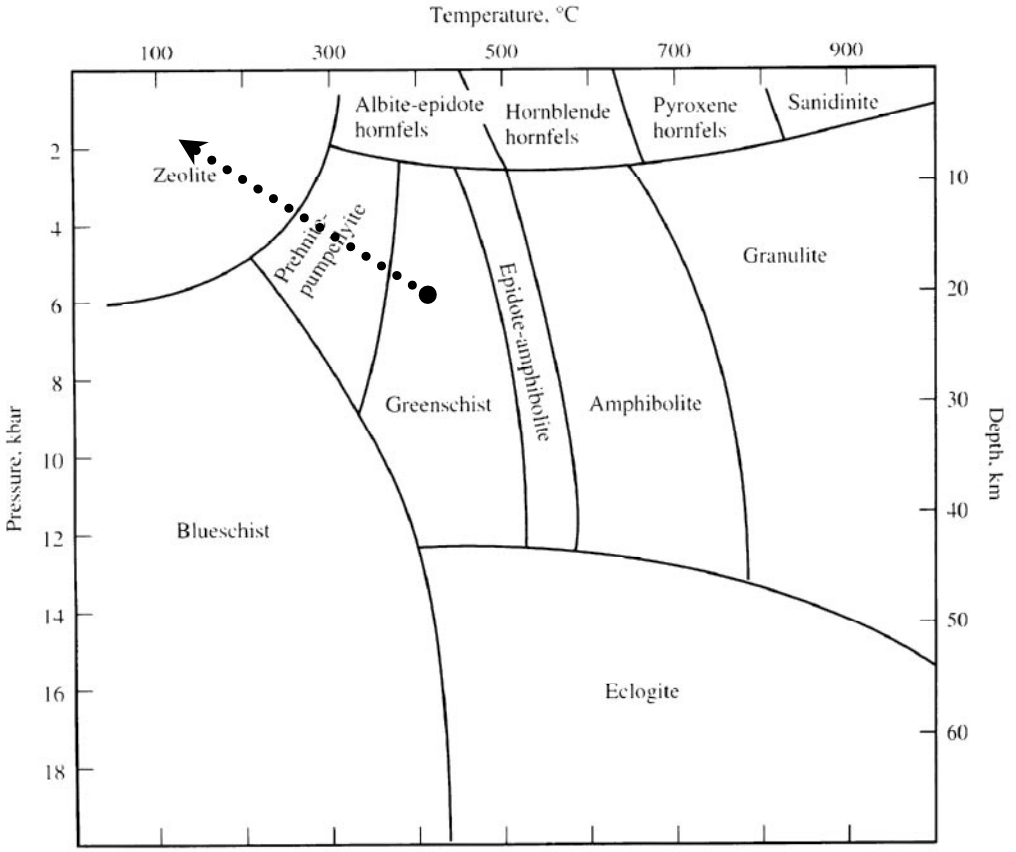

Figure 11-2. *P-T diagram showing the metamorphic facies, from /Blatt and Tracy, 2000, p. 378/. Inserted is a suggested path for the rock unit since formation, as revealed by the fracture mineralogy.*

Generation 1 and generation 4 are left out of this model since the dominating minerals in these generations, quartz and calcite, respectively, are not formed in well defined temperature-spans. The calcite and the quartz have also been formed at several different events. All of the possible depths where the minerals in the different generations have been formed are taken into consideration in this model.

The model gives further implications of gradually lower temperature origin of the different fracture filling generations. The model shows that the epidote-mylonite of generation 2 has been formed at a fairly well confined event, roughly at 1.6–1.45 Ga. The prehnite of generation 3 might have been formed at an event close to the epidote-mylonite (at "B" in Figure 11-1) but the formation temperature of prehnite may also infer formation at an event related to the erosion of the Sveconorwegian mountains ("E" in Figure 11-1). The issue is whether the sediment layers where thick enough to depress the present rock unit into prehnite-pumpellyite facies. The determination of the prehnite formation is crucial for the distinction of later formed generations. If the prehnite was formed at "E" the subsequent generations must have been formed later than 900 Ma. If the prehnite was formed at "B" the optional formation of the subsequent generations is less defined, with a span of possible formation of up to 1.5 billion years.

The hematite-cataclasite, consisting of low-temperature minerals like adularia, of generation 5 may have been formed prior to the intrusion of the 1.4 Ga. Götemar granite. It may also have been formed subsequent to the Sveconorwegian orogeny (D–F) and less likely subsequent to the Calcedonian orogeny (G), inferred by the lack of zeolites. As mentioned earlier, the position of the hematite-cataclasite in the model is dependent on the formation of the prehnite.

The low-temperature minerals in generation 6 may theoretically have been formed at several different events. The zeolites laumontite and harmotome confirm the low-temperature origin and position the formation of the generation at lower temperatures than the hematite-cataclasite. The presence of several generations of adularia might suggest that the adularia have been formed and re-crystallised at several events of subsidence and uplift. Observations of re-crystallisation of low-temperature K-feldspar and albite, related to subsidence and uplift caused by shallow burial from sedimentation have been observed by /Hagen et al. 2001/ and /Lee and Parsons, 1997/. The positions in the model, that indicate where the formation of the minerals of generation 6 might be theoretically possible, might not be reliable. If the zeolites where formed previous to the Götemar intrusion, they would surely have been dissolved and completely altered at the event subsequent to the Sveconorwegian orogeny. This is particularly true for the crystals situated in open fractures and for harmotome in particular, which has a lower formation temperature than laumontite. Laumontite crystals may have "survived" the Sveconorwegian event but the presence of unaltered harmotome in open fractures and the fact that observations of fairly contemporary harmotome and laumontite, may suggest that the minerals in generation 6 have been formed later than 700 Ma. Except for late calcite, pyrite, near surface Fe-oxyhydroxides and possibly some clay minerals /Tullborg, 1997/, the minerals in generation 6 have probably not been formed later than 300 Ma indicated by dating of illite minerals made by /Maddock et al. 1993/. However, as indicated from e.g. stable isotope results it is obvious that redistribution of calcites caused by meteoric and brackish water circulation have occurred at least down to 500 m depth and in some cases as deep as 1,000 m in the Äspö/Laxemar area /Tullborg, 2004/.

12 Summary

The fracture mineralogy as revealed in drill-core KSH01 shows several generations of mineralization. On the whole, the fracture mineralogy in KSH01 shows a decreasing temperature series, from greenschist facies to zeolite facies, although evidently formed during several events. The prevailing deformation inducing the fractures has also been changing through time, with an early ductile phase followed by brittle deformation. Indications of oxidising or reducing conditions have been recorded from the presence of hematite and pyrite, respectively. These indications interpret that reducing conditions prevailed at least during two phases; one early in the geological history and one beginning contemporaneously with the latest formed fracture fillings and is probably still prevailing. Oxidising conditions prevailed in between these phases, recorded by two events of extensive hematite formation, in the wall rock and in restricted fracture zones, respectively. The present reducing conditions are supported by presence of pyrite on the outermost fracture coatings and by the calcites showing signs of biogenic processes in situ.

An attempt to relate the different generations to geological events has been made by combining the characteristics of each mineral paragenesis (e.g. formation temperatures) with existing models of subsidence and uplift of the present land surface, contributed by Tullborg et al. 1996. This evaluation gives suggestions of when the fracture fillings of the different generations could possibly have been formed. It also gives implications of that the generations have been formed at several more or less restricted events, instead of at one continuous event.

13 Acknowledgement

We would like to thank the staff at the SKB site investigations at Simpevarp for their support. Owe Gustafsson at Geovetarecentrum in Göteborg has carried out the O and C isotope analyses and the ICP-MS analyses on the calcite leachates. Cees-Jan de Hoog is thanked for carrying out laser ICP-MS analyses Kjell Helge and Ali Firoozan have carried out the sample preparation

14 References

Andersson P, Byegård J, Dershowitz B, Doe T, Hermanson J, Meier P, Tullborg E L, Winberg A, 2002. Final report of the TRUE Block Scale. 1. Characterisation and model development. SKB TR-02-13. ISSN 1404-0344. Svensk Kärnbränslehantering AB.

Blatt H, Tracy R J, 2000. Petrology: igneous, sedimentary, and metamorphic, W.H Freeman and Company, 529 pp.

Bath A, Milodowski A, Ruotsalainen P, Tullborg E-L, Cortés Ruiz A, Aranyossy J-F, 2000. Evidences from mineralogy and geochemistry for the evolution of groundwater systems during the quaternary for use in radioactive waste repository safety assessment (EQUIP project). EUR report 19613.

Deer W A, Howie R A, Zussman J, 1992. An introduction to the rock forming minerals. Longman Scientific & Technical. 696 pp.

Didriksen K, Stipp S L S. In manuscript: Iron-oxides in fractures at Äspö. SKB. Svensk Kärnbränslehantering AB.

Drever S-I, 1973. The preparation of oriented clay mineral specimens for X-ray diffraction analysis by a filter-membrane peel technique. – Am. Miner, 58, 553–54.

Eliasson T, 1993. Mineralogy, geochemistry and petrophysics of red-coloured granite adjacent to fractures. In: SKB TR 93-06. 68 pp. Svensk Kärnbränslehantering AB.

Ehrenborg J, Stejskal V, 2004. Bore mapping of core drilled boreholes KSH01A and KSH01B, Oskarshamn Site Investigation, SKB P-04-01. Svensk Kärnbränslehantering AB.

Gaál G, Gorbatchev R, 1987. An outline of the Precambrian evolution of the Baltic Shield. Precambrian Research 35, 15–52.

Hagen E, Kelley S P, Dypvik H, Nilsen O, Kjölhamar B, 2001. Direct dating of authigenic K-feldspar overgrowths from the Kilombero Rift of Tanzania, Journal of Geological Society, London, Vol. 158, 801–807.

Kornfält K A, Persson P O, Wikman H, 1997. Granitoids from the Äspö area, SE Sweden – Geochemical and Geochronological data. Geologiska Föreningens i Stockholm Förhandlingar 119, 109–114.

Kornfält K-A, Wikman H, 1987. Description of the map of solid rock around Simpevarp. SKB Progress Report 25-88-12. 45 pp. Svensk Kärnbränslehantering AB.

Kornfält K-A, Wikman H, 1988. The rocks of the Äspö island, Description to the detailed maps of solid rocks including maps of 3 uncovered trenches. In: SKB Progress Report 25-88-12. Svensk Kärnbränslehantering AB.

Kresten P, Chyssler J, 1976. The Götemar massif in south-eastern Sweden. Geologiska Föreningens i Stockholm förhandlingar 98, 155–161.

Laaksoharju M, Smellie J A T, Gimeno M, Auqué L, Gómez J, Tullborg E-L, Gurban I, 2004. Hydrogeochemical evaluation of the Simpevarp area, model version 1.1. SKB R-report R-04-16. Svensk Kärnbränslehantering AB.

Landström O, Tullborg E-L, Eriksson G, 2001. Effects of glacial/post-glacial weathering compared with hydrothermal alteration – implications for matrix diffusion. Results from drillcore studies in porphyritic quartz monzodiorite from Äspö SE Sweden. SKB R 01-37. 60 pp. Svensk Kärnbränslehantering AB.

Larson S-Å, Berglund J, Stigh J, Tullborg E-L, 1990. The Protogine Zone, Southwest Sweden: A new model – An old issue. In C.F. Gower, T. Rivers & A.B. Ryan (eds.): Mid-Proterozoic Laurentia-Baltica, 317–333. Geological Association of Canada, Special Paper 38.

Larson S Å, Berglund J, 1992. A geochronological subdivision of the Transscandinavian Igneous Belt – three magmatic episodes? Geologiska Föreningens i Stockholm Förhandlingar 114, 459–461.

Lee M R, Parsons I, 1997. Dislocation formation and albitization in alkali feldspars from the Shap granite, American Mineralogist, Volume 82, 557–570.

Lidmar-Bergström K, 1991. Phanerozoic tectonics in southern Sweden. Zeitschrift für Geomorphologie N.F. 82, 1–16.

Lindström M, Lundqvist J, Lundqvist Th, 1991. Sveriges geologi från urtid till nutid. 398 pp. Studentlitteratur.

Maddock R H, Muir Wood R, Hailwood E A , Rhodes E J, 1993. Direct fault dating trials at the Äspö Hard Rock Laboratory. SKB TR 93-24. 189 pp. Svensk Kärnbränslehantering AB.

Milodowski A E, Gillespie M R, Pearce J M, Metcalfe R, 1998b. Collabration with SKB EQUIP programme: Petrographic characterisation of calcites from Äspö and Laxemar deep boreholes by scanning electron mocroscopy, electron microprobe and cathodoluminescence petrography. BGS Technical Report WG/98/45C.

Munier R, 1993. Segmentation, fragmentation and jostling of the Baltic shield with time. Thesis, Acta Universitatis Upsaliensis 37, 1–96

Nesse W D, 2000. Introduction to Mineralogy, Oxford University Press, 442 pp.

O´Neil J R, Clayton R N, Mayeda T K, 1969. Oxygen isotope fractionation in divalent metal carbonates. J. Chem. Phys. 51, 5547–5558.

Parsons I, 1978. Feldspars and fluids in cooling plutons. Mineralogical Magazine, vol. 42, 1–17.

Smellie J A T, Stuckless J S, 1985. Element mobility studies of two drill-cores from the Götemar granite, southeast Sweden. Chem. Geol. 51, 55–78.

Stanfors R, Rhén I, Tullborg E-L, Wikberg P, 1999. Overview of geological and hydrogeological conditions of the Äspö hard rock laboratory site, Applied Geocemistry 14, Pergamon, 819–834.

Tullborg E-L, 1988. Fracture fillings in the drillcores from Äspö and Laxemar. In: Wikman,.H, Kornfält, K.-A, Riad, L, Munier, R, Tullborg E.-L, 1988: Detailed investigations of the drillcores KAS02, KAS03 and KAS04 on Äspö Island and KLX01 at Laxemar. SKB PR 25-88-11. 30 pp. Svensk Kärnbränslehantering AB.

Tullborg E-L, 1997. Recognition of low-temperature processes in the Fennoscandian shield. PhD-thesis, Department of Geology, Göteborg University, Earth Sciences Centre, A17, 200 p.

Tullborg E-L, 2003. Palaeohydrogeological evidences from fracture filling minerals – Results from the Äspö/Laxemar area. MRS vol 807, Scientific basis for Nuclear Waste Management XXVII pp. 873–878.

Tullborg E-L, Larson S Å, Stiberg J-P, 1996. Subsidence and uplift of the present land surface in the souteastern part of the Fennoscandian Shield. Geologiska Föreningens i Stockholm Förhandlingar 118, 126–128.

Tullborg E-L, 2004. Palaeohydrogeological evidences from fracture filling minerals_ Results from the Äspö/Laxemar area. Mat. Res.Soc. Symp. Vol 807, pp 873–878.

Tullborg E-L, Smellie J A T, MacKenzie A B, 2004. The use of natural uranium series studies in support of understanding redox conditions at potential radioactive waste disposal sites. Mat. Res. Soc. Symp. Proc. Vol 2004, pp 571–576.

Wallin B, Peterman Z, 1999. Calcite fracture fillings as indicators of palaeohydrogeology at Laxemar at the Äspö Hard Rock Laboratory, southern Sweden. Applied Geochemistry, vol 14, pp 953–962.

Wahlgren C-H, Hermanson J, Curtis P, Forssberg O, La Pointe P, Tullborg E-L, 2004. Chapter 7: Resulting description of the Simpevarp subarea, In: Preliminary site description Simpevarp area – version 1.1. SKB R-04-25, 465 pp. Svensk Kärnbränslehantering AB.

Wikman H, Kornfält K-A, 1995. Updating the geological model at Äspö. SKB PR 2595-04, 42 pp. Svensk Kärnbränslehantering AB.

Wikström A, 1989. General geological-tectonic study of the Simpevarp area with special attention to the Äspö island. In: SKB Progress Report 25-89-06. Svensk Kärnbränslehantering AB.

Åberg G, 1978. A geochronological study of the Precambrian of southeastern Sweden. Geologiska Föreningens i Stockholm Förhandlingar 100, 125–154.

Åberg G, 1988. Middle Proterozoic anorogenic magmatism in Sweden and worldwide. Lithos 21, 279–289.

Åberg G, Löfvendahl R, Levi B, 1984. The götemar granite – isotopic and geochemical evidence for a complex history of an anorogenic granite. Geologiska Föreningens i Stockholm Förhandlingar 106, 297–400.

Åhäll K-I, 2001. Åldersbestämning av svårdaterade bergarter i sydöstra Sverige. SKB R-01-60, 28 pp. Svensk Kärnbränslehantering AB.

Åhäll K-I, Larson S Å, 2000. Growth-related 1.85-1.55 Ga magmatism in the Baltic Shield; a review addressing the tectonic characteristics of Svecofennian, TIB 1-related and Gothian events. Geologiska Föreningens i Stockholm Förhandlingar 122, p 193–206.

Appendix

A1 Thin-section descriptions

("* %" = below detection limit, SEM)

11.60–11.80 m:

Rock type: Quartz monzodiorite, equigranular to weakly porphyritic
Fracture: Closed, width: 10–14 mm
Orientation: 178°/73°

Minerals: Prehnite, Calcite, Epidote, Chlorite, Titanite, Quartz, Adularia, (Albite)

Order:

1. Idiomorphic quartz, calcite, titanite.
2. Epidote mylonite with a matrix of fine-grained epidote and earlier coarse-grained idiomorphic crystals of quartz, calcite and titanite, which have all been replaced by fine-grained epidote appearing as pseudomorphs of the earlier crystals.
3. Idiomorphic prehnite, fine-grained to coarse-grained. The epidote filling has been brecciated and prehnite is filling the space between the epidote fragments. The prehnite crystals are slightly dissolved.
4. Calcite (*% MnO_2), minor amount in prehnite.
5. Chlorite (Mg-rich, MgO: 22%, FeO: 12–16%), spherulitic, and fine-grained adularia, in dissolved cavities in prehnite. Also present are really small grains of an unidentifiable mineral with 6–8% BaO. The grains are too small for a reliable analysis.

Notable: Titanite appears as an individual fracture filling penetrated by prehnite. The crystals are elongated parallel to the orientation of the fracture. Small veins of fine-grained albite are also present.

Wall-rock alteration: Numerous red-stained and altered plagioclase crystals. Some k-feldspar crystals are also reddish but they appear to be less altered than the plagioclase. There are some chlorite and epidote crystals present. Some amphiboles remain but biotite does not.

Visible macroscopically: Prehnite is later than epidote and is using the same fracture as epidote. Prehnite is younger than the red coloured alteration of the wall-rock, adjacent to the fracture.

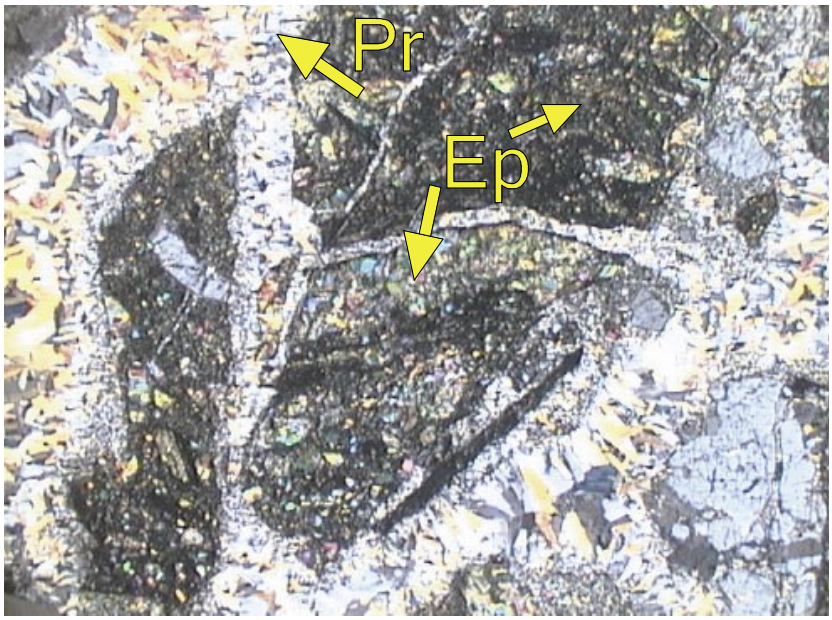

Figure A-1. *Idiomorphic crystals of prehnite (Pr) penetrating epidote mylonite (Ep). Photomicrograph, width c 5 mm.*

24.00–24.10 m (1):

Rock type: Quartz monzodiorite, equigranular to weakly porphyritic
Fracture: 2 Closed
Orientation: (1 Vertical + 1 horizontal)

Minerals: Quartz, Prehnite, Calcite, Epidote, Chlorite, Titanite, Fluorite, Pyrite, Adularia

Order:

1. Fine-grained quartz mylonite, elongated. Turning from more coarse-grained to more fine-grained and rounded crystals.
2. Epidote, idiomorphic in prehnite and wall-rock, not in quartz.
3. Idiomorphic prehnite, cuts quartz and penetrates epidote.

Postdates prehnite:

1. Calcite (MnO_2 = *%).
2. Chlorite (Mg-rich, FeO: 11–12%, MgO: 20–22%), maybe same generation as calcite.
3. Fluorite.

Postdates quartz mylonite:

1. Prehnite, fluorite (fluorite may be later), as fillings between the quartz crystals.
2. Chlorite (Mg-rich FeO: ~ 8% MgO ~ 23%), Pyrite, idiomorphic crystals.

Wall-rock alteration: The plagioclase crystals in the wall-rock have been saussuritized and sericitized. Red-stained with lots of chlorite, some allanite, lots of magnetite, but no biotite. Epidote is present, mostly as large crystals near the fractures.

Hypothetical order:

1. (Idiomorphic quartz).
2. Fine-grained quartz mylonite, re-crystallized, elongated.
3. (Epidote, idiomorphic).
4. Idiomorphic prehnite, fluorite.
5. Chlorite (Mg-rich, FeO: 8–12%, MgO: 20–23%) + some earlier Adularia.
6. Fluorite, single vein, Pyrite, idiomorphic crystals (may be of 5th generation).

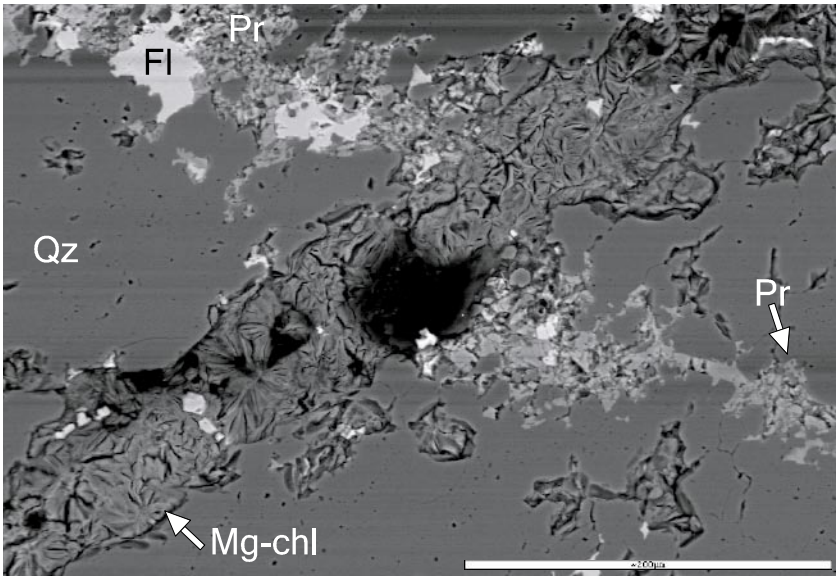

Figure A-2. *Quartz mylonite (Qz) has been penetrated by fine-grained prehnite (Pr) and fluorite (Fl). Mg-rich chlorite (Mg-chl) has later cut and offset the prehnite/fluorite vein. The black spot is carbon from the preparation of the thin-section. Backscattered electron image. Scale bar is 200 µm.*

24.00–24.10 m (2):

Rock type: Quartz monzodiorite, equigranular to weakly porphyritic
Fracture: Open, 4 mm fracture filling remaining
Orientation: (Vertical-subvertical)

Minerals: Pyrite, Chalcopyrite, Quartz, Prehnite, Calcite, Epidote, Chlorite, Titanite, Adularia, Fluorite

Order:

1. Idiomorphic pyrite with stains of chalcopyrite and idiomorphic quartz (with undulose extinction).
2. Fine-grained quartz, re-crystallised, almost mylonitic.
3. Epidote, idiomorphic and fine-grained.
4. Prehnite, cuts quartz.
5. Adularia, chlorite (Mg-rich, FeO: 5–15%, MgO: 18–24%), fluorite (fine-grained, in Mg-chlorite) and pyrite (fine-grained, in Mg-chlorite).

Notable: Titanite is present in pyrite, and is penetrated by epidote and later minerals. No relation to quartz has been noted.

Wall-rock alteration: Plagioclase has been altered (saussuritized) but k-feldspar remains fresh. Present are Chlorite, epidote (closer to the fracture) and also some remaining amphibole crystals. The wall-rock is not red coloured.

Visible macroscopically: Pyrite and quartz seems to be fairly contemporary.

44.65–44.75 m:

Rock type: Quartz monzodiorite, equigranular to weakly porphyritic
Fracture: Closed, 2–4 mm wide, red coloured wall-rock 1–2 cm on each side of the fracture.
Orientation: (Dip ~ 30–40°)

Minerals: Prehnite, Epidote, Quartz, Calcite, Chlorite, Titanite, Ilmenite, Pyrite

Order:

1. Idiomorphic quartz and epidote (pyrite).
2. Fine-grained epidote mylonite including fine-grained Fe/Mg-chlorite (few crystals, FeO: 21%, MgO: 17% – some titanites related to it), prehnite, calcite (MnO_2 = * % – few crystals).
3. Idiomorphic fine-grained to coarse-grained prehnite crystals, sometimes more mylonitic are cutting everything. Prehnite is also growing into old quartz grains in the epidote mylonite, replacing the quartz. Calcite (MnO_2 = * %) coarse-grained may be penetrated by prehnite. Titanite is present as thin fillings along the rim of the prehnite filled fracture.

Notable: Not easy to find any relation between 1 and 2 but this seems to be the most likely scenario.

Wall-rock alteration: Red coloured plagioclase is giving the wall-rock a red appearance. The quartz crystals are show signs of undulose extinction. Chlorite is present in the wall-rock as well as some amphibole crystals and some epidote crystals.

121.72–121.81 m:

Rock type: Quartz monzodiorite, equigranular to weakly porphyritic
Fracture: 2 closed fractures cutting one another at an angle of ~ 30°. Both fracture fillings are 1–2 mm thick
Orientation: (154°/26°)

Minerals: Epidote, Prehnite, Chlorite, Titanite, Apatite

Order:

1. Idiomorphic epidote and later idiomorphic chlorite in the wall-rock.
2. Epidote mylonite, with a matrix of fine-grained epidote. Also present in the matrix are earlier quartz and albite (may be from the wall-rock) + Fe/Mg- chlorite (with some titanite and apatite) which grows into the albite. Some ilmenite crystals form a diffuse filling – cutting the epidote.

3. Prehnite (fine-grained to coarse-grained/idiomorphic), partly dissolved, cutting the epidotes.
4. Chlorite (Mg-rich) is present in cavities in the dissolved prehnite.

Visible macroscopically: Prehnite filled fracture is clearly cutting older epidote filled fracture. The prehnite are apparently later than the red coloured alteration in the wall-rock.

Wall-rock alteration: Numerous red-stained and sericitized plagioclase crystals. Some k-feldspar crystals are also reddish but they appear to be less altered than the plagioclase. There are many chlorite (more some distance from the fracture) and epidote (closer to the fracture) crystals present. Some amphiboles remain but no biotite is visible.

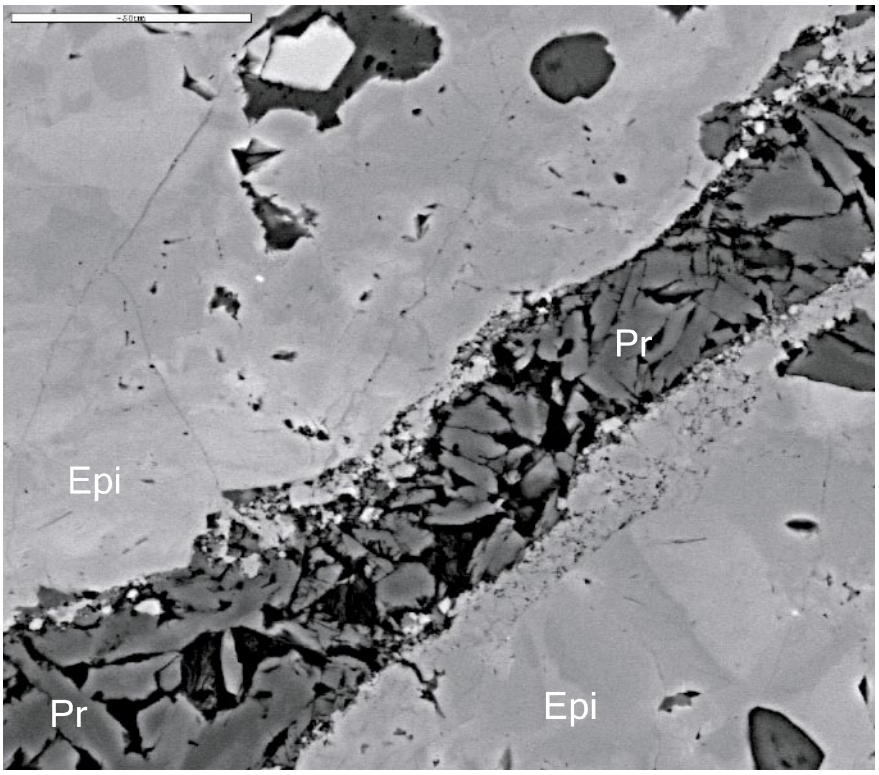

Figure A-3. *Fracture filling of idiomorphic prehnite (Pr) is cutting trough epidote mylonite (Epi). The prehnite crystals are partly dissolved. Backscattered electron image. Scale bar is 50 µm.*

130.83–131.19 m

Rock type: Quartz monzodiorite, equigranular to weakly porphyritic
Fracture: Open, cataclasitic, several closed fractures close to the open one
5–13 mm of fracture filling remaining
Orientation: 67°/65°

Minerals: Chlorite (3 generations), Calcite (2 generations), Epidote, Fluortie, Harmotome, Quartz, Titanite, Adularia

Order:

1. Idiomorphic Qz.
2. Re-crystalised Quartz and idiomorphic Calcite (MnO_2: * –0.7%).
3. Idiomorphic epidote (pseudomorphs of calcite etc). Fine-grained epidote (epidote-mylonite with idiomorphic epidote crystals in it).
4. Prehnite mylonite (both fine-grained and idiomorphic prehnite), with earlier idiomorphic and fine-grained epidote and quartz in it. Also veins of prehnite cutting through epidote, calcite and quartz. Fluorite is present in these veins.
5. Fe/Mg-chlorite (FeO: 26–28%, MgO 15–16%) spherulitic crystals with some related Titanite.
6. Calcite (MnO_2: *%) as a thin fracture filling, fluorite (small crystals).
7. Chlorite (Mg-rich; FeO: 19%, MgO: 21%).
8. Chlorite (Fe-rich; FeO: 18–21%, MgO: 11–12%), harmotome, both as thin fillings.

Notable: In prehnite-mylonite; Wall-rock minerals like k-feldspar, titanite, ilmenite are present. Adularia is present and at least younger than prehnite, epidote and idiomorphic calcite. It is difficult to decide whether “4” and “5” are of the same generation or not.

Wall-rock alteration: No wall-rock present.

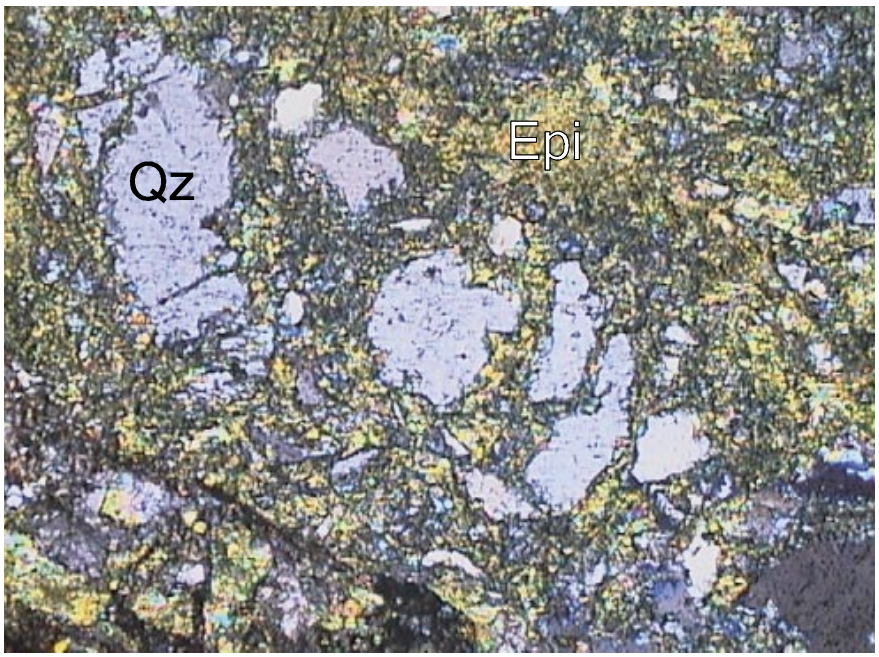

Figure A-4. *Fine-grained epidote (Epi) is penetrating through a big quartz (Qz) crytal. Photomicrograph, width c 1.25 mm.*

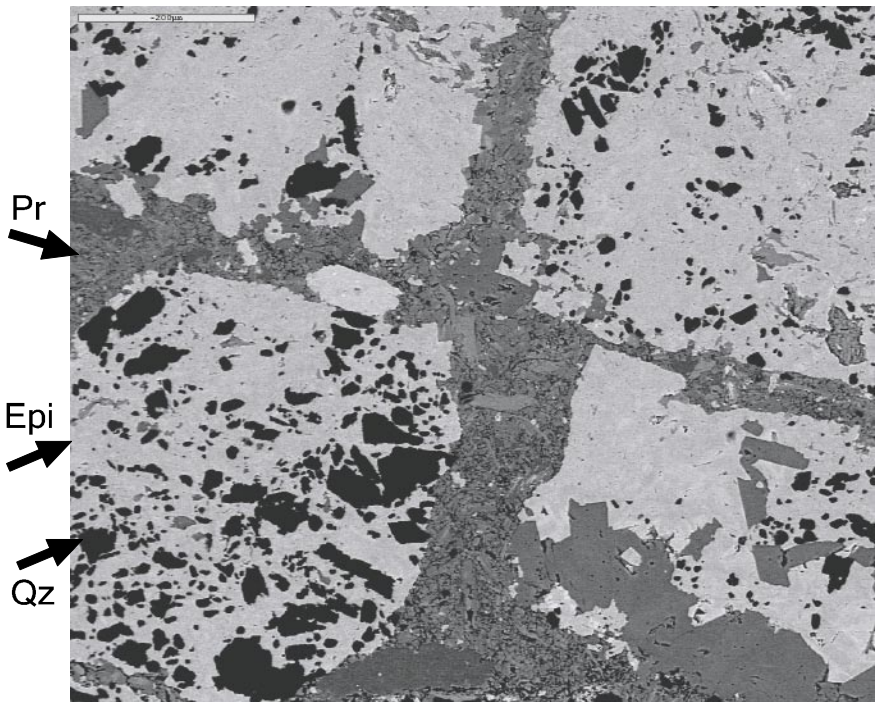

Figure A-5. *Fine-grained epidote (Epi) is surrounding older quartz (Qz) crystals. Two veins filled with fine-grained to idiomorphic prehnite (Pr) is cutting through the epidote. Backscattered electron image. Scale bar is 200 µm.*

198.00–198.10 m:

Rock type: Quartz monzodiorite, equigranular to weakly porphyritic
Fracture: Open, 2–16 mm fracture filling remaining
Orientation: 142°/31°

Minerals: Calcite, Albite, Adularia, Apatite, Chlorite (2 generations), Titanite

Two distinct groups of somewhat related minerals (not in order):

1. Calcite, scalenoedral (MnO_2 = * –0.93%) and albite
2. Fine-grained filling of (in order of appearance):
   - Adularia.
   - Apatite.
   - Mg-rich Chlorite (FeO: 9–12%, MgO: 19–22%). This chlorite trends to a more Fe-rich chlorite as it grows larger and more fibrous (FeO: 22%, MgO: 12%).
   - Red staining due to intensive oxidation. Small hematite grains coat silicate grains, making the silicates impossible to determine.

Notable: Not easy to make out the relation between the two groups. Also present are Fe/Mg-chlorite (FeO: 21%, MgO: 16%) with titanite. The chlorite is at least older than "2".

Wall-rock alteration: Red-stained and green-dotted by Fe and Chlorite respectively. The plagioclase crystals have been intensely red coloured and some k-feldspar crystals have also been red coloured. No biotite is present. Titanites are present in large amounts, but they have been altered by chlorite. The chlorite are of Fe/Mg composition (FeO: 25%, MgO: 16%) and is cut by adularia and albite. The chlorite has also been red coloured. Red coloured alteration are reaching far from the fracture (at least > 10 cm). No epidote is present in the wall-rock.

Visible macroscopically: Big scalenoedral calcite crystals are visible to the naked eye.

Figure A-6. *Photo of the drill-core, showing the open fracture with big calcite crystals. Drill-core diameter is 50 mm.*

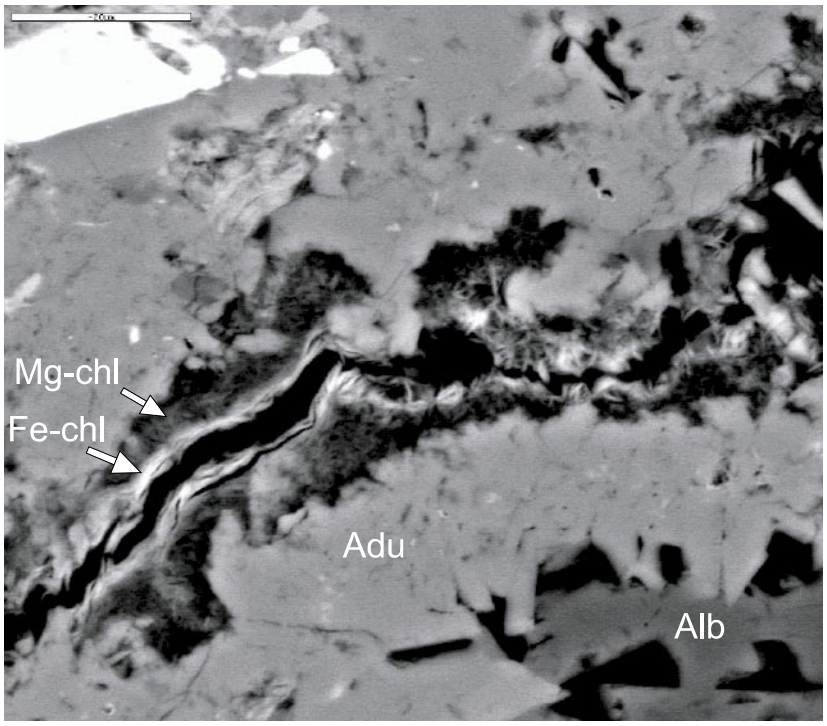

Figure A-7. *Albite (Alb) and adularia (Adu) is cut by Mg-rich chlorite (Mg-chl), which is cut by Fe-rich chlorite (Fe-chl). Backscattered electron image. Scale bar is 20 µm.*

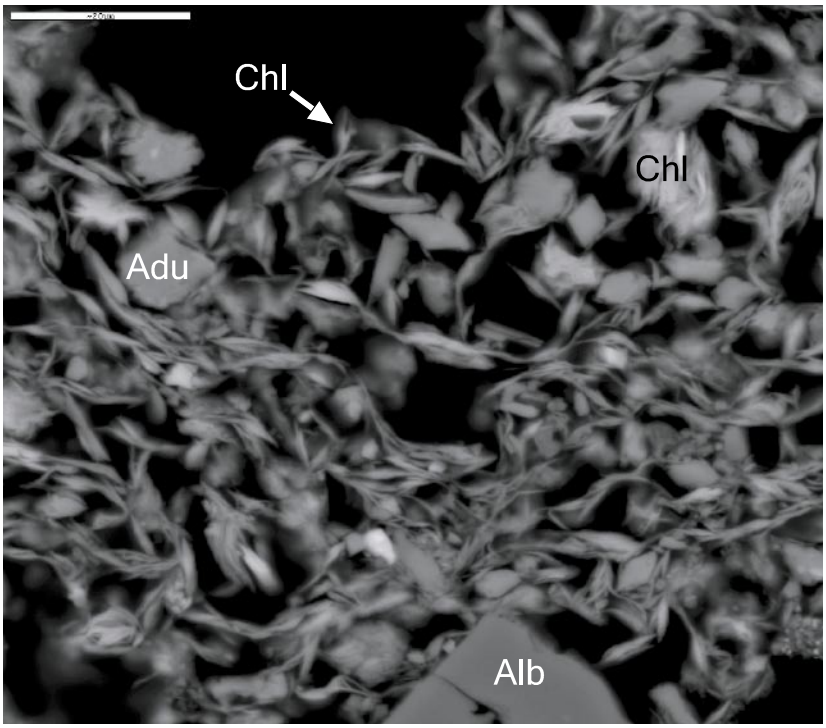

Figure A-8. *Albite (Alb) and later fine-grained matrix consisting of adularia (Adu) and even later Fe-rich chlorite (Chl). Backscattered electron image. Scale bar is 20 µm.*

208.60–208.65 m:

Rock type: Intermediate volcanic rock (quartz latite to andesite)
Fracture: Complex fracture-filling, open, but 25 mm of the old fracture filling is present
Orientation: 213°/14°

Minerals: Prehnite, Calcite, Epidote, Chlorite, Titanite, Adularia, Apatite, Hematite, Fluorite, Harmotome, Quartz, Albite, Pyrite, Laumontite

Order:

1. Idiomorphic prehnite, in several pulses, slightly dissolved
2. Thin fillings of calcite (MnO_2 = * %)
   - Later calcite pulse (MnO_2 = * %) more closely related in time to the minerals listed below.
   - Late quartz and albite crystals are present between the idiomorphic prehnite crystals. No relations to other minerals than prehnite are visible.
   - Fine-grained, idiomorphic adularia, + (later) idiomorphic apatite +hematite(?), (later) chlorite (Mg-rich, FeO: 10–11% MgO: 20–24%), harmotome + laumontite
   - Chlorite (Fe-rich, FeO: 26–35% MgO: 6–10%), cuts Mg-chlorite and is also present in open spaces between big idiomorphic prehnite crystals. Pyrite (small crystals in zeolites)

Notable: The relation between the Fe-oxide and the other minerals is somewhat unclear. Fe/Mg-chlorite (FeO: 21%, MgO: 15%) with titanite in it are present as old remnants in a later chlorite (Mg-rich), adularia, apatite matrix. Fluorite is present and is cutting prehnite.

Wall-rock alteration: Fine-grained matrix with some big crystals of plagioclase (extremely red coloured) and chlorite. The fine-grained plagioclase, K-feldspar and quartz matrix is also red coloured. This gives the wall-rock an intense red colour.

Visible macroscopically: Calcite is clearly cutting prehnite.

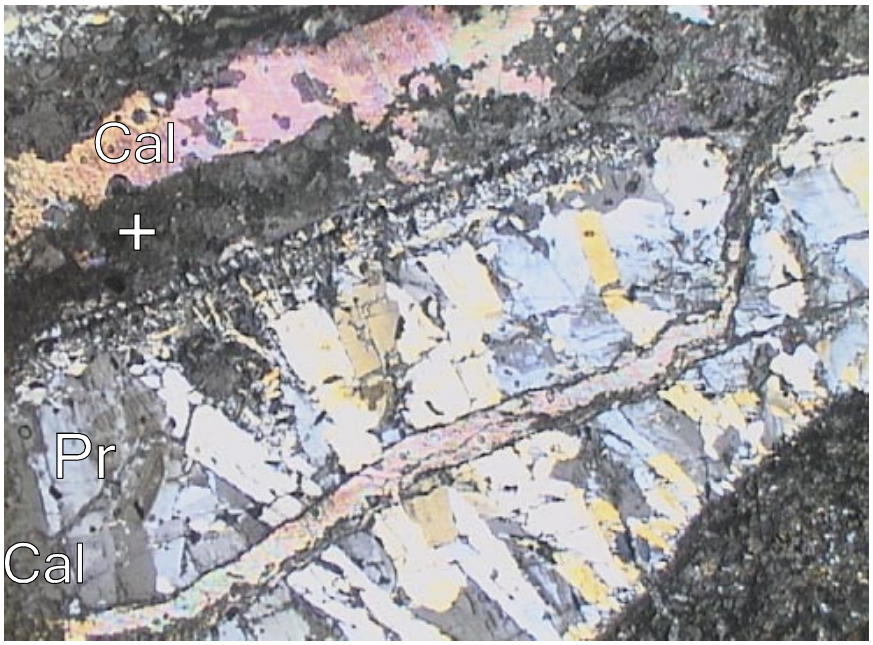

Figure A-9. *Idiomorphic prehnite (Pr) is cut distinctly by calcite (Cal). The calcite fillings are of two different generations. The upper calcite filling is oldest and is penetrated by a fine-grained matrix (+), consisting of adularia, Mg-rich chlorite, apatite, hematite etc. Photomicrograph, width c 1.25 mm.*

213.15–213.25 m (1):

Rock type: Intermediate volcanic rock (quartz latite to andesite)
Fracture: Closed, 4 mm thick
Orientation: 172°/74°

Minerals: Prehnite, Adularia, chlorite, Quartz, Epidote, Harmotome, Laumontite

Order:

1. Prehnite “mylonite” with older remnants of idiomorphic quartz and epidote crystals. Also present are later adularia, Fe-stained chlorite and ordinary Fe/Mg-chlorite (FeO: 15–17%, MgO: 8–10%).
2. Sealed fractures of idiomorphic prehnite (dissolved) are offsetting the mylonite. Present are later adularia, Fe-stained chlorite and ordinary Fe/Mg-chlorite (FeO: 15–17%, MgO: 8–10%).
3. Adularia and later chlorite (Mg-rich, FeO: 10–14%, MgO: 15–19%) + big laumontite crystals.
4. Harmotome and chlorite (Fe-rich, FeO: 27–36%, MgO: 6–10%), both as related thin fillings. The harmotome has been dissolved and only a few crystals are left in the filling.

Notable: Prehnite is cutting one thin filling of adularia but the rest of the adularia seems to be younger than prehnite, filling the space between the prehnite crystals and cutting through them.

Wall-rock alteration: Hydrothermally altered with red coloured feldspar (plagioclase in particular) and numerous big and small chlorite crystals replacing the biotites and amphiboles. Some small amphiboles are still present in the wall-rock though. The wall-rock is penetrated by several small fractures, in all directions, giving the wall-rock a slightly chaotic appearance.

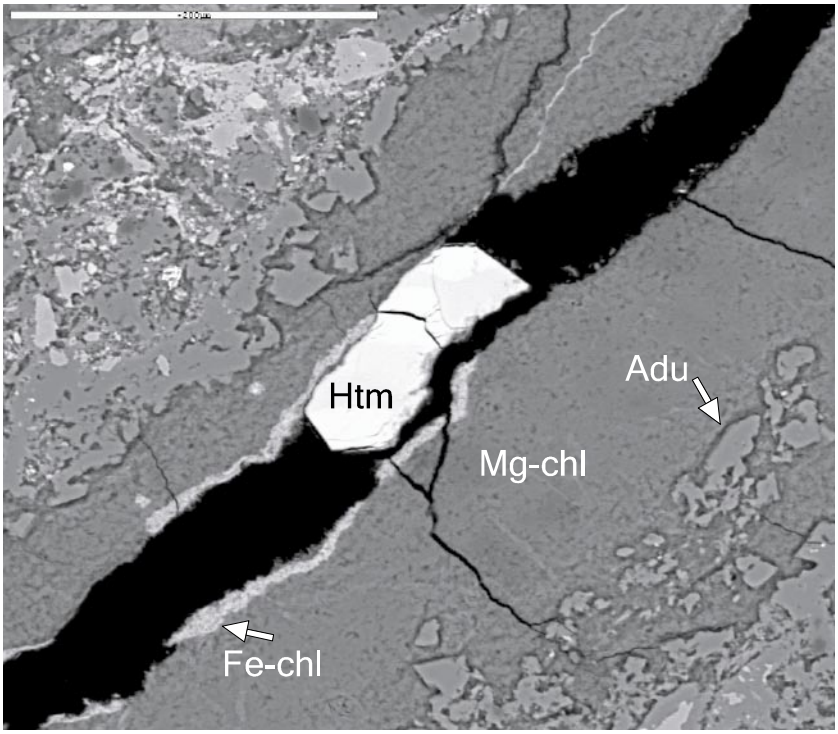

Figure A-10. *Adularia (Adu) and later Mg-rich chlorite (Mg-chl) are penetrated by a vein consisting of Fe-rich chlorite (Fe-chl) and harmotome (Htm). Backscattered electron image. Scale bar is 200 µm.*

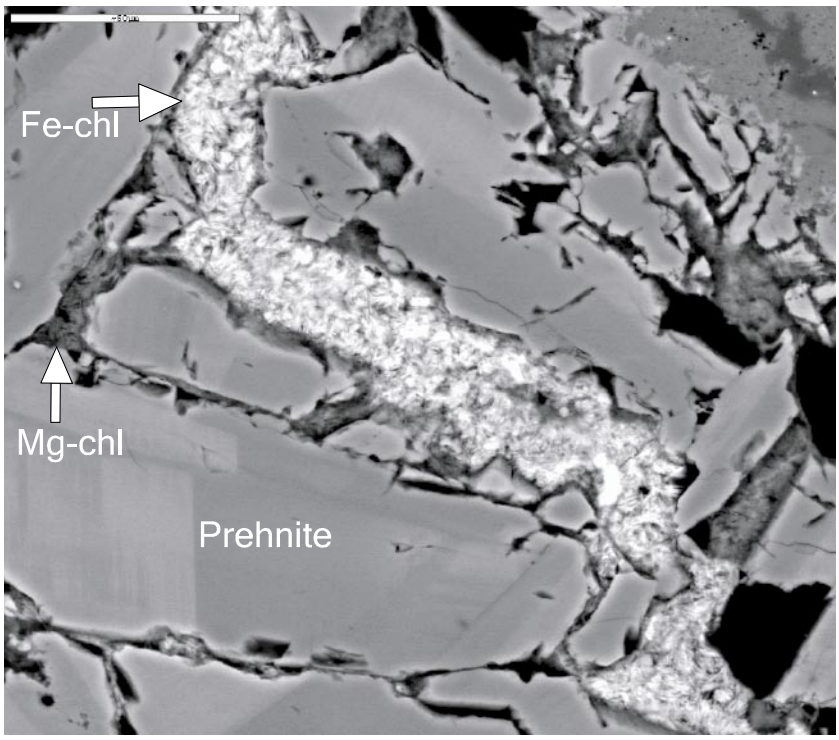

Figure A-11. *Idiomorphic prehnite, partly dissolved, with later Mg-rich chlorite (Mg-chl) in between the crystals have both been cut discordantly by even later Fe-rich chlorite (Fe-chl). Backscattered electron image. Scale bar is 50 µm.*

213.15–213.25 m (2):

Rock type: Intermediate volcanic rock (quartz latite to andesite)
Fracture: 2 closed fractures (prehnite and albite/calcite) intercepting at an angle of ~ 90°
Both fillings are 8–9 mm thick
Orientation: 172°/74° (Prehnite), 85°/38° (Calcite)

Minerals: Albite, Prehnite, Chlorite, Calcite, Epidote, Harmotome, Laumontite, Pyrite, Adularia, Quartz

Order:

1. Epidote-mylonite.
2. Thick filling of Idiomorphic prehnite crystals which have been dissolved.
3. Albite (and some fine-grained quartz) is filling the space between earlier dissolved prehnite crystals. Albite also forms a gigantic filling of idiomorphic crystals cutting the prehnite filling. The albite crystals are dissolved.
4. Calcite (MnO_2: * %), thin fillings and coarse-grained idiomorphic crystals, cuts the albite filling. Using the same fracture as albite.
5. Adularia, harmotome, laumontite. Adularia cuts the albite/quartz fillings. Harmotome (as single grains) and especially laumontite are filling holes in the dissolved idiomorphic albite. They are closely related in time with calcite but they seem to be a little bit later. No relation between adularia and the two zeolites has been found but they appear to be formed in the same time-span. Harmotome may be just later than laumontite. Laumontite crystals are very numerous in this thin-section.

6. Hematite, pyrite and chlorite (Fe-rich, FeO: 35–38%, MgO: 5%).
   - Hematite form fine-grained grained circular crystals, like small stains on earlier e.g. laumontite, calcite and albite.
   - Pyrite form fillings of xenomorphic crystals which clearly cut through “3” and “4”.
   - Fe-chlorite, fine-grained, cuts through, e.g. laumontite, calcite and albite and fill out holes in the dissolved albite and prehnite.

Notable: Mg-rich chlorite is present and is cutting prehnite and albite (no more relations are present).

Wall-rock alteration: Hydrothermal altered with red coloured feldspar (plagioclase in particular) and numerous big and small chlorite crystals replacing the biotites and amphiboles. Some small amphiboles are still present in the wall-rock though.

Visible macroscopically: Albite filling cutting older prehnite filling. Calcite is penetrating into older albite filling.

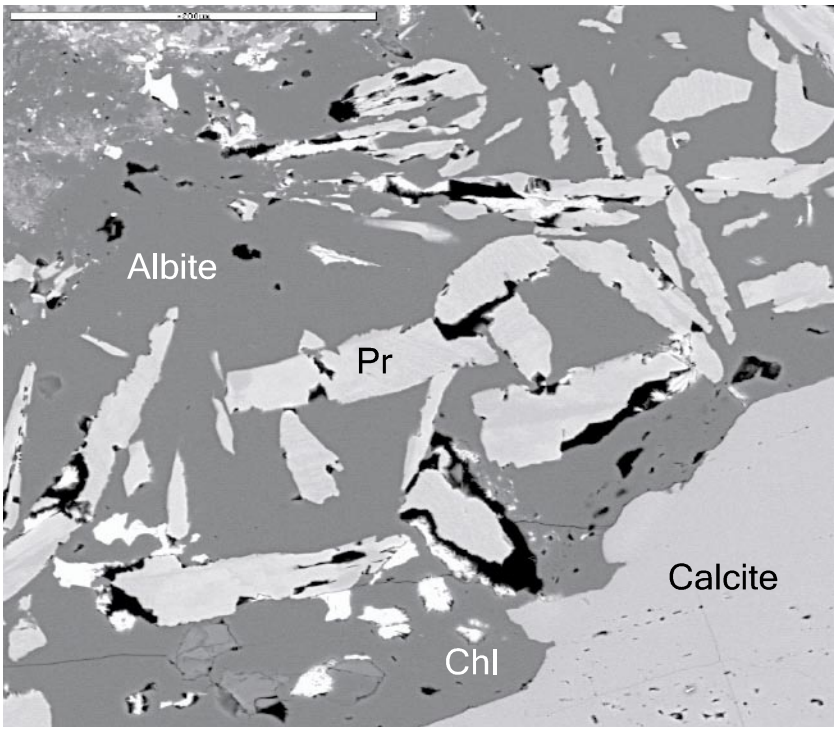

Figure A-12. *Idiomorphic and heavily dissolved prehnite (Pr) crystals are surrounded by albite. Calcite cuts the albite filling and Fe-rich chlorite (Fe-chl) occupy holes in the dissolved albite. Backscattered electron image. Scale bar is 200 µm.*

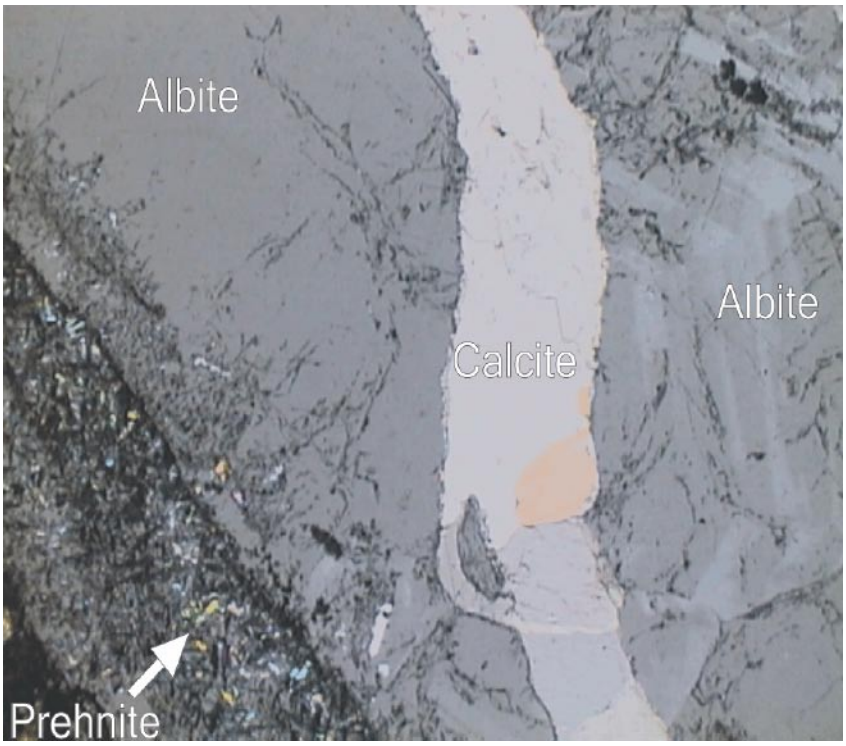

Figure A-13. *An early prehnite filling is cut by a filling of huge albite crystals. The albite filling is later cut by a calcite filling. Photomicrograph, width c 2.5 mm.*

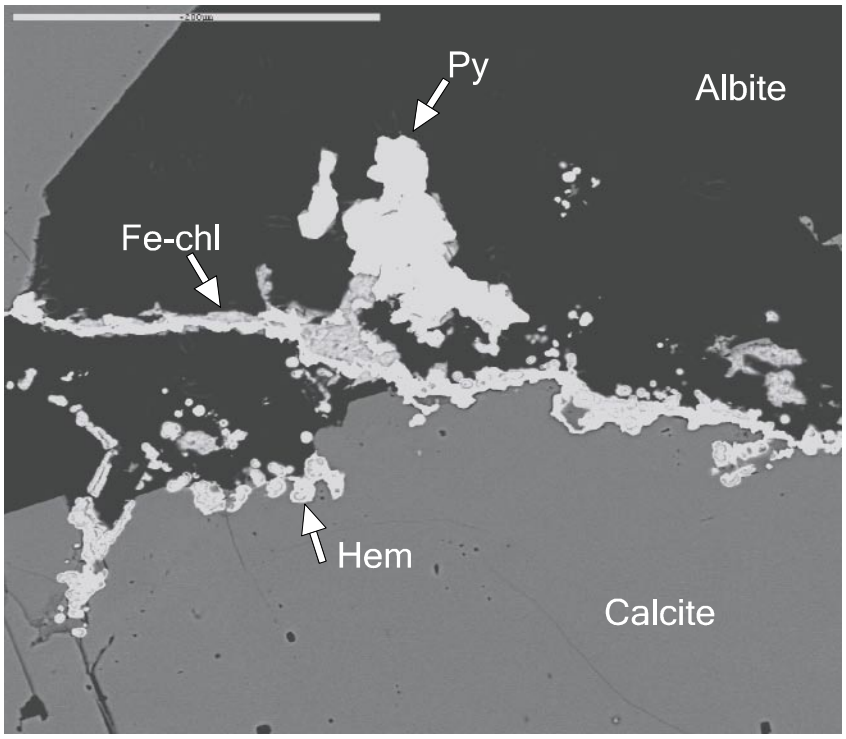

Figure A-14. *Albite and later calcite are penetrated by pyrite (Py), hematite (Hem) and Fe-rich chlorite (Fe-chl). Backscattered electron image. Scale bar is 200 µm.*

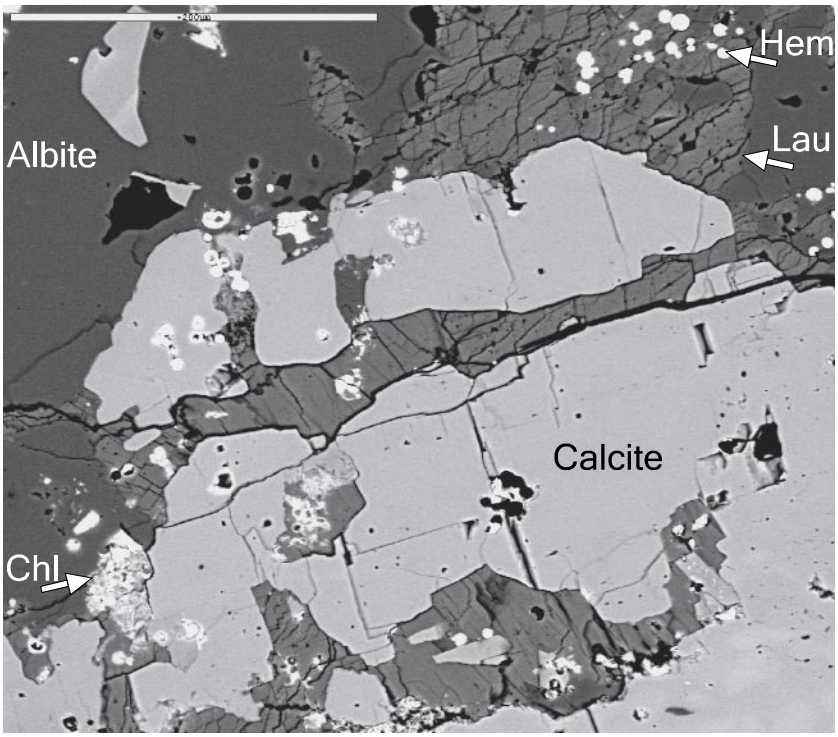

Figure A-15. *Albite and later calcite are penetrated by laumontite (Lau). Small stains of hematite (Hem) and Fe-rich chlorite (Chl) are the latest fracture minerals in this backscattered electron image. Scale bar is 200 µm.*

256.90–257.10 m:

Rock type: Quartz monzodiorite, equigranular to weakly porphyritic
Fracture: Several closed fractures, 2–10 mm wide
Orientation: Several sets of fractures, 3°/18°, 298°/22°

Minerals: Adularia, Calcite, Chlorite (3 generations), Hematite, Pyrite, Quartz, Epidote, Titanite, Prehnite, Apatite, Sphalerite

Order:

1. Old remnants of quartz and (later?) prehnite in later cataclasites.
2. Fine-grained red-coloured cataclasite with larger quartz crystals as xenocrysts (+some Fe/Mg-chlorite crystals with related titanite + epidote and apatite) and a matrix consisting of fine-grained adularia, chlorite (Mg-rich, FeO: 4%, MgO: 18–22%), chlorite (Fe-rich, FeO: 42%, MgO 5%) hematite (75% Fe) – causing the red colour. The hematite is present as small crystals and not as in other thin-sections just as a thin layer upon other crystals (often Fe-chlorite).
3. Fine-grained light-brown to dark-brown cataclasite. This cataclasite is breaking up the "2"-mylonite. The matrix of this cataclasite is still fine-grained but the crystals are all larger than that of "2". The minerals in this cataclasite are adularia and chlorite (Mg-rich: FeO 4–5%, MgO 14–18%) as in "2" but the Fe-rich chlorite (FeO: 42–52%, MgO: 10–15%, some extra Fe from hematite) and hematite are not as numerous, which gives the cataclasite a brown and not red colour as "2".
4. Calcite, thin fillings (MnO_2 = * %).

5. Chlorite (Mg-rich, FeO: 3–5%, MgO: 16–23%), same as in “2” and “3”. Fine-grained and clearly cutting “2” and “3”.
6. Cutting and penetrating “2”–“5”:
   – Adularia (idiomorphic yet fine-grained), (Mg-chlorite).
   – Pyrite (anhedral + one crystal of sphalerite) and Chlorite (Fe-rich, FeO: 35–45%, MgO 4–6%), thin tabular, feather-shaped crystals cutting pyrite and growing on adularia in an empty fracture.

Wall-rock alteration: Red-coloured plagioclase, quartz and k-feldspar are numerous. The wall-rock is penetrated by lots of fractures and chlorite is present in large amounts.

Visible macroscopically: Calcite is cutting older hematite stained fracture filling. Two different red coloured alterations are visible. One is very old (bright red) and hydrothermal, the other darker one is later and related to hematite.

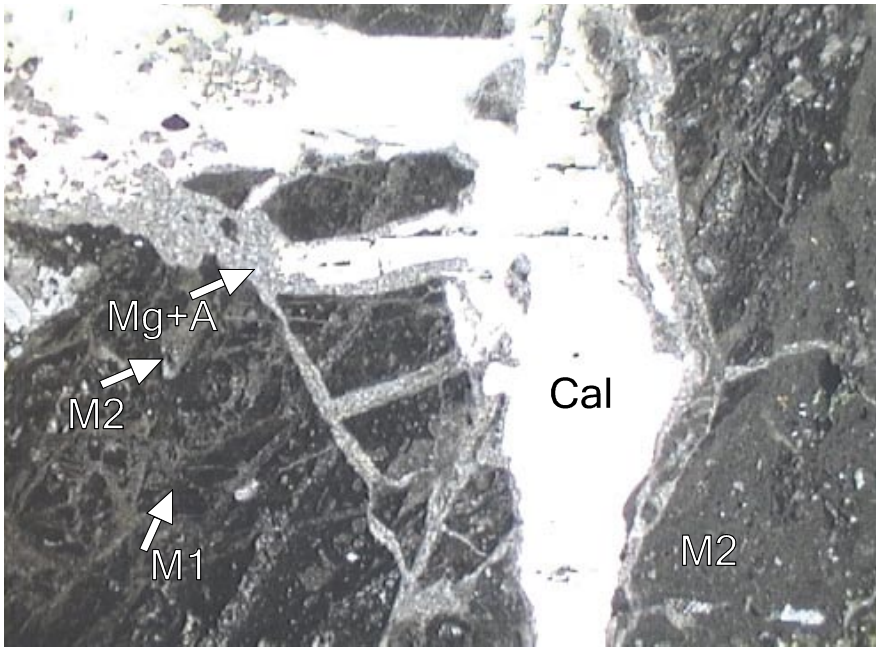

Figure A-16. *Dark red/brown cataclasite (M1 – “2” in order) is cut by a brighter cataclasite (M2 – “3” in order). Calcite cuts both M1 and M2. Calcite is later penetrated by Mg-rich chlorite and adularia (Mg+A). Photomicrograph, width c 5 mm.*

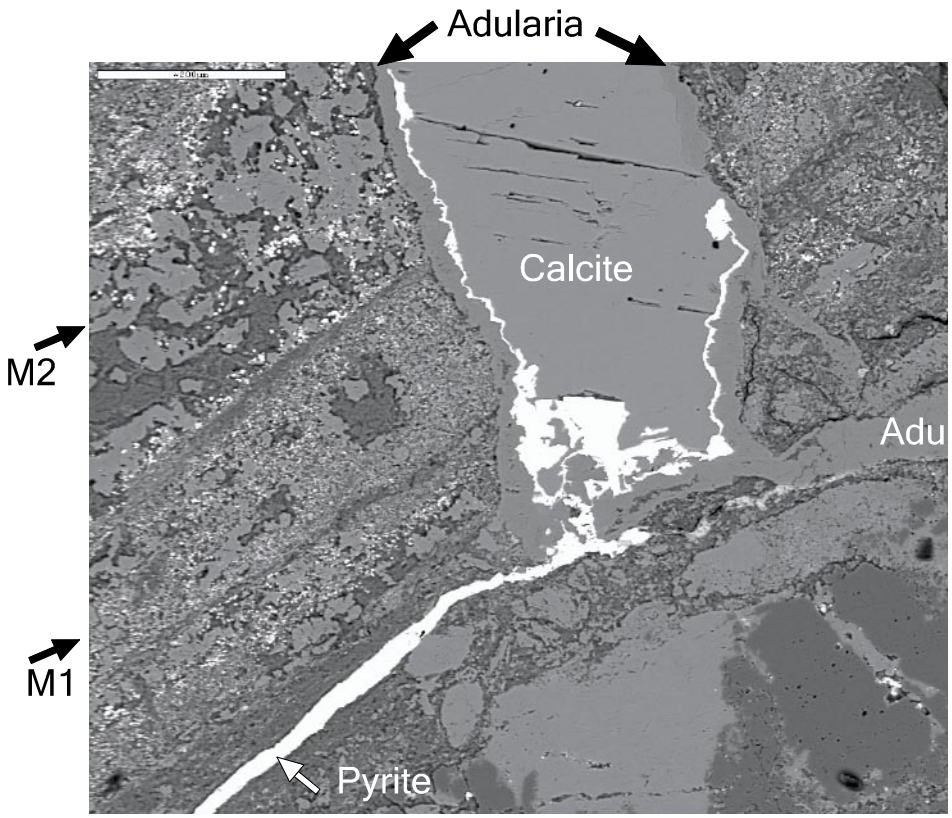

Figure A-17. *Fine-grained cataclasite (M1 – "2" in order) is cut by a more coarse-grained cataclasite (M2 – "3" in order). Calcite cuts both M1 and M2. Adularia (Adu) is coating the fracture walls of the calcite filled fracture. Later, a thin filling of pyrite penetrates between the calcite and the adularia. Backscattered electron image. Scale bar is 200 µm.*

275.70–275.75 m:

Rock type: Quartz monzodiorite, equigranular to weakly porphyritic
Fracture: Open, 3 mm of the old fracture filling is remaining
Orientation: 33°/61°

Minerals: Quartz, Calcite, Adularia, Chlorite, Hematite, (Albite)

Order:

1. Calcite, (MnO_2 = 0.3–0.4%).
2. Fe/Mg-chlorite (FeO: 23–25%, MgO: 16%) with titanite inclusions.
3. Calcite (MnO_2 = * %).
4. Adularia and Chlorite (Mg-rich; FeO: 4–16%, MgO = 20–28%) and hematite. These minerals appear randomly in several pulses, cutting one another.
5. Calcite (thin filling on fracture surface).

Wall-rock alteration: Red-coloured plagioclase (saussuritized) and k-feldspar (less red coloured) appears in great numbers. Chlorite is present but epidote is not.

287.40–287.47 m:

Rock type: Quartz monzodiorite, equigranular to weakly porphyritic
Fracture: Open, 3–4 mm of old fracture filling is remaining
Orientation: 3°/67°

Minerals: Quartz, Albite, Calcite, Chlorite, Adularia, Hematite, Fe-stained mineral, Pyrite

Order:

1. Idiomorphic quartz and albite (possibly altered wall-rock).
2. Calcite, thin fillings, and also some subhedral crystals. MnO_2 = * % (thin fillings) and MnO_2 = * –0.7% (subhedral crystals).
3. Chlorite (Fe-rich), spherulitic, trending towards extreme Fe-richness (FeO: 24–55%, MgO: 6–13%).
4. Adularia, hematite (FeO: 75%) and chlorite (Mg-rich, FeO: 11–16% MgO: 20–23%), also some Fe-stained silicate of unknown origin. The Mg-rich chlorite is growing into adularia, which means that it is a little bit later. Big pyrite crystals are present and are penetrating the calcite. Pyrite seems to be contemporary with hematite.
5. Chlorite (Fe-rich, FeO: 30–31%, MgO: 9–10%), penetrating pyrite diffusely.

Notable: Calcite may be of several different generations, indicated by the shape of the crystals and the inconsequent Mn-values. At least some of the crystals are older than Fe-rich chlorite (“3”) and all are older than (“4”). Prehnite is present and is penetrating quartz, no other relation with prehnite included are visible. Some of the Fe-stained mineral grains seem younger than adularia and some seem older. This means that they are probably closely related in time.

Wall-rock alteration: Red coloured but many of the plagioclase, k-feldspar and quartz crystals are relatively fresh in there appearance. Some hematite filled micro-fractures are cutting through the wall rock. Chlorite is rare and epidote is not present.

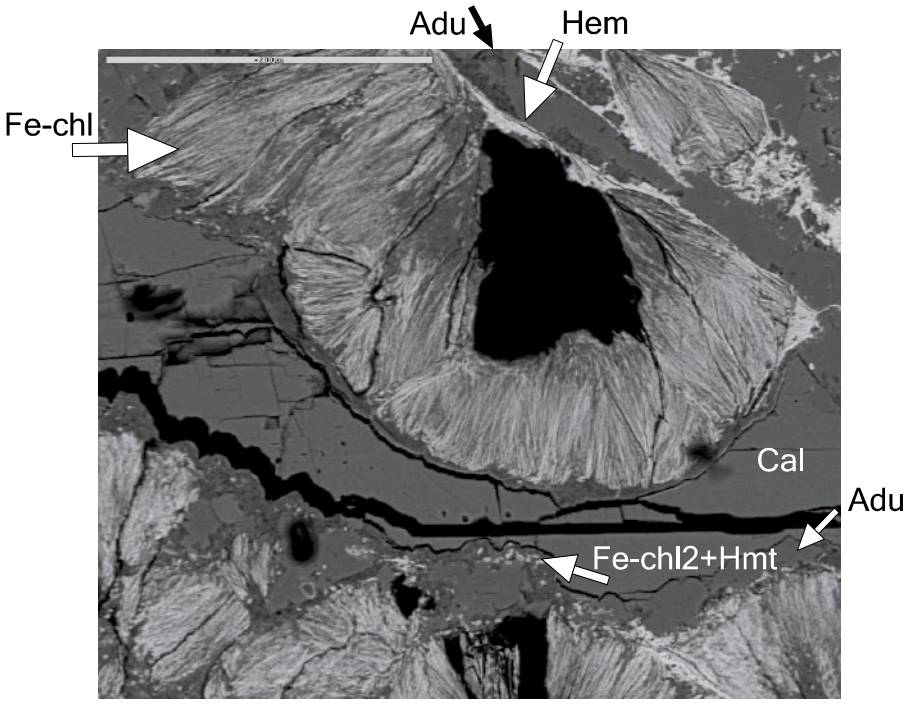

Figure A-18. *The chlorite is coated by adularia (Adu), hematite (Hem) and a later generation of fine-grained Fe-rich chlorite (Fe-chl2). Calcite (Cal) presumed to later than the Fe-rich chlorite and adularia in this photo. Backscattered electron image. Scale bar is 200 µm.*

289.80–289.95 m:

Rock type: Quartz monzodiorite, equigranular to weakly porphyritic
Fracture: Open (289.95), 10–20 mm of old fracture filling is remaining
Orientation: 150°/53°

Minerals: Prehnite, Epidote, Adularia, Hematite, Chlorite, Pyrite, Calcite, Titanite, Quartz

Order:

1. Idiomorphic quartz and epidote.
2. Epidote-mylonite with fine-grained epidote (the matrix includes prehnite, chlorite [Fe/Mg-rich], epidote, quartz) surrounding idiomorphic epidote and titanite (+quartz).
3. Fine-grained prehnite with later pulses of idiomorphic prehnite in veins cutting the mylonite. Present between the prehnite crystals are older idiomorphic quartz and calcite.
4. Calcite (MnO_2 = * –0.4%), thin fillings.
5. In order
   – Adularia.
   – Chlorite (Mg-rich: FeO: 10%, MgO: 21%).
6. Hematite and Chlorite (Fe-rich: FeO: 38% MgO: 5%).

Wall-rock alteration: Red coloured alteration, reaching far (> 15 cm) from the fracture. The red colour is concentrated to the altered plagioclase and K-feldspar (not as altered) crystals. Chlorite is slightly numerous.

Visible macroscopically: Over 90% of this wide fracture filling is consisting of prehnite.

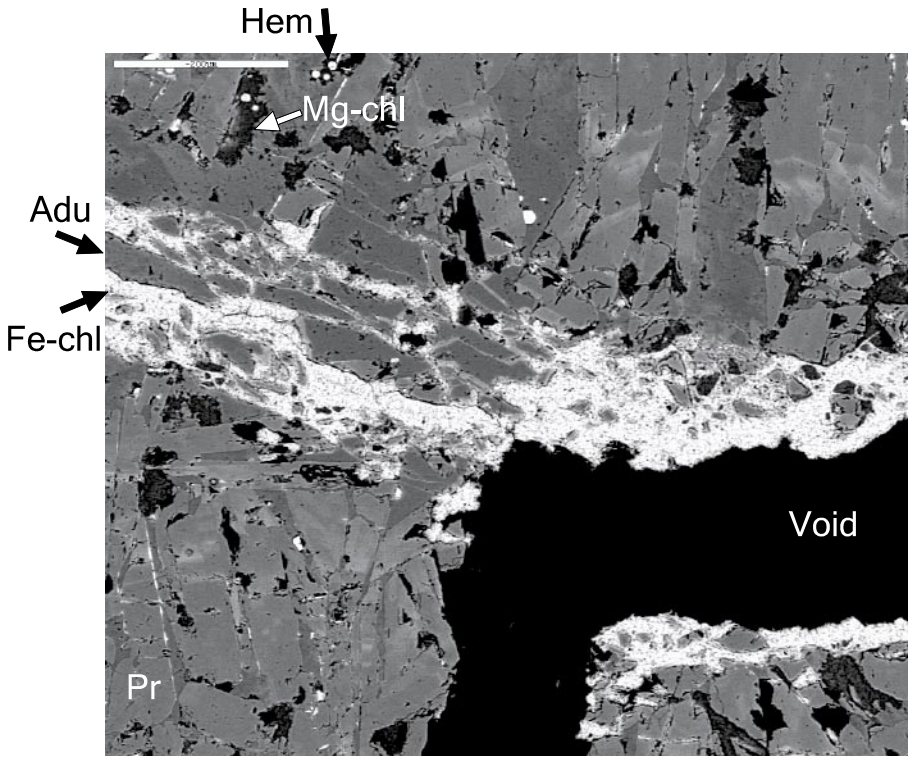

Figure A-19. *Idiomorphic prehnite (Pr) crystals, which have been partly dissolved, are cut by adularia (Adu) and even later Fe-rich chlorite (Fe-chl). Mg-rich chlorite (Mg-chl) and later hematite (Hem – bright round crystals) are filling the dissolution holes in the prehnite. Backscattered electron image. Scale bar is 200 µm.*

363.65–363.67 m:

Rock type: Granite, fine to medium-grained
Fracture: Closed, mylonite, 20–30 mm wide filling
Orientation: 270°/70°

Minerals: Quartz, Albite, Prehnite, Calcite, Epidote, Chlorite, Titanite, Ilmenite, Adularia, Apatite, Hematite, Fe-stained minerals, Fluorite, Ti-oxide, Muscovite

Order:

1. Mylonite with mainly quartz, fine-grained, also muscovite, K-feldspar, albite, epidote and some chlorite ("2") in the matrix.
2. Fe/Mg-chlorite (FeO: 20–29%, MgO: 11–17%) with titanite and ilmenite + Fe-stained minerals, in more dark-green mylonite.
3. Red-black cataclasite, with a matrix of hematite, Fe-stained silicates and adularia.
4. Thin fillings of calcite, several pulses (MnO_2 = * –1%) + Ti-oxide (95% TiO_2 = anatase or rutile).Calcite is mostly cutting the red-black cataclasite (like in 257) but hematite is penetrating the calcite at some locations which means that "3" and "4" are closely related in time.
5. Fluorite (related to calcite, but later).

Notable: The relations are somewhat unclear in general, but "3"–"5" are fairly contemporary.

Wall-rock alteration: The wall-rock (if it is not a part of the fracture filling) is more or less cataclastic – mylonitic.

Visible macroscopically: Calcite is cutting through the mylonite.

Figure A-20. *Quartz mylonite (Qz-myl) is penetrated by a dark red cataclasite, with hematite in it (Hem). Both the mylonite and the cataclasite are cut discordantly by calcite and even later fluorite. The fracture with the fluorite filling is partly empty. Photomicrograph, width c 2.5 mm.*

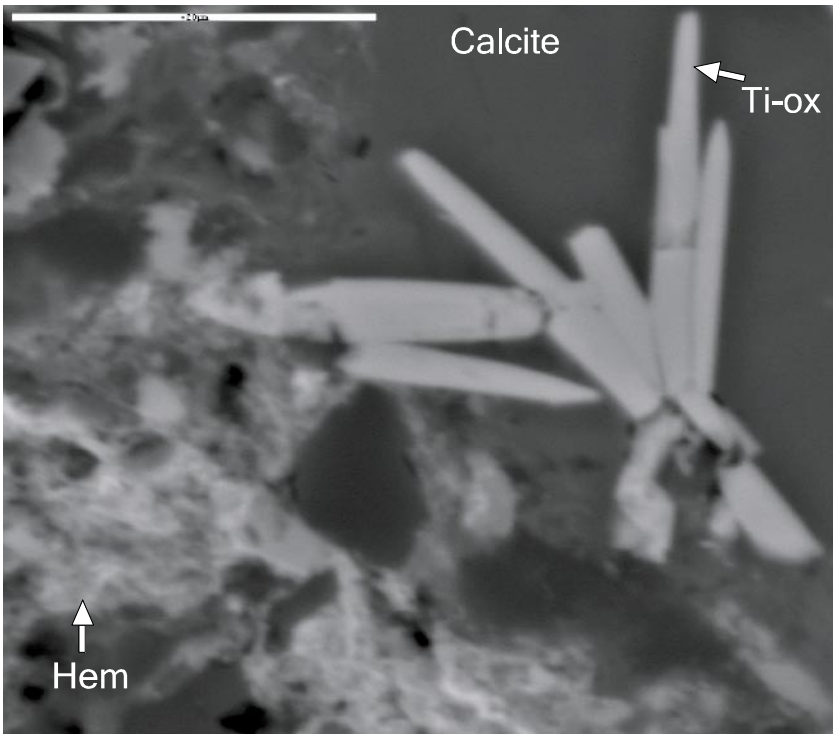

Figure A-21. *Hematite stained mylonite (Hem) is cut by calcite. Needle-like crystals of Ti-oxide (Ti-ox) are probably formed contemporary to calcite. Backscattered electron image. Scale bar is 20 µm.*

376.44–376.56 m:

Rock type: Fine-grained dioritoid
Fracture: Open with thick (7 mm) fracture filling attached to the wall-rock
Orientation: 185°/68°

Minerals: Quartz, Calcite, Chlorite, Epidote, Prehnite, Titanite, Adularia

Order:

1. Big idiomorphic quartz crystals.
2. Fine-grained quartz (re-crystallised), idiomorphic epidote.
3. Idiomorphic prehnite, few crystals, different crystals compared to other thin-sections.
4. Idiomorphic calcite (MnO_2 = 0.4–0.8%).
5. Idiomorphic Fe/Mg-chlorite (FeO: 24–26% MgO: 11–16%), with stains of titanite.
6. Calcite (MnO_2 = * %), thin vein.
7. Fine-grained quartz and adularia (penetrating “6”).
8. Chlorite (Mg-rich). Merely one observation in this thin-section.

Notable: The Mg-rich chlorite might be related to the fine-grained quartz and adularia. Titanite is present as small stains in the idiomorphic prehnite.

Wall-rock alteration: Chlorite is present but there are much biotite and amphibole crystals left + some ilmenite. No red coloured alteration.

Visible macroscopically: Chlorite is penetrating big crystals of calcite.

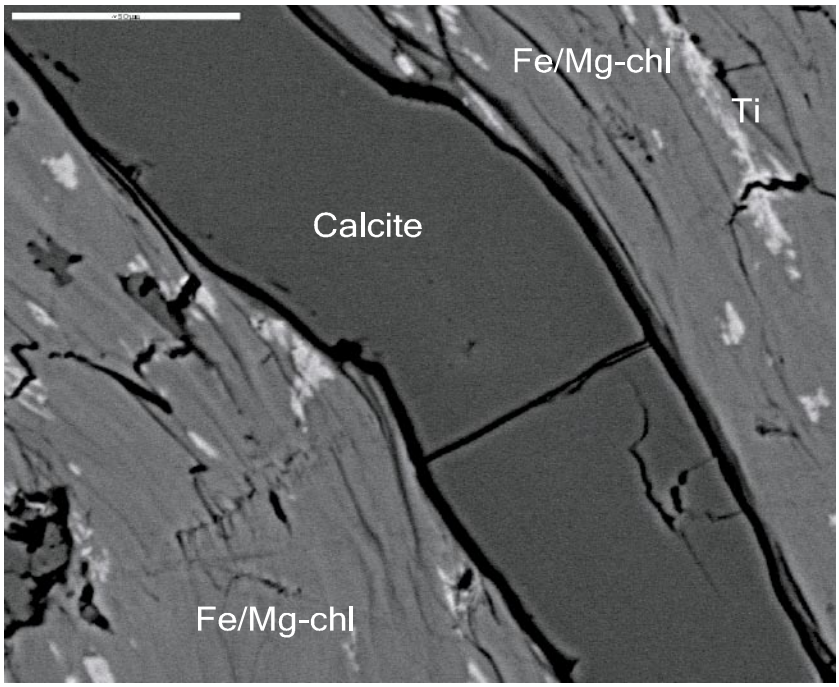

Figure A-22. *Fe/Mg-chlorite (Fe/Mg-chl), with titanite in it, is cut by a later calcite vein. Backscattered electron image. Scale bar is 50 µm.*

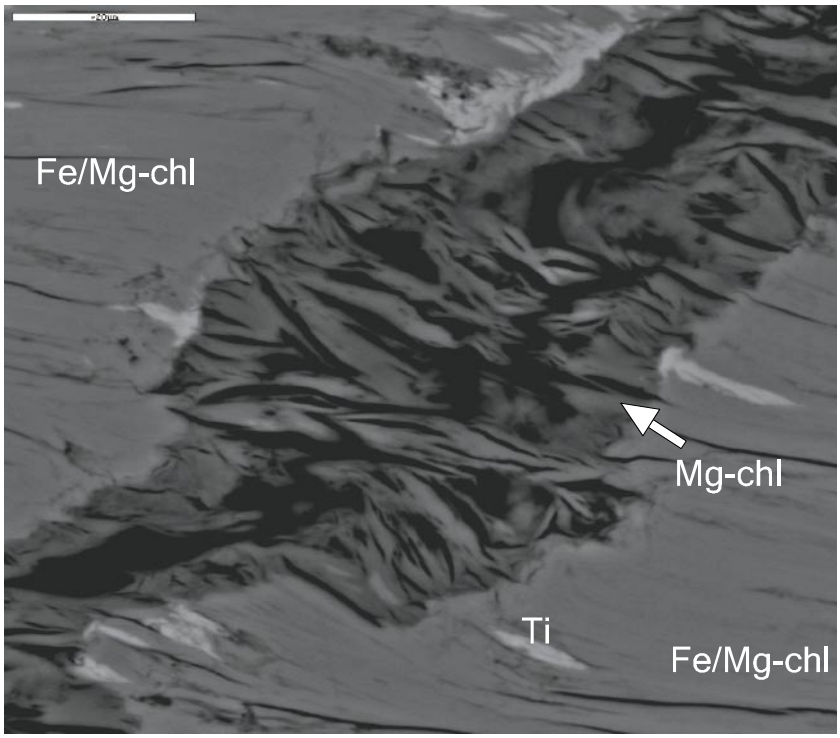

Figure A-23. *Fe/Mg-chlorite (Fe/Mg-chl), with some titanite (Ti) in it, is cut by a calcite vein. The calcite has later been replaced by Mg-rich chlorite (Mg-chl). Backscattered electron image. Scale bar is 20 µm.*

401.05–401.23 m:

Rock type: Intermediate volcanic rock (quartz latite to andesite)
Fracture: Open, 5 mm of old fracture filling remaining
Orientation: 185°/65°

Minerals: Calcite, Epidote, Chlorite, Prehnite, Titanite, Adularia, (Albite)

Order:

1. Calcite: idiomorphic (MnO_2 = 0.7%).
2. Epidote and Chlorite:
   - Epidote, fine-grained, two contemporary compositions: one with 3 times more calcium than aluminium, and one with equal amount of calcium and aluminium.
   - Fe/Mg-chlorite (FeO: 21–26%, MgO: 9–15% + titanite).
3. Prehnite, appears to be at least younger than epidote.
4. Thin filling of calcite (MnO_2= * %).
5. Adularia.

Wall-rock alteration: Very fine-grained wall-rock with lots of quartz and feldspars and some fine-grained calcite. The plagioclase has been slightly saussuritized. Numerous chlorite crystals give the wall rock a pale green appearance. Epidote is present close to the fracture. Ilmenite, which has altered to titanite and rutil (anatase?), are concentrated app. 1 mm into the wall rock but are also present well inside the wall rock. No red coloured alteration is present. Some allanite crystals are present.

Visible macroscopically: Calcite looks old and seems to be penetrated by chlorite.

409.85–410.00 m:

Rock type: Intermediate volcanic rock (quartz latite to andesite)
Fracture: Closed, 15–35 mm thick, hydrothermal
Orientation: 360°/31°

Minerals: Prehnite, Epidote, Chlorite, Quartz, Calcite, Titanite

Order:

1. Idiomorphic quartz.
2. Fine-grained epidote mylonite (with fine-grained Fe/Mg-chlorite [FeO: 27%, MgO: 16% – with some titanite] and later prehnite + some calcite) penetrating idiomorphic quartz which is found in the mylonite as fenocrysts.
3. Idiomorphic and coarse-grained and fine-grained prehnite of several pulses are clearly cutting the epidote mylonite. The prehnite filling is using the same fracture as the epidote filling, breaking up the epidote filling like an intrusive micro breccia, leaving fragments of the epidote mylonite in the prehnite filling.

Notable: The wall-rock and the minerals earlier than “3” are red-stained.

Wall-rock alteration: The plagioclase crystals are red-stained, giving the wall-rock an intense red colour, due to alteration. Other minerals like K-feldspar and quartz are also altered but they are not as red coloured as plagioclase. The wall-rock is fine-grained with subhedral character. No indications of shear are visible. Chlorite is present in a fairly large amount.

Visible macroscopically: The prehnite filling seems to be later than the red coloured alteration of the wall-rock, adjacent to the fracture.

596.00–596.10 m:

Rock type: Intermediate volcanic rock (quartz latite to andesite)
Fracture: A set of closed fractures, 1–20 mm wide
Orientation: Mostly flat-moderate, but several steep fractures are connecting the flat fractures to one another. (4°/40°)

Minerals: Quartz, Calcite, Adularia, Chlorite, (Pyrite) (Albite)

Order:

1. Quartz-mylonite.
2. Calcite, two pulses, thin fillings (MnO_2 = * %).
3. Penetrating calcite – in order:
   - Quartz, fine-grained but sometimes clearly idiomorphic.
   - Adularia – related to quartz but younger (penetrates quartz).
   - Chlorite (Mg-rich, FeO: 9–12%, MgO: 17–21%) – almost always with adularia but penetrates adularia.
   - Chlorite (Fe-rich, FeO: 20–25%, MgO: 13–15%) – not very common.

Notable: The second pulse of calcite (one small vein), may be earlier or contemporary with quartz. (No relation in thin-section)

Wall-rock alteration: Slightly fine-grained wall-rock with undulose extinction with re-crystallized quartz. Quartz-mylonitic veins, bordered by extremely red-coloured “fluid-structures” are present at some locations of the thin-section. Red coloured plagioclase and less altered K-feldspar are present in small amounts, as well as chlorite and epidote.

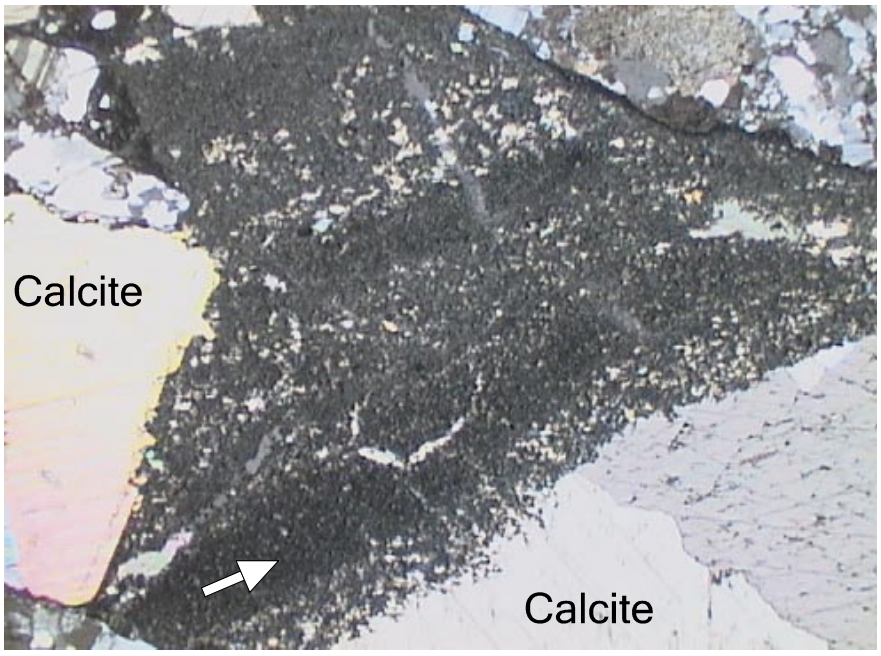

Figure A-24. *A fracture filling of idiomorphic calcite is penetrated by a brown and very fine-grained matrix (arrow) of adularia and Mg-rich chlorite. Photomicrograph, width c 5 mm.*

600.22–600.32 m:

Rock type: Intermediate volcanic rock (quartz latite to andesite)
Fracture: Several sets of closed fractures. The main fracture has a thickness of 3–7 mm
Orientation: 216°/53°

Minerals: Calcite, Epidote, Prehnite, Adularia, Quartz, Hematite, Chlorite, Titanite, (Albite)

Order:

1. Epidote-mylonite, with a matrix of fine-grained epidote, quartz and some chlorite (+titanite). Also present are more coarse-grained quartz, epidote and albite.
2. Idiomorphic and fine-grained prehnite.
3. Calcite (MnO_2 = * –0.4%). Cutting distinct through the earlier fillings.
4. Fine-grained quartz + later adularia and hematite grow into the calcite fracture fillings.

Notable: There are some veins of quartz present. These veins are penetrated by adularia. Idiomorphic epidote is penetrated by prehnite and adularia.

Wall rock alteration: Fine-grained wall-rock with lots of re-crystallized quartz, chlorite and epidote. The fine-grained minerals seem to be elongated. Some of the big plagioclase crystals close to the fracture seem to have been sheared by some fracture related movement.

Visible macroscopically: Prehnite is cutting epidote, using the same fracture as epidote. Calcite is cutting the prehnite, using the same fracture as prehnite and epidote.

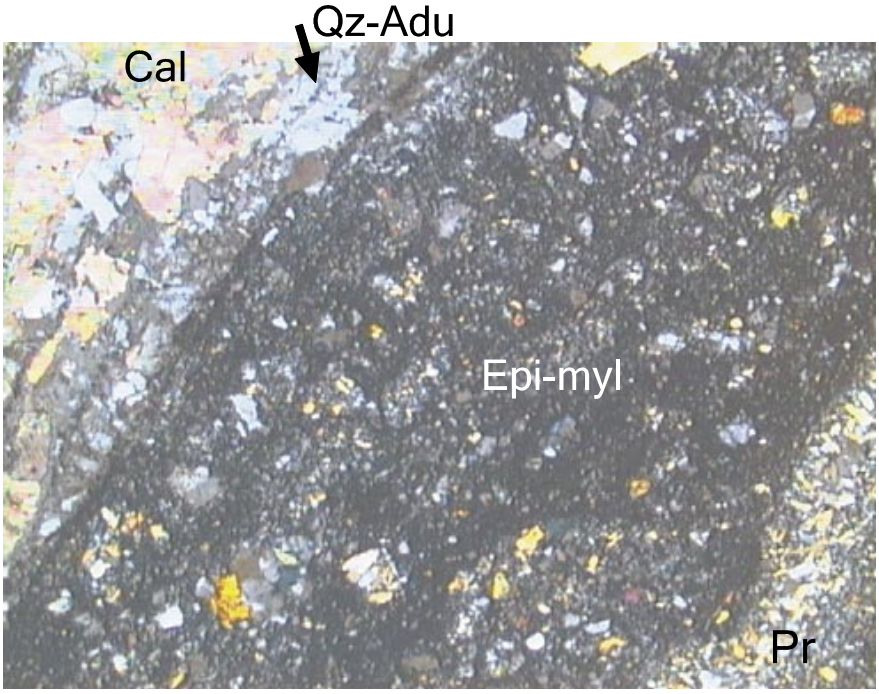

Figure A-25. *Epidote mylonite (Epi-myl) is cut by idiomorphic prehnite crystals (Pr). The prehnite is cut by calcite (Cal, the relation between prehnite and calcite is not visible in this photograph). The calcite is penetrated by later quartz and even related but even later adularia (Qz-Adu). Photomicrograph, width c 2.5 mm.*

602.45–602.85 m:

Rock type: Intermediate volcanic rock (quartz latite to andesite)
Fracture: 1 closed fracture cutting a set of older fractures. The older fracture set (prehnite) has fractures of 3–8 mm width and the younger (calcite etc) fracture is 3–4 mm wide
Orientation: 164°/19° (Prehnite), 240°/33° (Calcite).

Minerals: Epidote, Prehnite, Quartz, Adularia, Calcite, Albite, Chlorite, Titanite

Order:

1. Epidote mylonite with a matrix consisting of fine-grained, epidote, quartz, prehnite (later), Fe/Mg-chlorite (FeO: 23–24%, MgO: 16–17%) and albite. Also present are coarse-grained crystals of epidote and quartz.
2. Prehnite – idiomorphic crystals, coarse grained to very fine-grained, 2 pulses cutting one another. In the fine-grained matrix are remnants of quartz and epidote + titanite present. Between the partly dissolved prehnite crystals are later albite and even later adularia.

----------Distinct age difference----------

3. Calcite thin fillings, several pulses, contemporary (MnO_2 = * %).
4. Penetrating calcite in order:
   – (Fine-grained epidote) – hard to relate.
   – Quartz, fine-grained but also idiomorphic.
   – Adularia (+ earlier albite?).

Wall-rock alteration: In this thin section the wall-rock alteration is demonstrated by the presence of red coloured, saussuritized and sericitized plagioclase crystals, chlorite and epidote crystals and fine-grained quartz crystals.

Visible macroscopically: Younger calcite is clearly cutting a set of older prehnite fractures. The calcite is younger than the red coloured alteration of the wall-rock, adjacent to the fracture.

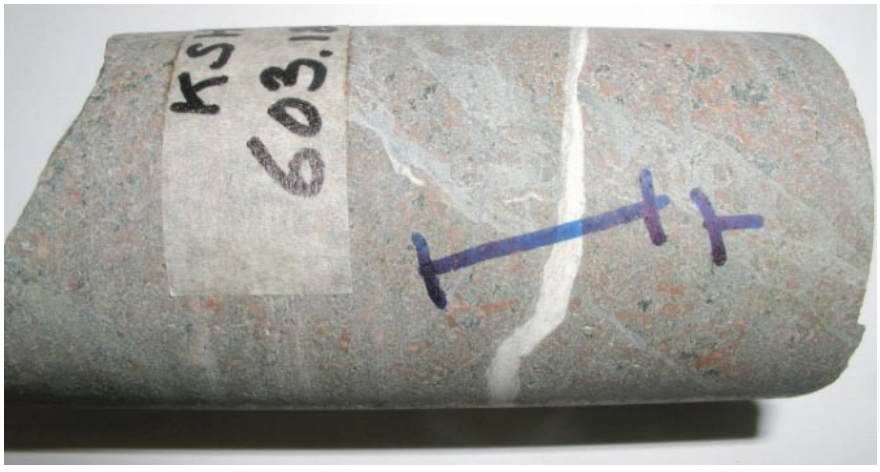

Figure A-26. *Photo of the drill-core, showing the fracture and the orientation of the thin-section (T). Fillings of prehnite (light green) are distinctly cut by calcite (white). Drill-core diameter is 50 mm.*

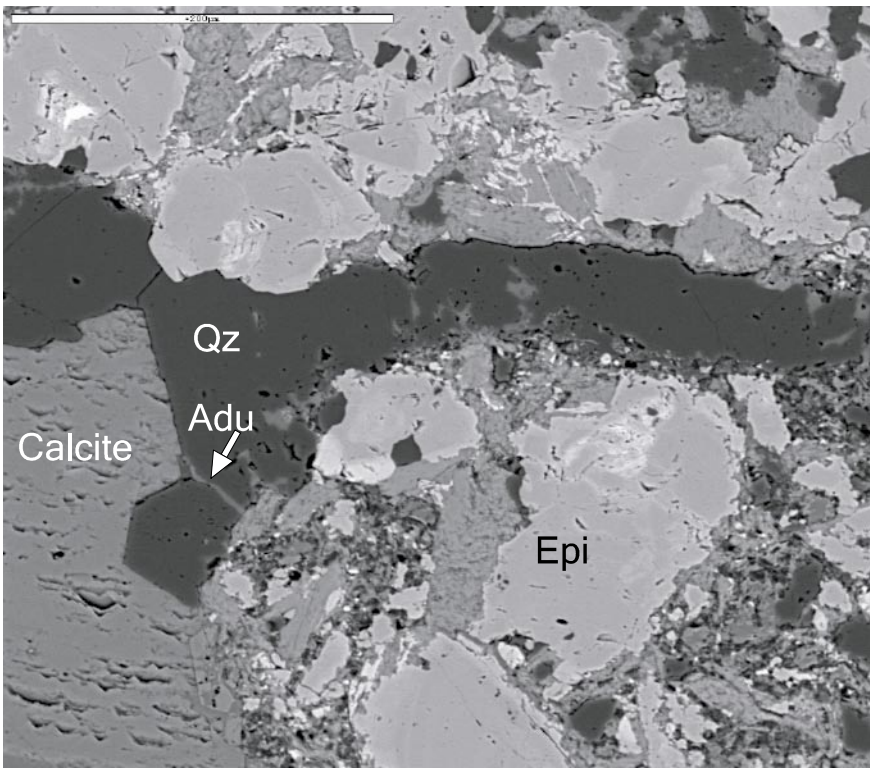

Figure A-27. *Mylonite ("1" in order) with coarse-grained epidote (Epi) is cut by calcite and quartz (Qz). The quartz crystals have been penetrated by even later adularia (Adu). Backscattered electron image. Scale bar is 200 µm.*

626.00–626.05 m:

Rock type: Intermediate volcanic rock (quartz latite to andesite)
Fracture: Open, 2 cm of the old fracture filling is remaining
Orientation: 205°/40°

Minerals: Calcite, Chlorite, Quartz, Adularia, Hematite, Muscovite, Titanite, Apatite, (Albite)

Order:

1. Quartz mylonite, with later growth of muscovite (some epidote is present within the muscovite and as individual crystals in the quartz mylonite) and some chlorite (Mg-rich, FeO = 7–8 %, MgO = 15–17%) and Fe/Mg-chlorite (FeO: 26%, MgO: 13%). Also present are a few albite crystals and some later adularia.
2. Chlorite – cataclasite/mylonite, matrix consisting almost entirely of fine-grained chlorite (Mg-rich, FeO: 6–8%, MgO: 14–16% and Fe/Mg-chlorite: FeO: 17–25%, MgO: 10–15%). Quartz mylonite is found as xenocrysts in the chlorite matrix along with some crystals of K-feldspar, Fe-chlorite (~ 44% FeO) and apatite.
3. Calcite, thin filling (MnO_2 = * %), with deformation twins.
4. Red matrix of adularia, Mg-rich chlorite, hematite, Fe-rich chlorite (35% FeO), same as in 257.
5. Quartz, fine-grained veins cutting the mylonites/catataclasites and growing into "3–4".

6. Penetrating 1–4 are in order:
   - Adularia (closely related to quartz and Mg-chlorite).
   - Chlorite (Mg-rich, FeO = 7–8%, MgO = 15–17%).
   - Fe-stained minerals – trending towards pure Fe-oxide (hematitization) particularly of chlorite. Some of the pure hematite form veins cutting through all mineral phases listed above.
7. Calcite, (MnO_2 = 0.3–2%).

Notable: Quartz "4", are cutting through the chlorite mylonite but the quartz vein is later penetrated by merely the Mg-rich chlorite from the mylonite. It is really hard to distinguish age-relations.

Also present are small lenses of elongated albite mylonite with adularia (microcline?) and Fe/Mg-chlorite (FeO: 26–28%, MgO: 14–16%) in it. These lenses are surrounded by later "2".

Visible macroscopically: Quartz mylonite is present as fragments in the later chlorite dominated mylonite. One of the calcite fillings seems to be very old and deformed and one of the calcite fillings looks fairly young and fresh.

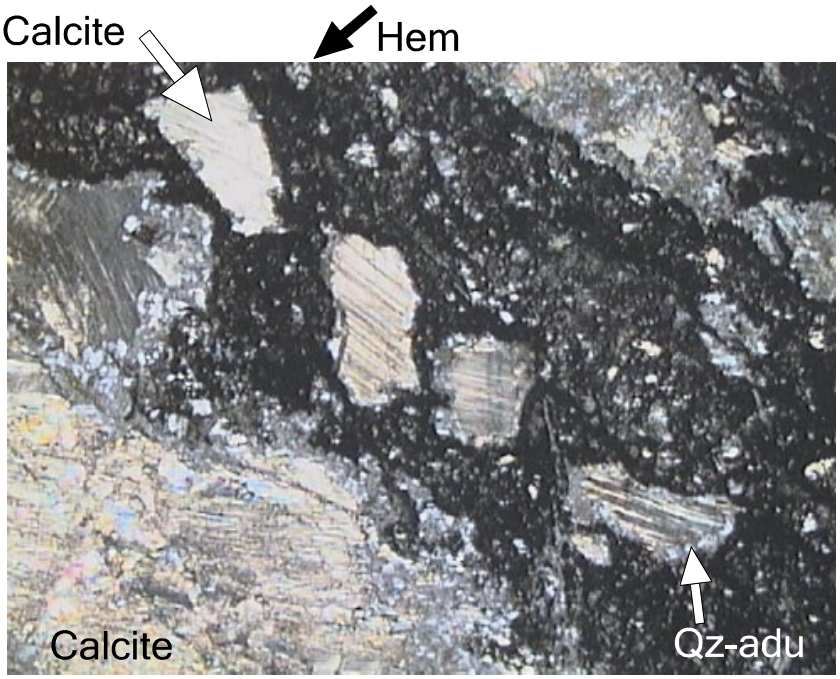

Figure A-28. *Early calcite ("3" in order), is penetrated by a dark-red cataclasite (Hem – "4" in order). Quartz and adularia (Qz-adu – "5"–"6" in order) are growing on the "rim" of the cataclasite and are penetrating into the calcite. Photomicrograph, width c 5 mm.*

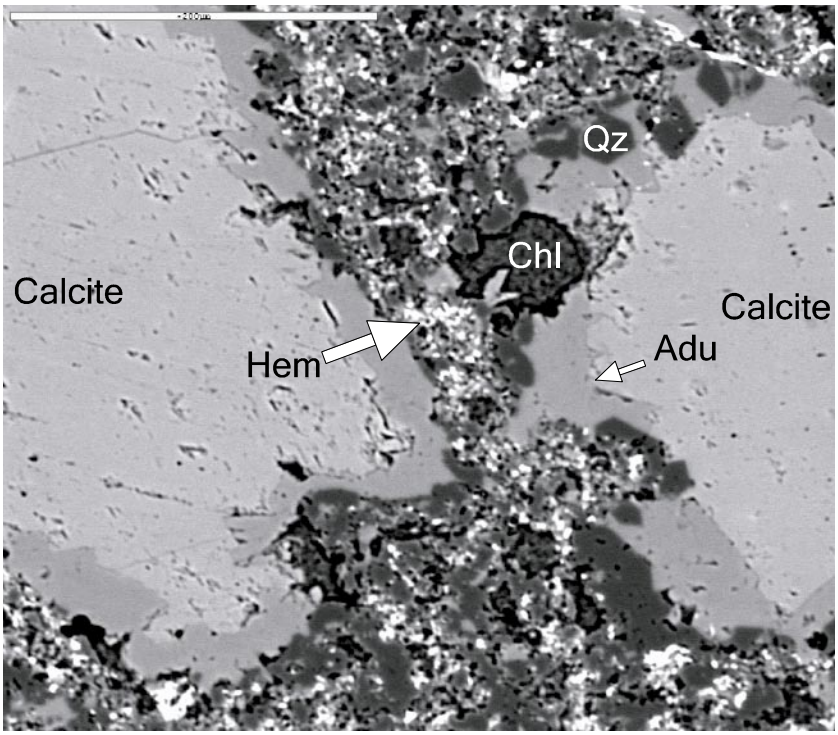

Figure A-29. *Calcite is penetrated by a hematite-rich cataclasite (Hem). Quartz (Qz) and even later Mg-rich chlorite (Chl) and adularia (Adu) are all later than the hematite-rich "cataclasite". Backscattered electron image. Scale bar is 200 µm.*

793.70–793.80 m:

Rock type: Granite to quartz monzodiorite, generally porphyritic.
Fracture: Closed, 2–4 mm wide.
Orientation: (Steep)

Minerals: Amphibole, Prehnite, Fluorite

Order:

1. Big idiomorphic crystals of prehnite (> 1 mm) are penetrating the amphibole. The prehnite crystals show growth-zonation with Fe-rich (7% FeO) and less Fe-rich (5% FeO) horizons. Fluorite is related to the prehnite cutting the wall-rock but the fluorite does not grow in to the amphibole at any visible location in this thin-section.
2. Big idiomorphic crystals of Ca-Fe amphibole, > 2 mm.

Wall-rock alteration: Plagioclase is slightly altered but is not very red coloured. The quartz in the wall-rock show undulose extinction and growth of sub-grains are visible. Chlorite and epidote are present.

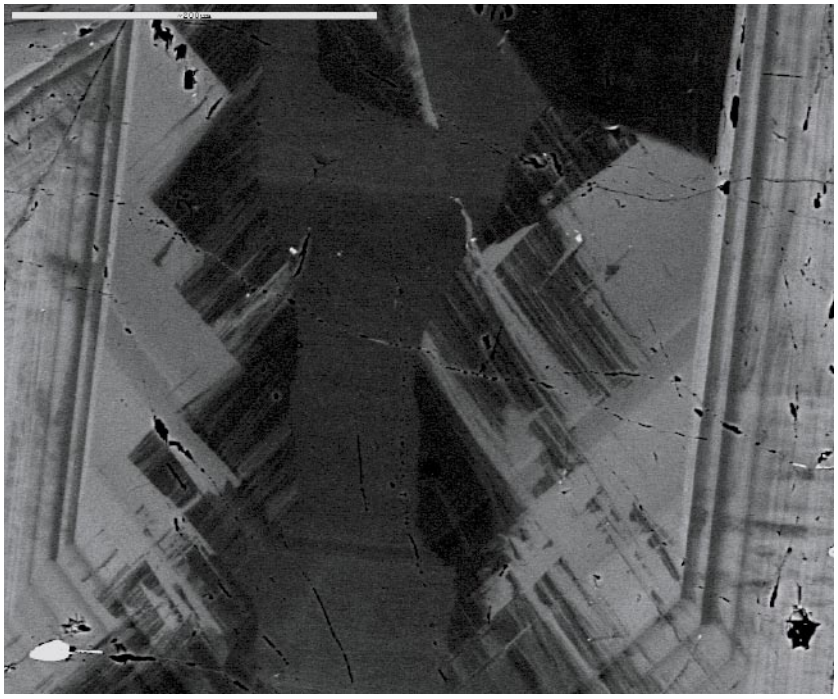

Figure A-30. *Interior of a big idiomorphic prehnite crystal. Bright fields are more Fe-rich (7% Fe) than dark fields (5% Fe). Backscattered electron image. Scale bar is 200 µm.*

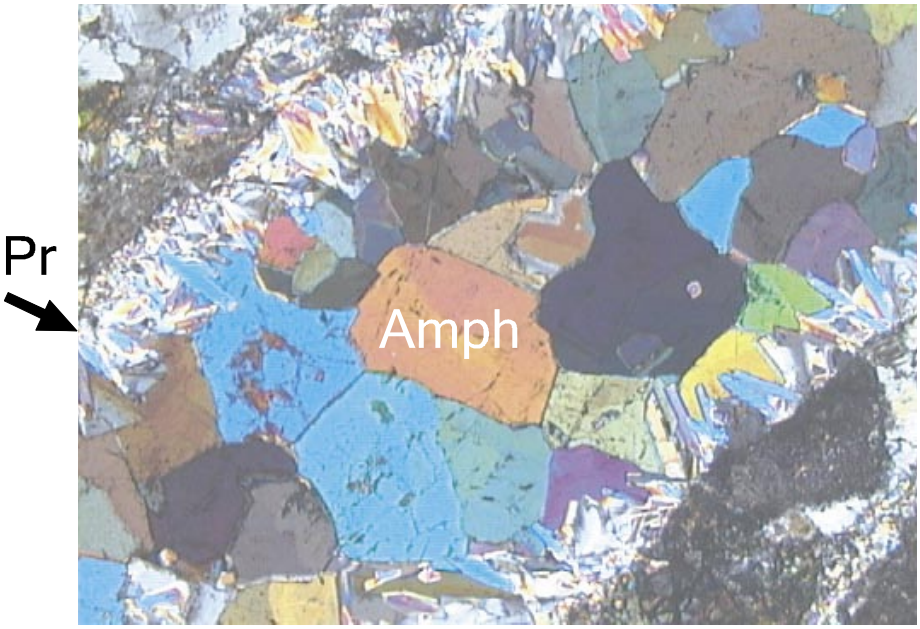

Figure A-31. *Fracture with idiomorphic amphibole (Amph) is coated by idiomorphic prehnite (Pr). Photomicrograph, width c 5 mm.*

873.55–873.60 m:

Rock type: Granite, medium- to coarse-grained
Fracture: Open, 8–9 mm of the old fracture filling is remaining
Orientation: 337°/29°

Minerals: Pyrite, Muscovite, Calcite (2-3 generations), Chlorite, Adularia, Quartz, Titanite, Fluorite, Albite, Chalcopyrite

Order:

In the wall-rock:

1. Re-crystallised, fine-grained quartz.
2. Titanite (cut by fine-grained epidote) – chlorite (Fe-rich, FeO: 23%, MgO: 19%), muscovite.

(2?): Calcite cutting fine-grained quartz.

In the big fracture:

1. Idiomorphic quartz.
2. Idiomorphic pyrite (with some chalcopyrite), coarse-grained calcite (MnO_2 = 0.7–1%) and re-crystallised quartz.
3. Fine-grained calcite (MnO_2 = * –1.2%) and Fe/Mg-chlorite.

The small fracture – cutting the big:

1. Calcite (MnO_2 = * %) including earlier idiomorphic epidote crystals.
2. Fe/Mg-chlorite (FeO: 21–24%, MgO: 16–19%), spherulitic, and adularia, with remnants of (early) epidote and quartz in it.

Also present:
- Albite,thin filling: Earlier than “2”, no relation to “1” is present.
- Fluorite: Later than calcite.
- Muscovite is present but is hard to relate to the different generations.

Wall-rock alteration: Not very red coloured. Pyrite grains are visible. Re-crystallised quartz fillings and extremely sericitized idiomorphic plagioclase crystals are numerous in the wall-rock. Fine-grained K-feldspars and some idiomorphic chlorite crystals are also present but they are not as red as the plagioclase crystals are.

Visible macroscopically: The pyrite present in the big fracture seems to be related in time with the quartz and calcite crystals, also present in the big fracture.

A2 Fracture surface sample descriptions

(* = below detection limit, SEM)

211.74-211.77 m:

Rock type:
Fracture: Open
Orientation: 228°/37°

Minerals: Harmotome, Calcite

Order:

1. Idiomorphic harmotome and calcite (scalenoedral crystals).

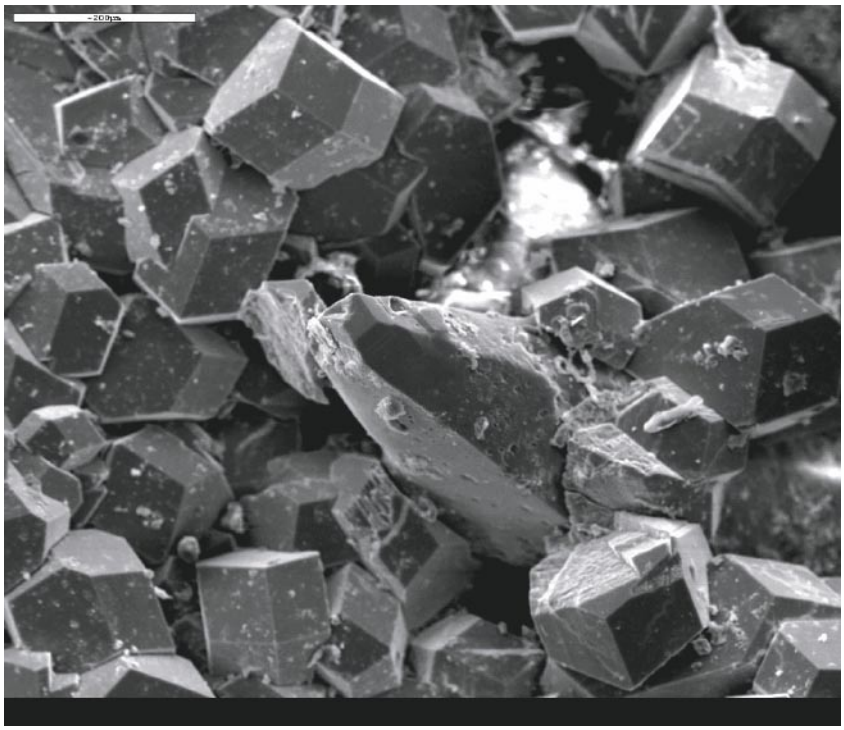

Figure A-32. *A single scalenoedral calcite crystal, surrounded by idiomorphic harmotome crystals. Electron image. Scale bar is 200 µm.*

242.40–242.48 m (1):

Rock type: Intermediate volcanic rock (quartz latite to andesite)
Fracture: Open, thin surface filling is present
Orientation: Flat

Minerals: Laumontite, Calcite, Quartz, some green mineral

Order:

1. Quartz.
2. Calcite and laumontite (elongated fibrous crystals).

Notable: The relation between calcite and quartz are unclear. Quartz may possibly by of wall-rock origin.

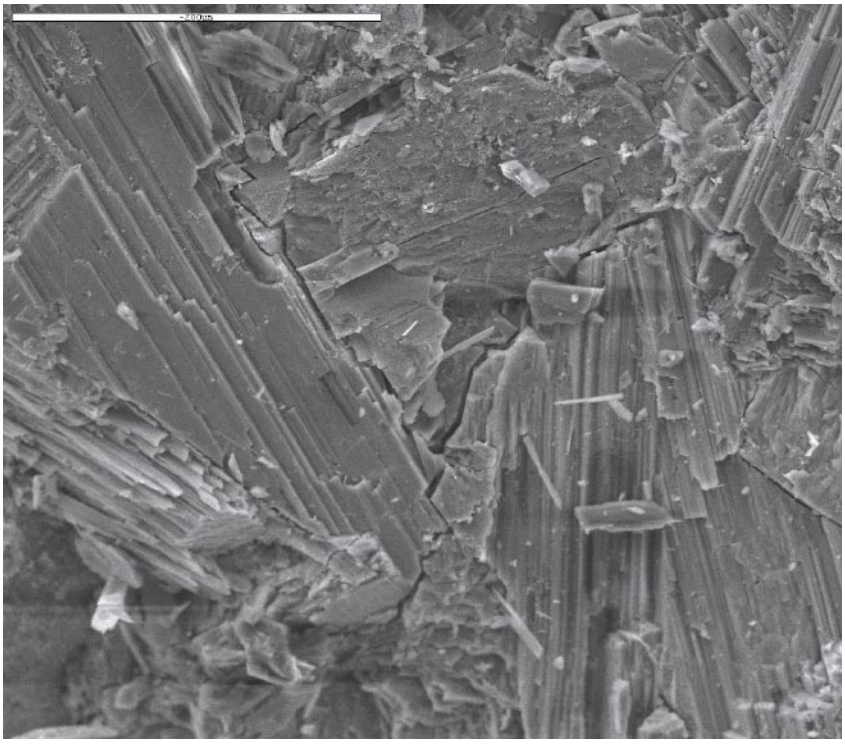

Figure A-33. *Laumontite crystals. Electron image. Scale bar is 200 µm.*

242.40–242.48 m (2):

Rock type: Intermediate volcanic rock (quartz latite to andesite)
Fracture: Open, thin surface filling is present
Orientation: (Vertical-subvertical)

Minerals: Barite, Harmotome, Calcite, Chlorite, Adularia, Hematite, Pyrite, Chalcopyrite

Order:

1. Chlorite (Fe-rich), striated.
2. Fe-rich (to extremely Fe-rich) chlorite, trending towards hematite, adularia (earlier than hematite).
3. Latest: In order (are probably closely related in time):
   - Barite, very big, idiomorphic crystals.
   - Calcite, scalenoedral, only a few crystals.
   - Harmotome, idiomorphic in huge numbers (closely related in time with calcite only a little less covered with Fe-rich chlorite).
   - Chlorite (Fe-rich) is present in small amount on the surface of the calcite and harmotome.

Notable: No relation between the sulfides and barite, adularia etc is found. Sulfides seem to have fresh crystal surfaces and might be of the latest generation (4).

Relations are not all clear, e.g. hard to tell if (2) are older than (3).

Visible macroscopically: Striated chlorite is oldest. The later mineral assemblages have grown upon its striated surface.

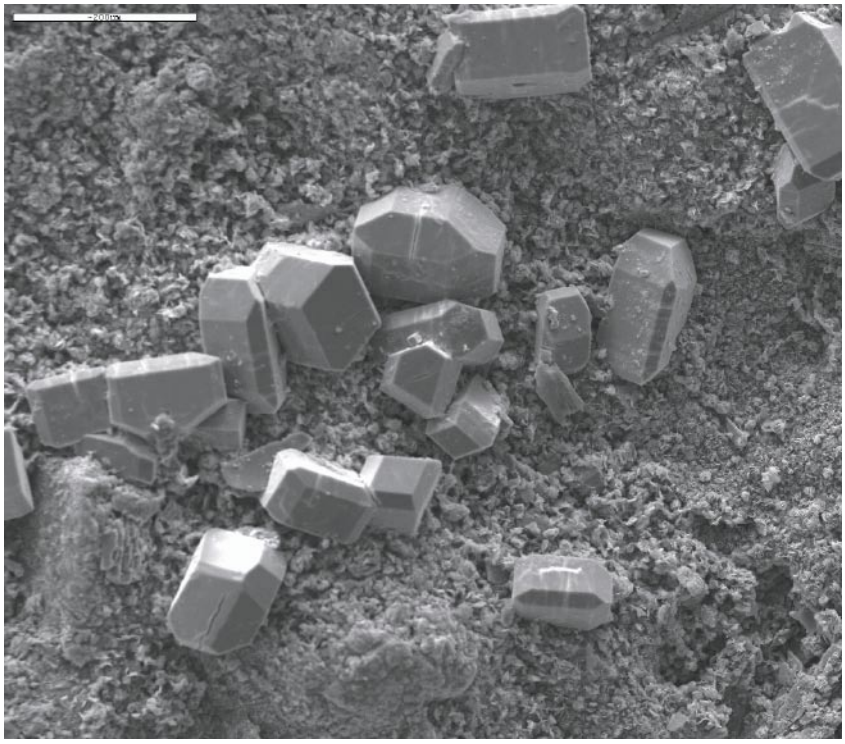

Figure A-34. *Idiomorphic harmotome crystals. Electron image. Scale bar is 200 µm.*

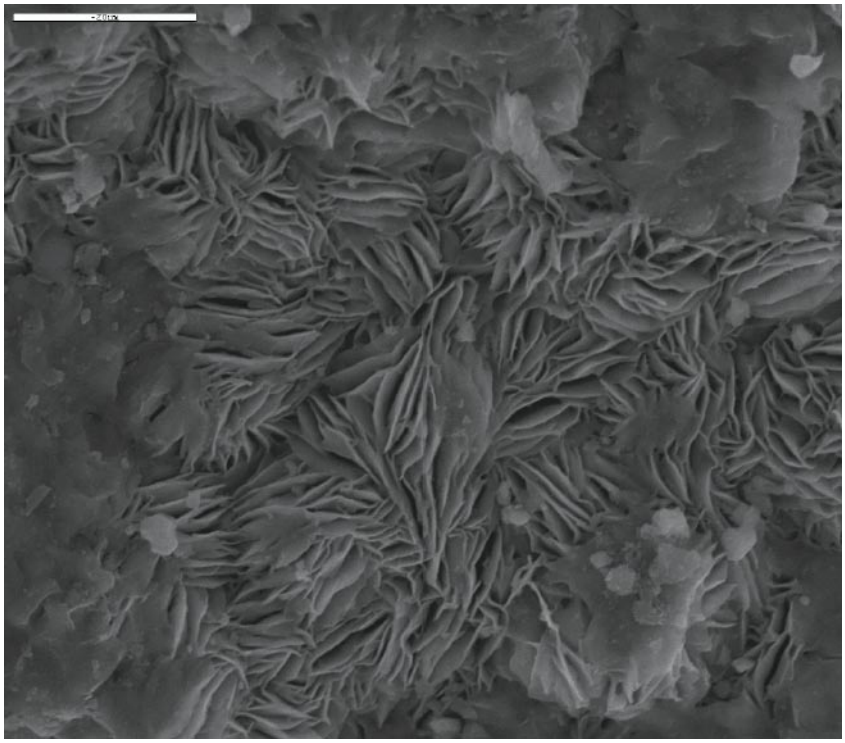

Figure A-35. *Fe-rich chlorite/mixed layer clay. Electron image. Scale bar is 20 µm.*

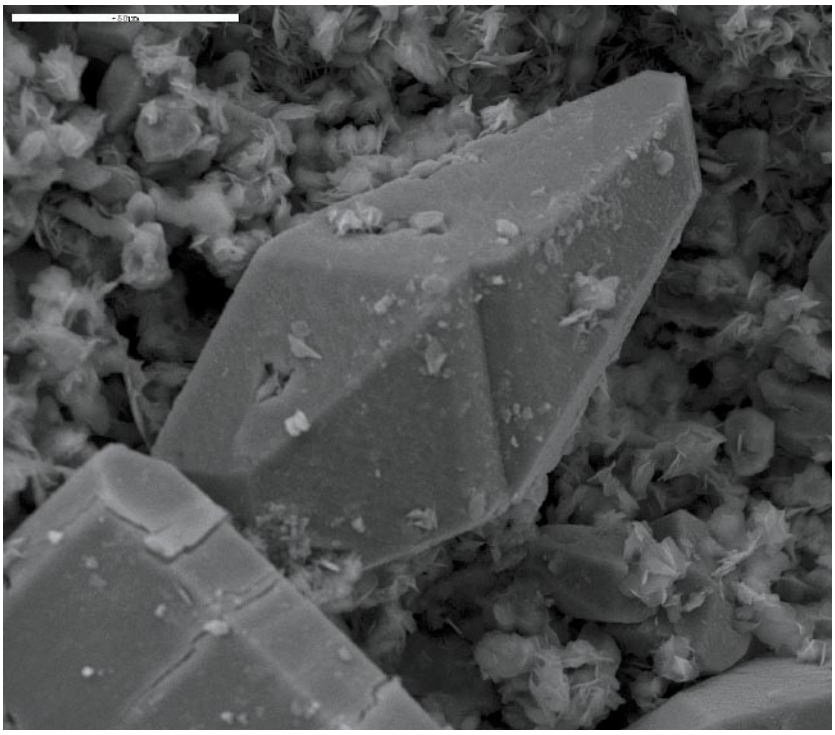

Figure A-36. *Idiomorphic harmotome crystal and a scalenoedral calcite crystal. The calcite crystal has some Fe-rich chlorite on the surface. Electron image. Scale bar is 50 µm.*

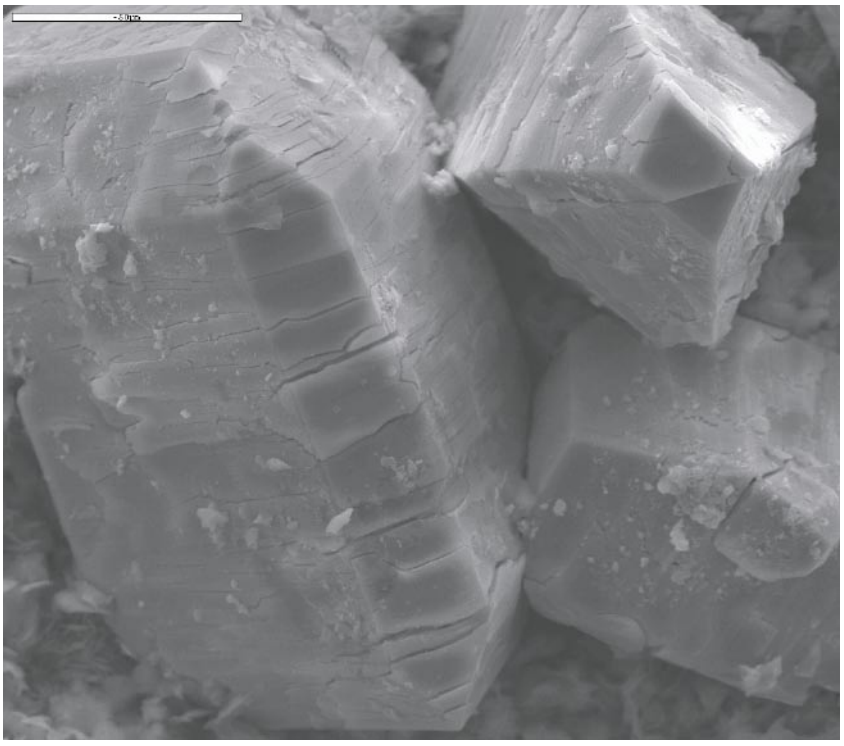

Figure A-37. *Idiomorphic harmotome crystals. Electron image. Scale bar is 50 µm.*

289.80–289.95 m:

Rock type: Quartz monzodiorite, equigranular to weakly porphyritic
Fracture: Open (289.80)
Orientation: 172°/50°

Minerals: Calcite, Chlorite, REE-carbonate

Order all are late:

1. Calcite, very big and numerous, scalenoedral and as bigger aggregates. (MnO_2 = * %).
2. Chlorite, (Fe-rich, FeO ~ 27–30%). May be closely related in time with calcite.
3. REE-rich carbonate. Growing on and "burying" calcite. La-Ce-Nd-Ca(-Na) rich mineral.

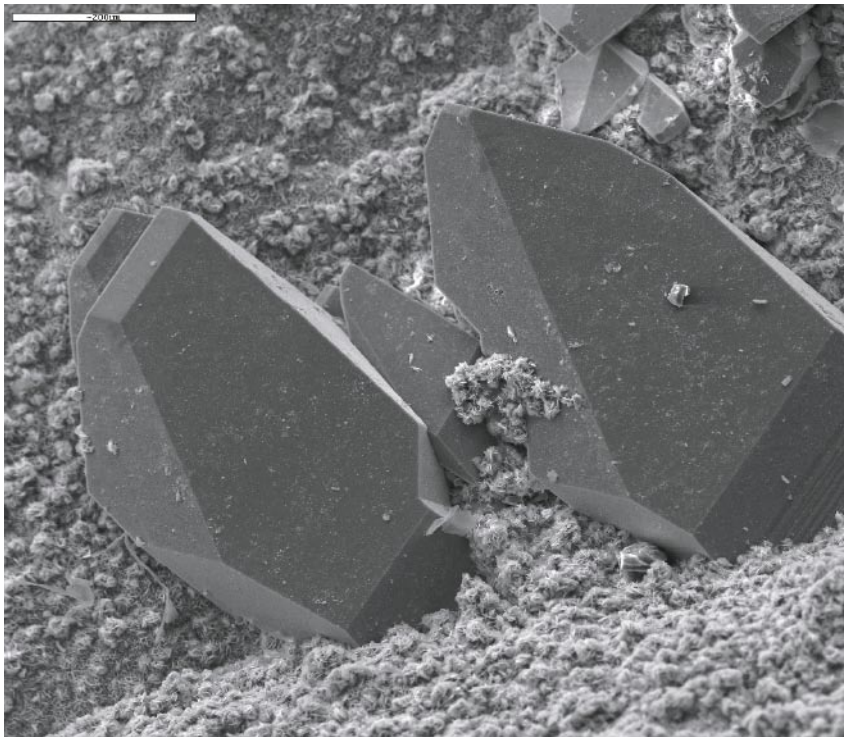

Figure A-38. *Big scalenoedral calcite crystals, with small stains of chlorite on the surfaces. Scale bar is 200 µm.*

611 m:

Surface sample.
Rock type: Intermediate volcanic rock (quartz latite to andesite)

Minerals: Calcite (equant with * % MnO_2)

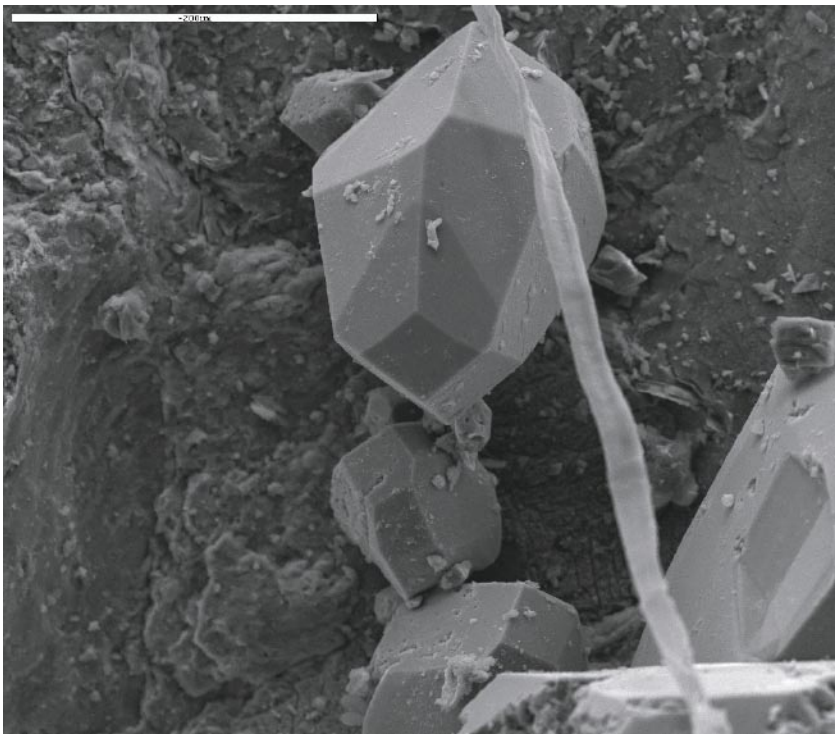

Figure A-39. *Electron image showing some equant calcite crystals. Scale bar is 200 µm.*

A3 SEM-EDS analyses

* = below detection limit (< 0.1 oxide%) (except Na20< 0.3 oxide %)

	MgO	Al2O3	SiO2	K2O	CaO	TiO2	MnO	FeO	Total
208-Fe/Mg-Chlorite	15.40	14.99	30.29	0.18	0.49	*	0.27	21.45	83.06
376-Fe/Mg-Chlorite	15.94	17.05	28.20	*	0.14	*	0.48	24.76	86.58
401-Fe/Mg-Chlorite	13.78	16.26	26.75	*	0.32	*	0.39	28.08	85.57
626-Fe/Mg-Chlorite	13.34	17.39	25.80	*	*	*	0.58	26.82	83.93
130-Fe/Mg-Chlorite(sph)	14.72	21.08	25.71	*	*	*	*	26.10	87.61
208-Mg-Chlorite	17.27	13.86	38.47	3.16	1.55	*	0.34	9.75	84.39
257-Mg-Chlorite	20.17	22.25	40.12	*	*	*	*	4.50	87.03
596-Mg-Chlorite	21.18	14.29	32.03	0.15	3.66	*	0.66	10.93	82.90
596-Mg-Chlorite(2)	22.45	13.70	36.44	0.75	1.43	*	0.57	9.96	85.30
208-Fe-Chlorite	6.95	14.61	30.35	*	2.46	*	0.78	34.07	89.22
257-Fe-Chlorite	4.97	12.78	27.34	*	*	*	0.38	37.42	82.90
257-Fe-Chlorite(2)	3.99	12.62	27.94	0.23	0.51	*	*	43.24	88.52
257-Fe-Chlorite(3)	4.18	11.91	27.91	0.18	0.43	*	0.23	43.04	87.89
289-Fe-Chlorite	4.22	16.73	27.54	*	0.59	*	0.41	38.06	87.55
257-Fe-stained-Chlorite	9.96	11.74	28.13	3.38	0.80	1.15	0.38	39.00	94.54
257-Fe-stained-Chlorite	5.31	5.99	10.50	0.35	0.21	0.99	0.22	68.35	91.94

	SiO2	Al2O3	CaO	FeO	Total
289-Prehnite	42.31	20.85	26.00	5.75	94.92
795-Prehnite	43.60	23.23	26.88	2.29	96.00

	MgO	Al2O3	SiO2	CaO	FeO	Total
130-Epidote	*	20.46	37.85	22.25	16.41	96.98
401-Epidote(odd variety)	0.64	12.39	34.04	29.91	15.95	92.93

	Na2O	MgO	Al2O3	SiO2	K2O	CaO	FeO	BaO	Total
130-Harmotome	2.23	1.02	18.96	51.64	1.03	0.35	2.11	17.44	94.79
208-Harmotome	2.88	*	19.63	49.16	0.67	0.11	*	22.35	95.55

	Na2O	Al2O3	SiO2	K2O	CaO	Total
213-Laumontite	0.18	21.84	51.64	0.15	11.24	85.06

	MgO	Al2O3	SiO2	K2O	FeO	Total
626-Muscovite	1.41	32.11	47.08	10.70	3.88	95.18

	MgO	SiO2	CaO	MnO	FeO	Total
795-Amphibole	1.40	54.40	20.14	1.83	20.11	97.87

	Na2O	Al2O3	SiO2	K2O	CaO	BaO	Total
213-1-K-feldspar(1)	0.33	18.98	64.75	15.97	0.36	1.01	101.40
376-K-feldspar(1)	0.61	19.06	64.57	15.65	*	0.67	100.60
376-K-feldspar(2)	0.78	18.78	64.90	15.35	*	0.30	100.06
257-Adularia-gen5	*	18.82	66.15	15.24	*	0.48	100.69
257-Adularia-gen6(1)	*	18.68	64.30	16.30	*	*	99.24

	Na2O	MgO	Al2O3	SiO2	K2O	CaO	TiO2	MnO	FeO	BaO	Total
376-Biotite(1)	*	10.30	14.40	36.22	9.83	0.14	3.85	0.28	21.06	*	96.43
376-Biotite(2)	0.36	10.10	14.72	36.46	9.40	0.14	2.99	0.29	22.18	*	96.82

A4 ICP-MS analyses

ICP-MS analyses (ppm): Harmotome; BaO is set to 20%, based on SEM-EDS analyses.

	Harmotome 1	Harmotome 2	Harmotome 3	Harmotome 4
Si29	605,793.3	572,779.4	517,268.5	605,793.3
Si30	638,077.3	574,765.3	542,316.6	689,762.1
K39	3,323.6	2,564.2	2,080.9	3,281.1
Ca43	6,706.9	5,342.2	2,739.3	16,949.8
Ca44	5,127.4	2,563.1	< 2,100	9,292.8
Rb85	39.2	39.7	34.3	43.5
Sr88	60.9	63.3	61.4	53.0
Y89	5.1	4.8	3.9	5.2
La139	9.5	3.6	2.3	3.7
Ce140	10.5	5.0	3.3	5.0
Pr141	1.52	0.96	0.45	0.60
Nd146	5.6	2.8	1.39	2.5
Sm147	0.99	< 0.8	< 1.3	< 0.9
Eu151	2.2	2.0	1.85	2.3
Eu153	4.1	3.7	3.8	4.2
Gd157	< 0.7	0.73	< 1	< 0.7
Tb159	< 0.09	0.110	< 0.12	< 0.08
Dy163	< 0.5	0.54	< 0.6	0.55
Ho165	< 0.08	0.098	< 0.11	< 0.08
Er166	< 0.4	< 0.4	< 0.6	< 0.4
Tm169	< 0.07	< 0.06	< 0.09	< 0.07
Yb172	< 0.8	< 0.6	< 1.1	< 0.7
Lu175	< 0.08	< 0.07	< 0.11	< 0.08
Th232	< 0.32	< 0.26	< 0.4	< 0.3
U238	< 0.17	0.136	< 0.23	0.27

ICP-MS analyses (ppm): Biotite.

	Si30	K39	Ca43	Ca44	Ti47	Fe57	Rb85	Sr88	Ba137
Biotite1	268,169	41,822.4	< 1,600	< 1,600	28,641	86,807	385	1.32	1,298
Biotite2	189,318	46,944.4	< 2,400	< 2,400	31,495	102,046	482	2.5	1,791
Biotite3	259,929	42,986.5	< 1,300	< 1,300	28,595	101,220	424	1.24	1,547

ICP-MS analyses (ppm: K/Ba-ratio): K-Feldspar (wall-rock), Adularia (in fractures).

	K39/Ba137
K-feldspar1	85.1
K-feldspar2	91.2
K-feldspar3	82.9
K-feldspar4	63.8
Adularia1	30.0
Adularia2	25.3
Adularia3	12.4
Adularia4	15.6
Adularia5	19.0
Adularia6	15.7
Adularia7	41.0
Adularia8	33.9
Adularia9	90.5
Adularia10	31.1
Adularia11	25.6
Adularia12	22.8

A5 XRD analyses of fracture material from open fractures in borehole KSH01 (Analyses carried out by SGU, Uppsala)

Sample Core length	Qtz	K-fsp	Alb	Ca	Chl	Py	Hem	Amp	Bi	Pre	Epi	Apo	Clay	Corr	M-l Clay	Ill	Smec
3.7–3.87	x			xxx	(x)								xx	yy’			y
24.0	xx	xx	x		x	x		x					x				yy
67.8–67.9	xx	xx	xx	x	xx								x		yy	(y)	
81.35	xx	xx	xx	x	x								x		y	yy	
82.2	xx	xx	xx	x	xx								x		yy	y	
95.0		xx	xx	xxx	x			x			x		x	y	y	(y)	
130.83	xx		x	xxx	x			x					(x)*				
159.20 m (I)	xx	x	x	xxx	xx			x					x	yy			
159.20 m (II)	xx	xx	x	xx	xxx			x					xx*			y	
178.25–178.35			xx	xx	x							xxx	x	yy			
249.0	x	x	x	xx	x								(x)*				
250.4	xx	xx		x	xx		x						(x)			(y)	
255.78–255.93	xx	xx		x	xx		x						X	yy’			
259.3	xx	xx		xx	xx		x						X		yy	y	
267.97–268.02	xx	xx		Xx	xx		x						xx	yy			
289.8–289.95	xx	xx			xxx								x				yy
290.9	xx	x	xxx	xx	xx								x	yy			
306.77	x	x	x	xxx	x								x	yy			
325.93	xx		x		x				xx			xx	x	yy			
447.34	xx	x			xx					xx	x	xx	x	yy			
514.46	xx			xx	xx								x	y	yy		
558.60–558.65	xx	xx		x	xx		x						x	yy			
590.35–590.52	xx	xx	xx		xx								x		y	yy	

Qz = quartz, K-flsp = K-feldspar usually adularia, Alb = Na-plagioclase (albite), Chl = chlorite, Py = pyrite, Hem = hematite

Amp = amphibole, Bi = biotite, Pre = prehnite, Ep = epidote, Apo = apophyllite, Clay = presence of clay minerals indicated in the random oriented sample, the clay minerals are identified in fine fraction oriented sample, results are marked with y.

xxx = dominates the sample, xx = significant component, x = minor component, OBS this is only semi-quantitative.

Corrensite = swelling mixed layer clay with chlorite/smectite or chlorite/vermiculite regularly interlayered, M-l clay = mixed layer clay with illite/smectite layers, ill = illite, Smec = smectite * = indicates swelling chlorite, ‘ = indicates corrensite without 1:1 layering.

yy = dominating clay mineral in the fine fraction, y = identified clay mineral in the fine fraction.

( ) = potentially present

* = swelling chlorite

A6 Table showing all samples analysed for stable isotopes and trace element composition from borehole KSH01

Sample	Comment (morphology/ generation)	$\delta^{18}O$	$\delta^{13}C$	$^{87}Sr/^{86}Sr$	Chemical analyses
KSH01B:1.25–1.45		–7.43	–11.06		
KSH01B:3.7–3.87		–12.41	–15.4		
KSH01B:20.77–21.01		–9.18	–6.86		
KSH01B:40.1–40.38		–7.47	–3.2		
KSH01B:67.8–67.9		–6.61	–11.69		
KSH01B:72.6–72.7		–7.44	–23.85		
KSH01B94.8–94.9		–8.88	–8.7		
KSH01A:130.83–131.0	Short C-axis Nailheaded	–8.61	–11.17		
KSH01A:130.83–131.0	Elongated C-axis Scalenohedral	–5.89	–9.8		
KSH01A:159.2	Equant	–7.16	–13.49		
KSH01A:198.0–198.1	Elongated C-axis Scalenohedral	–12.78	–15.44	0.712814	ICP-leachate
KSH01A:198.1B	Elongated C-axis Scalenohedral	–12.64	–25		
KSH01A:198.0–198.2		–8.49	–26.25	0.714992	
KSH01A:208.65	Gen 4 or 6?	–10.68	–6.47	0.709307	ICP-leachate
KSH01A:211.74–211.77	Equant	–8.2	–14.92		
KSH01A:249.65		–12.97	–15.58	0.713193	ICP-leachate
KSH01A:250.4-5		–11.98	–15.62		
KSH01A:255.78-93		–8.91	–23.74		
KSH01A:257.8	Gen 6	–9.57	–12.68	0.711258	ICP-leachate
KSH01A:259.4		–13.37	–13.04		
KSH01A:259.4		–11.75	–15.86		
KSH01A:267.97(I)		–9.84	–17.6		
KSH01A:267.97 (II)		–7.04	–23.28		
KSH01A:287.4	Gen 6	–8.59	–9.42	0.712097	
KSH01A:289.802–289.95	Equant	–6.6	–21.72		
KSH01A:289.802–289.96	Elongated C-axis Scalenohedral	–6.4	–17.68	0.715985	
KSH01A:306.7	Equant	–8.13	–5.95		
KSH01A:363.6	Equant	–9.87	–6		
KSH01A:363.65 B		–10.08	–6.3		ICP-leachate
KSH01A:363.65 A	Gen 6	–10.38	–6.34	0.712575	
KSH01A:401.05	Gen 2	–20.33	–3.82	0.707743	ICP-leachate
KSH01A:557.3-5		–19.52	–3.59		
KSH01A:590.36-52		–7.97	–9.02		
KSH01A:600.22	Gen 4	–20.72	–3.92	0.709479	
KSH01A:603.18	Gen 4	–18.11	–3.41	0.709966	ICP-leachate
KSH01:611	Contaminated with Ba-zeolite	–7.96	–6.52	0.715798	ICP-leachate
KSH01A:626.8 (1)	Gen 4?	–14.97	–2.3	0.711238	ICP-leachate
KSH01A:626.8 (3)	Gen 6	–15.537	–9.78	0.712868	
KSH01A:875.79	Gen 2	–20.99	–4.16	0.707551	

A7 ICP-MS analyses of calcite samples, KSH01

Sample:		198.0	249.65	401.25	208.65	257.80	363.65	603.28-1	603.28-2	611	626.8
Weight	**mg**	9.7	13.89	3.08	12.88	13.82	13.99	13.66	13.47	12.56	13.17
						dissol.rest	dissol.rest				dissol.rest
Na/23	ppm	< 20	< 20	115	197	215	94	40	44	86	59
Mg/24	ppm	103	154	2,294	495	1,992	351	127	120	227	79
Al/27	ppm	119	8	803	792	2,163	46	237	249	497	75
K/39	ppm	45	40	176	130	976	63	191	197	213	90
Ca/43	ppm	472,579	458,514	454,628	464,981	349,951	484,480	462,151	457,785	456,495	485,471
Sc/45	ppm	0.36	1.48	2.31	0.51	1.20	8.67	0.37	0.42	0.54	0.39
Mn/55	ppm	287	19,812	3,886	80	147	6,553	543	537	425	980
Fe/57	ppm	1,261	1,109	5,978	1,927	2,708	1,173	1,204	1,265	1,543	991
Rb/85	ppm	0.06	0.05	0.63	0.20	4.72	0.06	0.73	0.80	1.51	0.18
Sr/88	ppm	46	66	307	80	55	45	214	215	112	134
Y/89	ppm	1.87	167.77	9.12	2.39	3.82	41.45	0.17	0.16	0.86	6.83
Ba/137	ppm	1	2	14	132	33	2	6	4	4,852	10
La/139	ppm	7.08	68.91	0.65	1.59	12.26	50.41	14.49	13.61	6.05	2.20
Ce/140	ppm	6.00	239.25	0.97	1.56	13.00	106.32	14.50	14.06	7.18	4.07
Pr/141	ppm	0.51	28.81	0.10	0.25	2.36	11.96	1.18	1.06	0.64	0.41
Nd/146	ppm	2.26	133.04	0.55	1.11	9.84	43.86	3.93	3.67	2.81	2.75
Sm/147	ppm	0.44	30.45	0.11	0.24	1.07	9.19	0.14	0.18	0.40	0.74
Eu/153	ppm	0.09	6.63	0.06	0.05	0.18	1.32	0.01	0.02	0.53	0.16
Gd/157	ppm	0.61	32.01	0.32	0.37	0.97	8.76	0.14	0.11	0.30	1.14
Tb/159	ppm	0.06	4.47	0.07	0.04	0.11	1.26	0.01	< 0.01	0.04	0.15
Dy/163	ppm	0.28	24.53	0.84	0.28	0.52	6.66	0.01	0.03	0.20	0.83
Ho/165	ppm	0.05	4.74	0.29	0.05	0.12	1.32	< 0.01	< 0.01	0.02	0.16
Er/166	ppm	0.13	12.28	1.48	0.13	0.31	3.87	< 0.01	0.03	0.05	0.52
Tm/169	ppm	0.02	1.73	0.34	< 0.01	0.06	0.69	< 0.01	< 0.01	< 0.01	0.08
Yb/172	ppm	0.11	11.22	3.69	0.10	0.34	5.48	< 0.01	< 0.01	0.06	0.41
Lu/175	ppm	0.02	2.01	1.02	0.01	0.04	1.04	< 0.01	< 0.01	< 0.01	0.08
Th/232	ppm	0.02	0.01	0.09	0.01	0.23	0.03	0.02	0.02	0.34	0.02
U/238	ppm	0.02	0.01	0.04	2.68	1.55	0.05	0.02	0.02	0.05	0.16

A8 Macroscopic mapping of KSH01

Title GEOLOGY IN KSH01A **Appendix: A8**

Site	SIMPEVARP	**Coordinate System**	RT90-RHB70
Borehole	KSH01A	**Northing [m]**	6366013.45
Diameter [mm]	76	**Easting [m]**	1552442.98
Length [m]	1003.000	**Elevation [m.a.s.l.]**	5.32
Bearing [°]	173.60	**Drilling Start Date**	2002-08-22 13:00:00
Inclination [°]	-80.43	**Drilling Stop Date**	2002-12-18 21:10:00
Date of mapping	2003-07-04 17:24:00	**Plot Date**	2004-10-21 21:05:26
Rocktype data from	p_rock_XXXXX	**Fracture data from**	p_fract_core

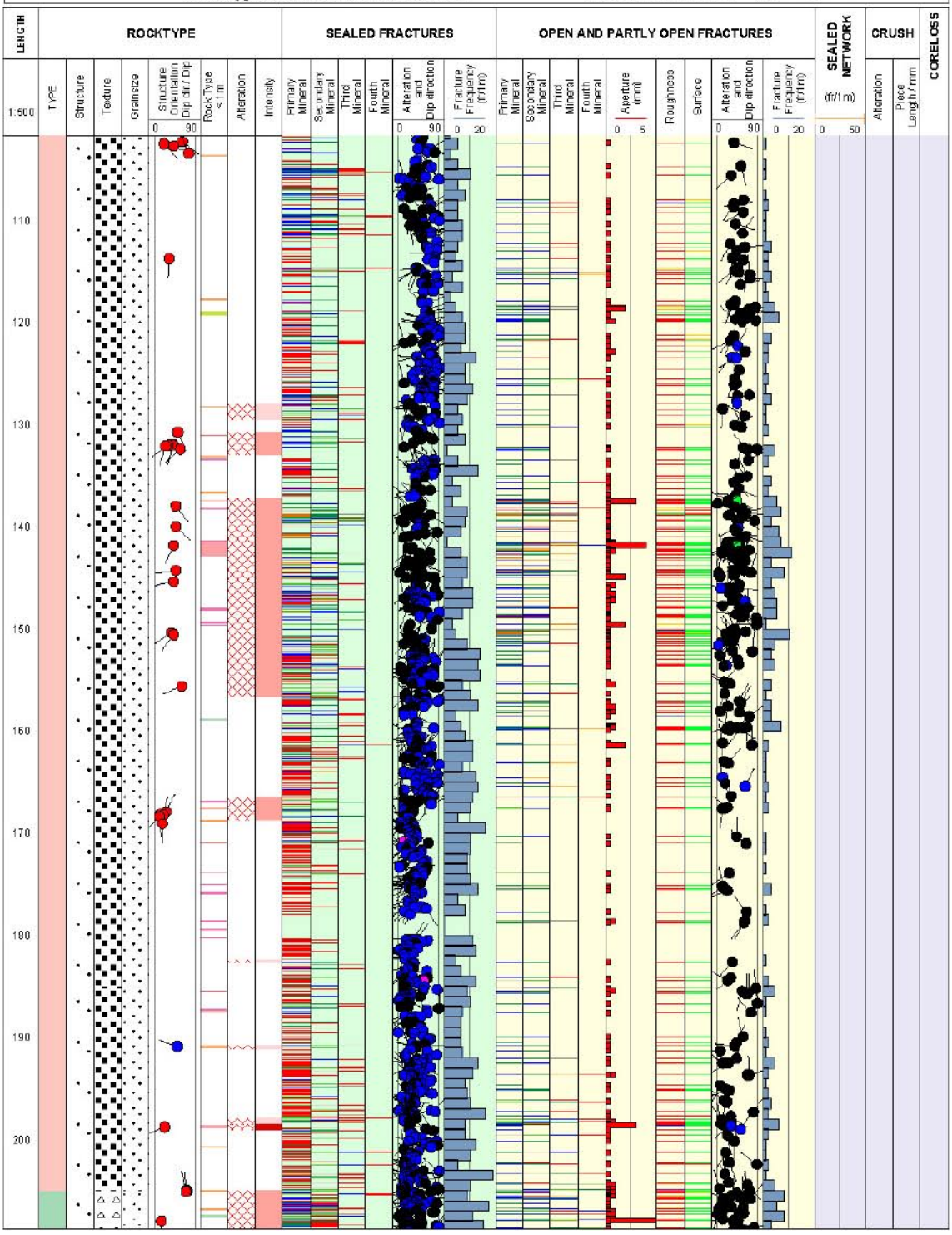

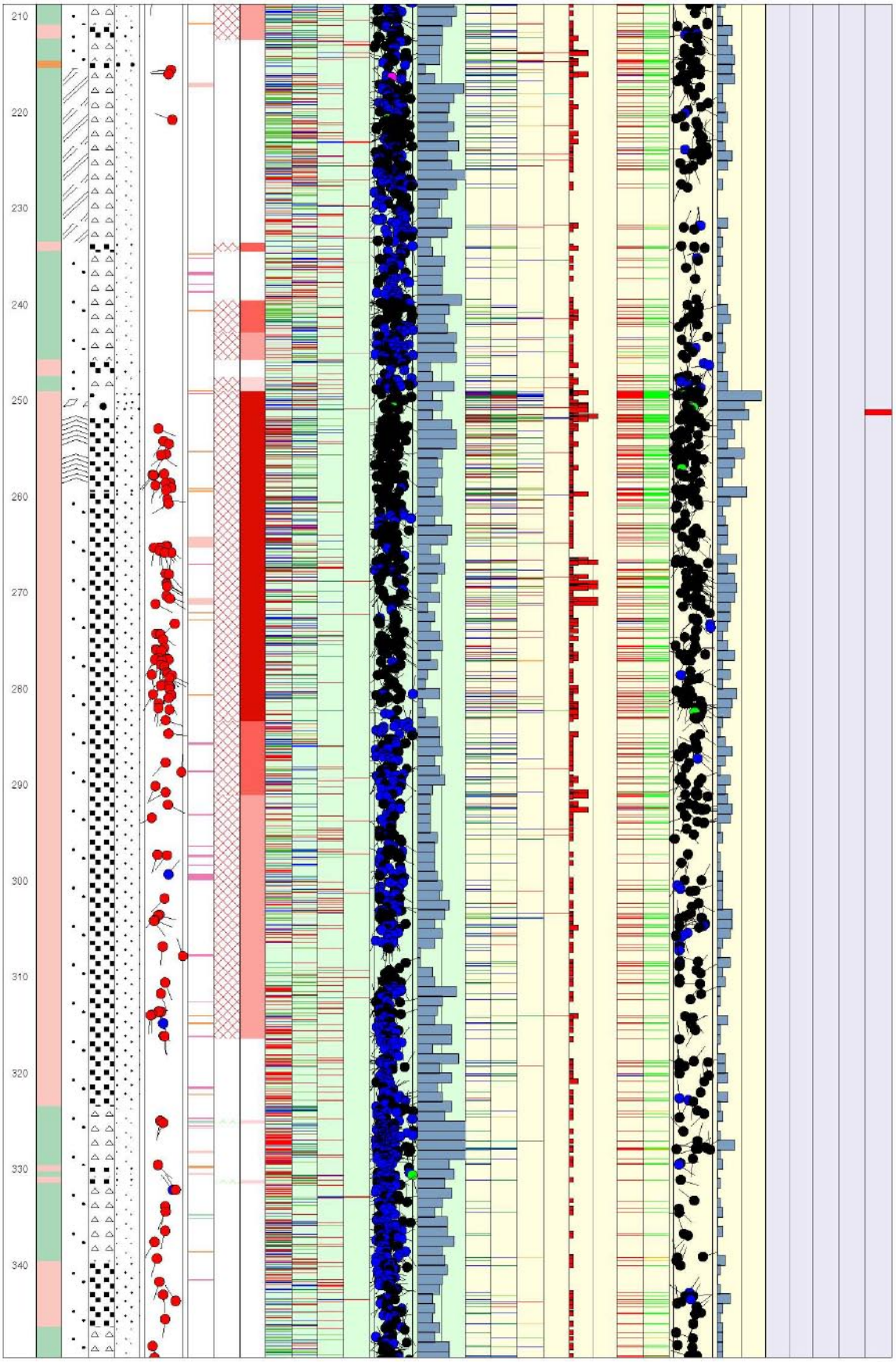
210
220
230
240
250
260
270
280
290
300
310
320
330
340

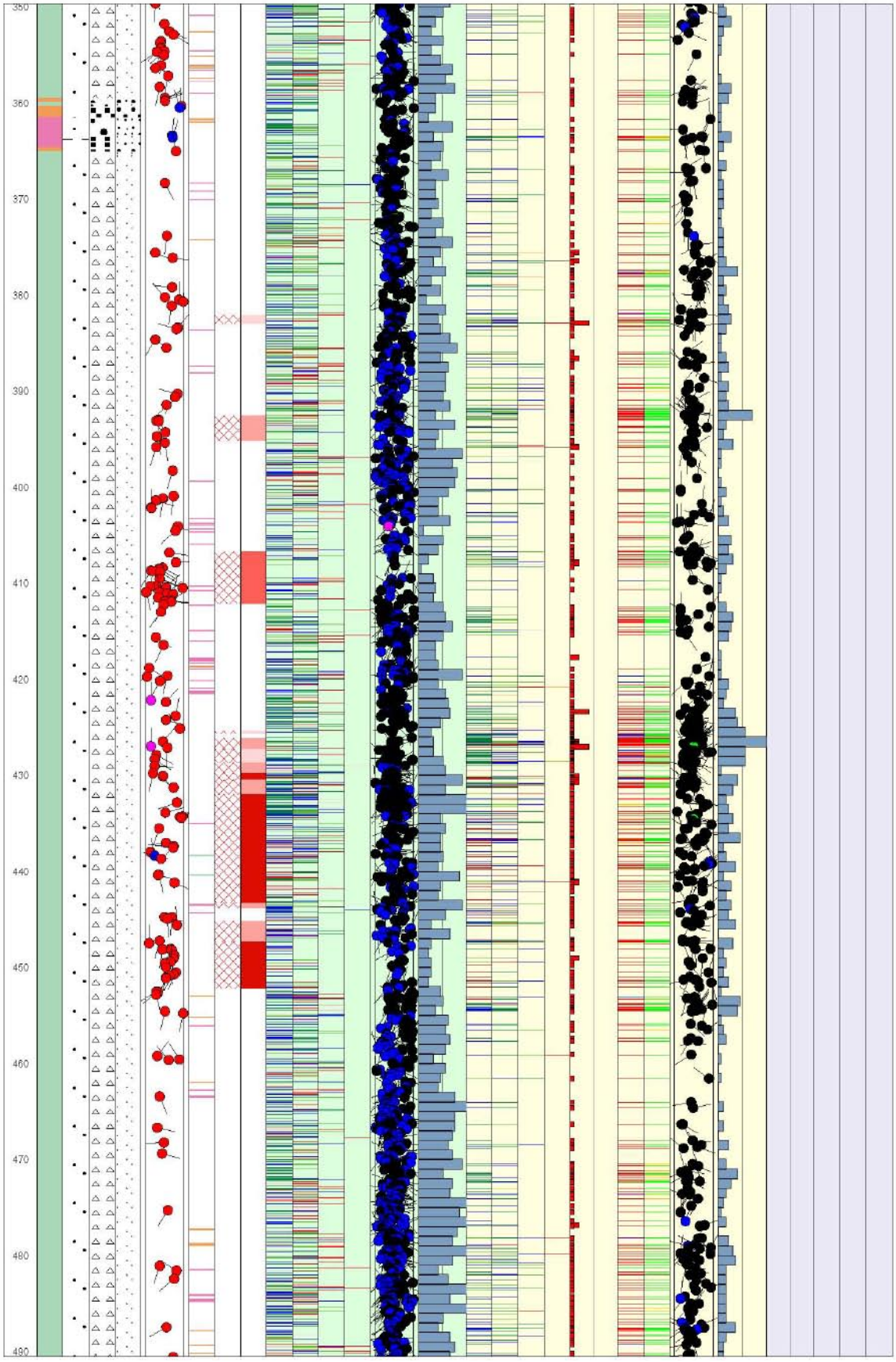
350
360
370
380
390
400
410
420
430
440
450
460
470
480
490

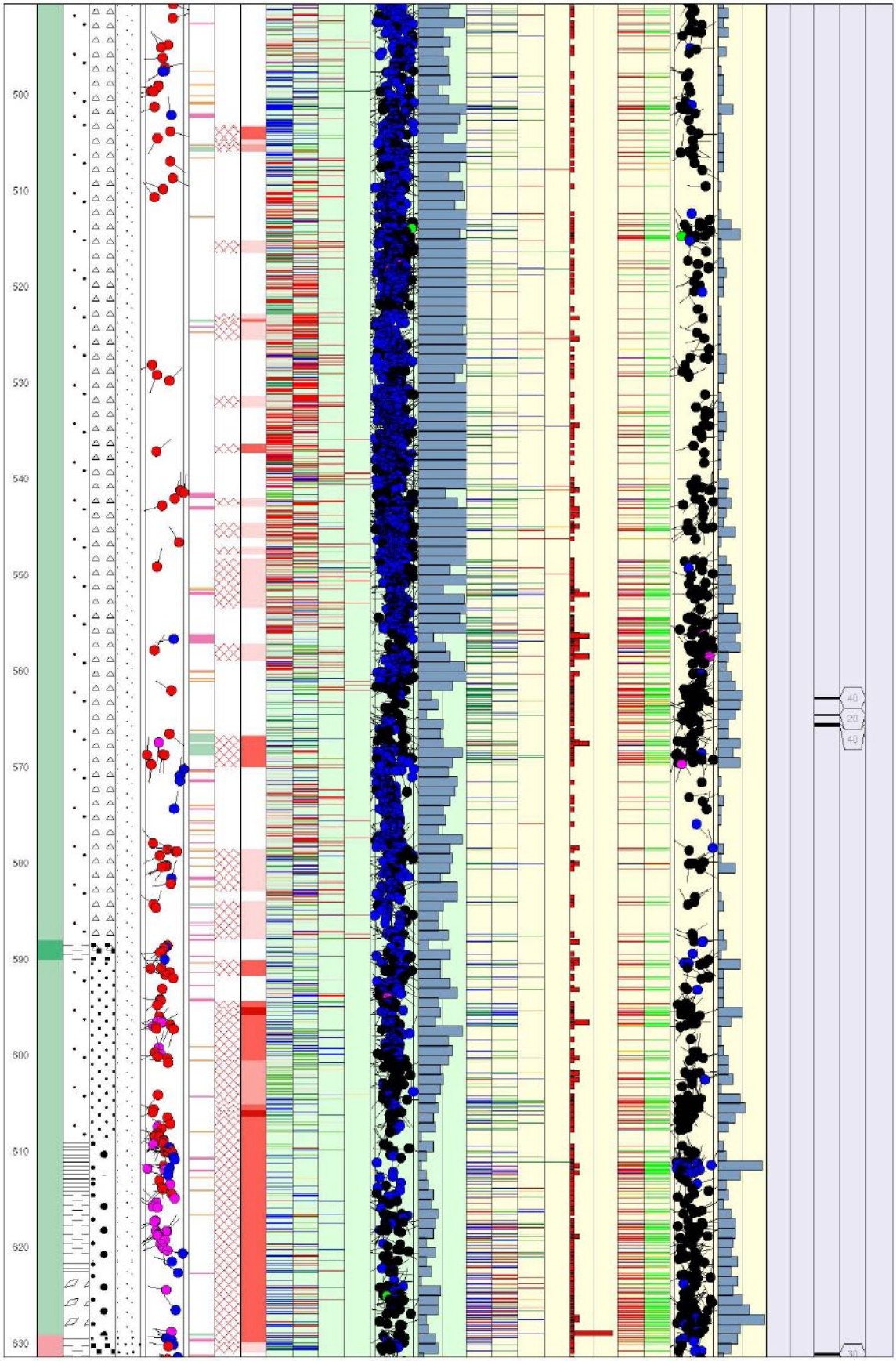
500
510
520
530
540
550
560
570
580
590
600
610
620
630
40
20
40

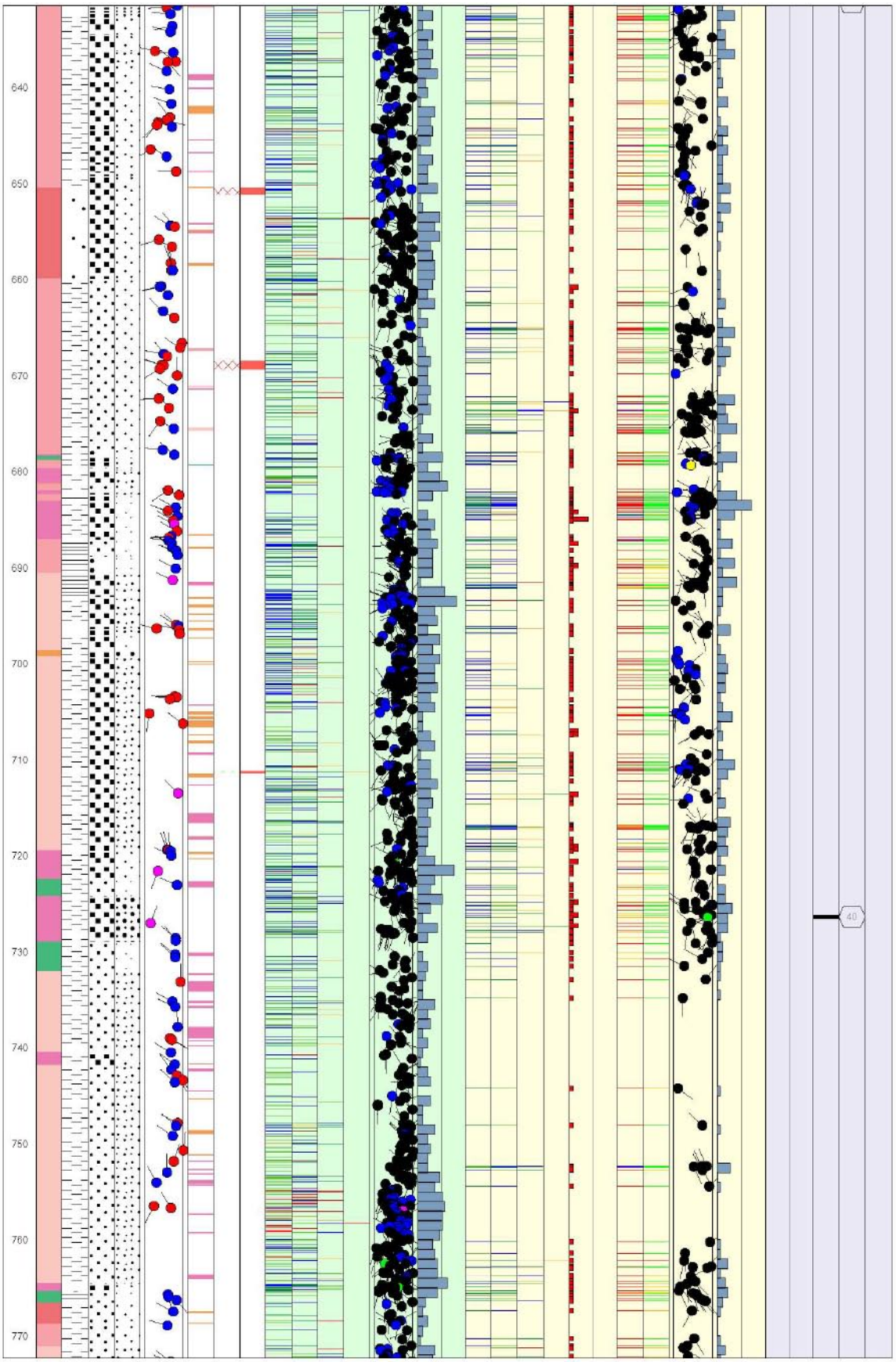
640
650
660
670
680
690
700
710
720
730
740
750
760
770
40

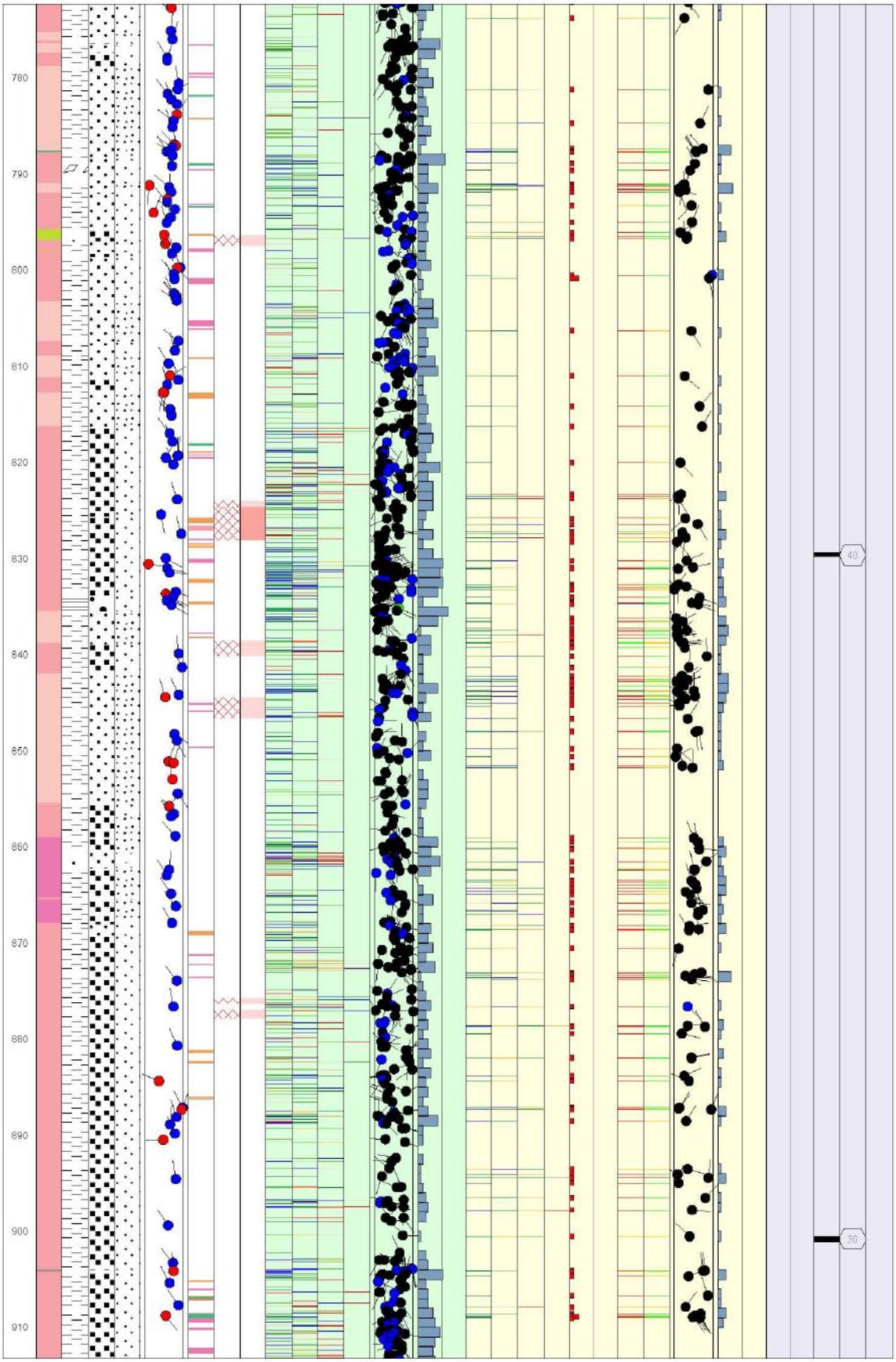
780
790
800
810
820
830
840
850
860
870
880
890
900
910
40
30

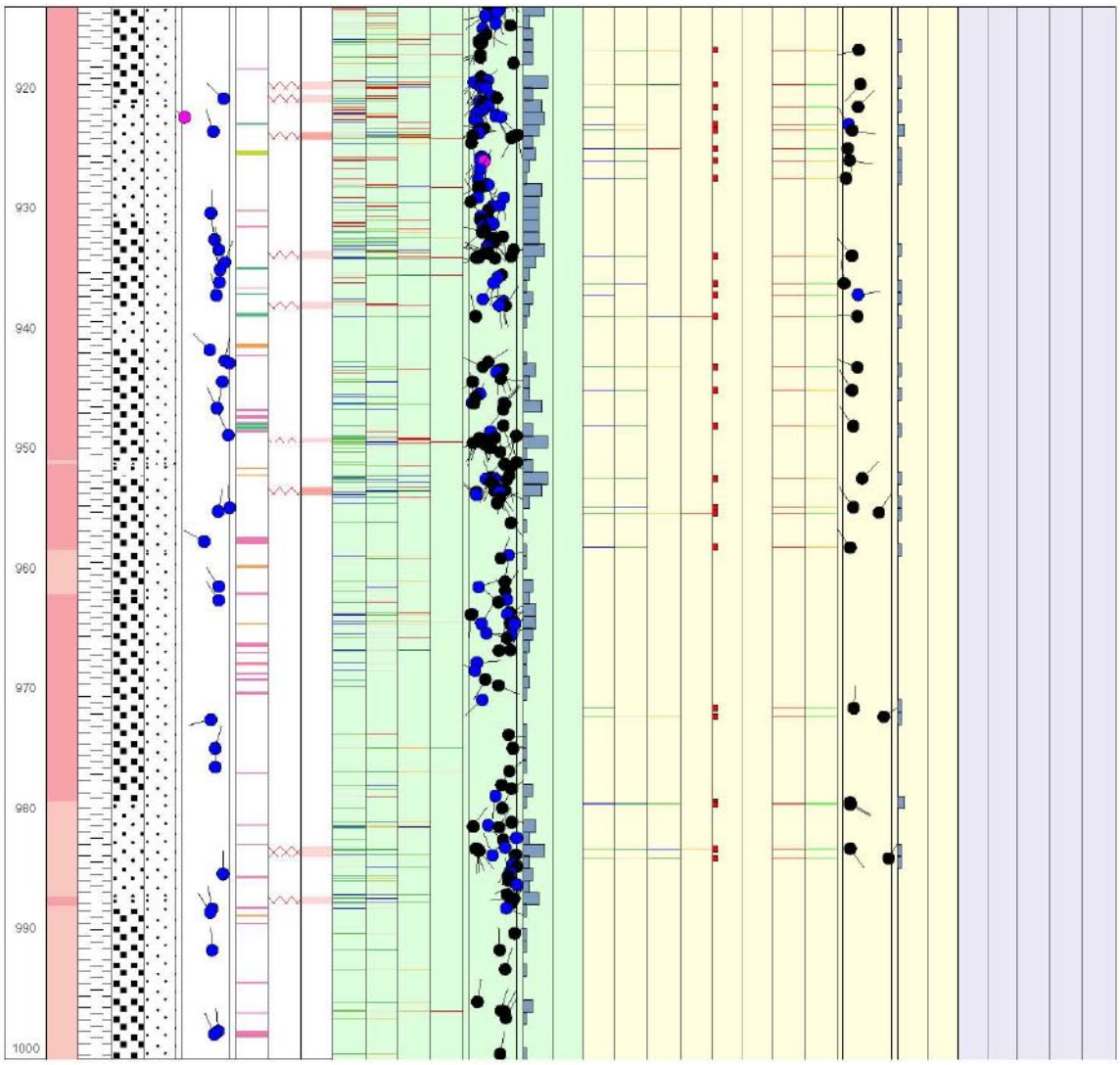
920
930
940
950
960
970
980
990
1000

Title GEOLOGY KSH01B

Site	SIMPEVARP	**Coordinate System**	RT90-RHB70
Borehole	KSH01B	**Northing [m]**	6366014.03
Diameter [mm]		**Easting [m]**	1552442.89
Length [m]	100.250	**Elevation [m.a.s.l.]**	5.20
Bearing [°]	177.76	**Drilling Start Date**	2003-01-17 12:00:00
Inclination [°]	-87.88	**Drilling Stop Date**	2003-01-27 19:00:00
Remark		**Plot Date**	2004-03-10 21:03:30

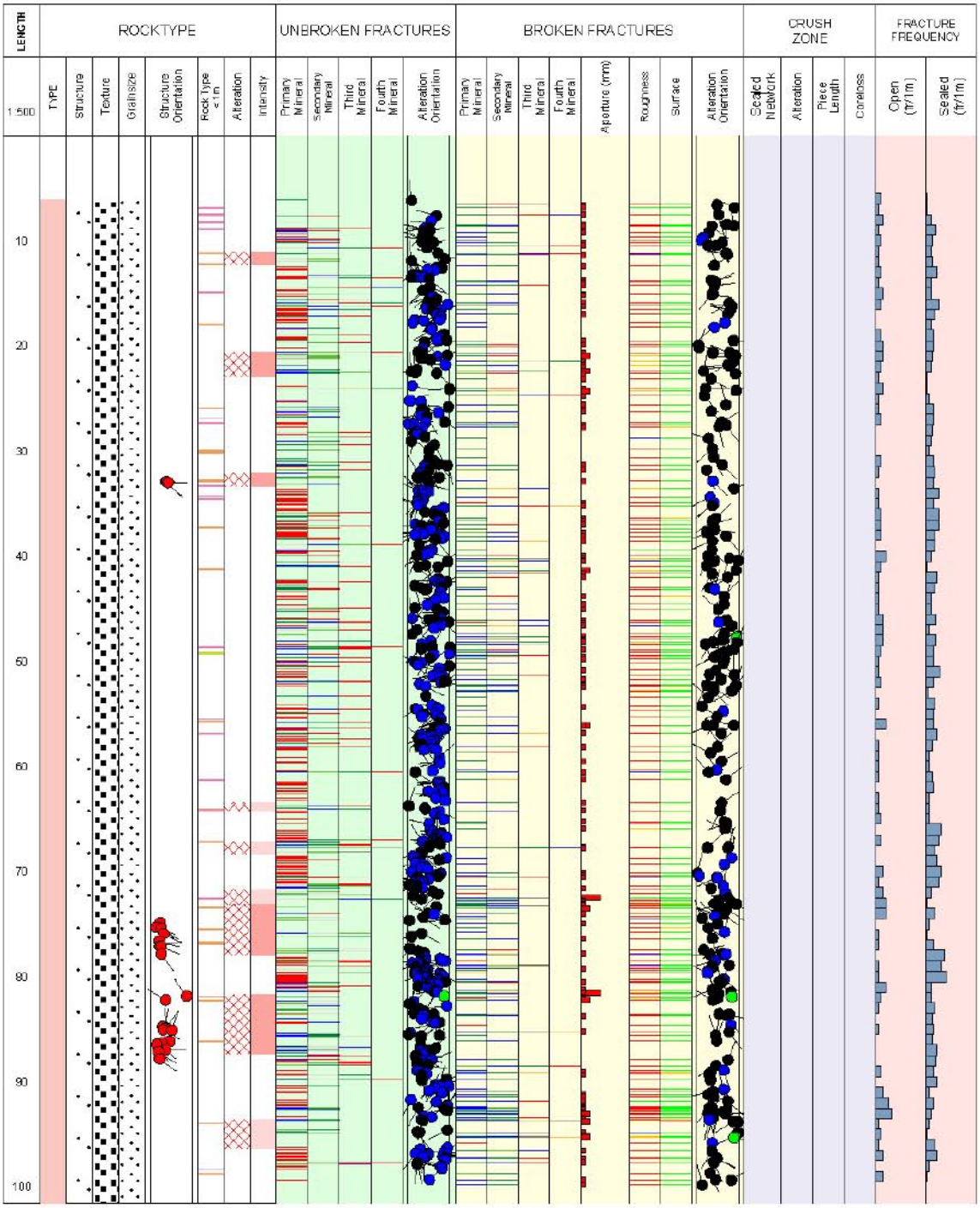

Title LEGEND FOR SIMPEVARP KSH01A + B

Site SIMPEVARP
Borehole KSH01A
Plot Date 2004-03-15 21:03:26

ROCKTYPE - SIMPEVARP

- Dolerite / Diabas
- Fine-grained Götemargranite
- Coarse-grained Götemargranite
- Fine-grained granite
- Pegmatite
- Granite
- Ävrö granite
- Quartz monzodiorite
- Diorite / Gabbro
- Fine-grained dioritoid
- Fine-grained diorite-gabbro
- Sulphide mineralization
- Sandstone

STRUCTURE

- Schistose
- Gneissic
- Mylonitic
- Ductile Shear Zone
- Brittle-Ductile Zone
- Veined
- Banded
- Massive
- Foliated
- Brecciated
- Lineated

TEXTURE

- Hornfelsed
- Porphyritic
- Ophitic
- Equigranular
- Augen-Bearing
- Non_equigranular
- Metamorphic

GRAINSIZE

- Aphanitic
- Fine grained
- Fine to Medium Grained
- Medium coarse
- Coarse grained
- Medium grained

ROCK ALTERATION

- Oxidized
- Cloritisized
- Epidotisized
- Weathered
- Tectonized
- Sericitisized
- Miarolitic
- Silicification
- Argillization
- Albitization
- Carbonatization
- Saussuritization
- Steatitization
- Uralitization

INTENSITY

- No intensity
- Faint
- Weak
- Medium
- Strong

ROUGHNESS

- Planar
- Undulating
- Stepped
- Irregular

SURFACE

- Rough
- Smooth
- Slickensided

CRUSHALTERATION

- Slightly Altered
- Moderately Altered
- Highly Altered
- Completley Altered
- Gouge
- Fresh

MINERAL

- Epidote
- Hematite
- Calcite
- Chlorite
- Chalcopyrite
- Quartz
- Pyrite
- Clay Minerals
- Laumontite
- Prehnite
- Iron Hydroxide
- Oxidized Walls

FRACTURE ALTERATION

- Fresh
- Gouge
- Completely Altered
- Highly Altered
- Moderately Altered
- Slightly Altered

FRACTURE DIRECTION